PhD degree in Systems Medicine (curriculum in Molecular Oncology)
European School of Molecular Medicine (SEMM)
University of Milan and University of Naples “Federico II”
Settore Disciplinare: BIO/11

Molecular mechanisms orchestrating lysosome-mediated degradation of ribosomes in aneuploid cells

Sonia Viganò

European Institute of Oncology (IEO), Milan (Italy)

Tutor: Prof. Stefano Santaguida
European Institute of Oncology (IEO), Milan (Italy)
University of Milan, Milan (Italy)

PhD coordinator: Prof. Saverio Minucci

Academic year 2021-2022

Table of content

Figure index

Table index

List of Abbreviations

17-AAG	17-allylamino-17-demethoxy-geldanamycin
26S	26 Svedberg, eukaryotic proteasome
40S	40 Svedberg, eukaryotic small ribosomal subunit
60S	60 Svedberg, eukaryotic large ribosomal subunit
80s	80 Svedberg, eukaryotic ribosome
Aneu	Aneuploid sample (treated with Mps1 inhibitor)
ap>myrT, bub3-i	apterous-specific Gal4 driving bub3-RNAi fused with MyrT for *Drosophila* model
APC/C	Anaphase Promoting Complex / Cyclosome
ArCK	Arrested cells with Complex Karyotype
ATF3	Activating Transcription Factor 3
ATF4	Activating Transcription Factor 4
ATF6	Activating Transcription Factor 6
ATG	Autophagy-related protein
ATG5	Autophagy-related protein 5
ATM/Chk2	Ataxia Telangiectasia Mutated serine/threonine kinase/Checkpoint kinase 2
AZC	L-Azetidine-2-Carboxylic acid
$BafiloA_1$	Bafilomycin A_1
BiP	Binding immunoglobulin Protein (also known as GRP78)
Bre5	Brefeldin-A sensitivity protein 5 (yeast Ubp3 cofactor)
BSA	Bovine Serum Albumine
BUB1	Budding Uninhibited by Benzimidazole 1
BUB3	Budding Uninhibited by Benzimidazole 3
BUBR1	Budding Uninhibited by Benzimidazole-Related 1
$CaCl_2$	Calcium Chloride
Cas9	CRISPR-associated protein 9
CCLE	Cancer Cell Line Enciclopedia
CDC20	Cell Division Cycle protein 20
CDK	Cyclin-Dependent kinase
cGAS	Cyclic GMP-AMP Synthase
CH21	human Chromosome 21
CHOP	C/EBP-Homologous Protein (also known as DDIT3)
CHX	Cycloheximide
CIN	Chromosomal Instability
CLEM	Correlative Light Electron Microscopy
CRISPR	Clustered Regularly Interspaced Short Palindromic Repeats
Ctrl	Pseudo-diploid control sample (treated with DMSO)

Cue2	Coupling of ubiquitin to ER degradation 2 (yeast homologue of human N4BP2)
DABCO	1,4-diazabicyclo[2.2.2]octane
DAPI	4′,6-diamidino-2-phenylindole
DAVID	Database for Annotation, Visualization and Integrated Discovery
Dcp1	Death caspase-1 (*Drosophila* homologue of human Caspase-7)
DDIT3	DNA damage-inducible transcript 3 (also known as CHOP)
DepMap	the cancer Dependency Map
DMSO	Dimethyl Sulfoxide
DNA	Deoxyribonucleic Acid
DS	Down Syndrome
Dub	De-ubiquitylating enzyme
E1	Ubiquitin-activating Enzyme
E2	Ubiquitin-conjugating Enzyme
E3	Ubiquitin-protein ligase
EC_{50}	Half maximal effective concentration
ECL	Enhanced Chemiluminescence
EDF1	Endothelial Differentiation-related Factor 1
EDTA	Ethylenediaminetetraacetic Acid
eIF2α	eukaryotic translation Initiation Factor 2, subunit alpha
eIF4G	eukaryotic translation Initiation Factor 4 G
EM	Electron Microscopy
ER	Endoplasmic Reticulum
ERAD	ER-Associated Degradation
ey>bub3-i	eye-specific Gal4 driving bub3-RNAi for *Drosophila* model
FACS	Fluorescence-Activated Cell Sorting
FAM134A	Family with sequence similarity 134, member A (also known as RETREG2)
FAM134B	Family with sequence similarity 134, member B (also known as RETREG1)
FAM134C	Family with sequence similarity 134, member C (also known as RETREG3)
FBS	Foetal Bovine Serum
FRP	Fraction of Ribosomes in Polysomes
G3BP1	Ras-GTPase-activating SH3-domain-Binding Protein 1
GAPDH	Glyceraldehyde-3-Phosphate Dehydrogenase
GCN2	General Control Non-depressible 2
Geld	Geldanamycin
GFP	Green Fluorescent Protein
GOBP	Gene Ontology of Biological Processes
GO	Gene Ontology
GRP78	Glucose-Regulated Protein 78 (also known as BiP)
GRP94	Glucose-Regulated Protein 94

GSEA	Gene Set Enrichment Analysis
GTP	Guanosine-5'-triphosphate
HA-tag	Hemagglutinin tag
HBS	HEPES-buffered saline
HCT116	Human Colorectal carcinoma cell line (HCT-116)
HEPES	4-(2-hydroxyethyl)-1-piperazineethanesulfonic acid
HRI	Heme-Regulated Inhibitor
HRP	Horseradish Peroxidase
HSF1	Heat Shock Factor 1
Hsp(s)	Heat shock protein(s)
Hsp27	Heat shock protein 27 KDa
Hsp70	Heat shock protein 70 KDa
Hsp90	Heat shock protein 90 KDa
IEO	European Institute of Oncology
iPS	Induced Pluripotent Stem cells
IRE1	Inositol Requiring Enzyme 1
JNK	Jun N-terminal Kinase
K48-Ub	Poly-Ubiquitin chains linked to lysine residue 48
K63-Ub	Poly-Ubiquitin chains linked to lysine residue 63
KEGG	Kyoto Encyclopaedia of Genes and Genomes
LC3	microtubule-associated protein Light Chain 3
LDHB	Lactate Dehydrogenase B
LIR	LC3-Interacting Region
Ltn1	Listerin E3 ubiquitin protein ligase 1
MAD1	Mitotic Arrest Deficient 1
MAD2	Mitotic Arrest Deficient 2
MCC	Mitotic Checkpoint Complex
Met	Methionine
MFI	Mean Fluorescence Intensity
MiDAS	Mitotic DNA Synthesis
MN / MNi	Micronucleus / Micronuclei
Mps1	Monopolar spindle protein 1
mRNA	Messenger RNA
MS/MS	Tandem mass spectrometry
mTOR	mammalian Target of Rapamycin
MyrT	MyrTomato red fluorescence protein
n=	Number of independent biological replicates
N4BP2	NEDD4-binding protein 2 (human homologue of yeast Cue2)
$NaAsO_2$	Sodium arsenite

NF-kB	Nuclear Factor kappa-light-chain-enhancer of activated B cells
NGD	No-Go Decay pathway for mRNA degradation
NK	Natural Killer cells
NUFIP1	Nuclear Fragile X mental retardation-Interacting Protein 1
ORF	Open Reading Frame
OTUD3	Ovarian Tumour Deubiquitinase 3
p53	Tumour Protein 53 KDa
p62	Ubiquitin-binding protein 62 KDa (also known as SQSTM1)
P-body	Processing body
PBS	Phosphate-Buffered Saline
PCR	Polymerase Chain Reaction
PERK	Protein Kinase R (PKR)-like Endoplasmic Reticulum Kinase
pH	Potential of Hydrogen
PI3K	Phosphoinositide 3-Kinase
PKR	Protein Kinase R
PN	Primary Nucleus
Poly(A)	Polyadenylated sequence
RACK1	Receptor for Activated C Kinase 1
RAMP4	Ribosome-Associated Membrane Protein 4
RBP	RNA Binding Protein
RETREG1	Reticulophagy Regulator family, member 1 (also known as FAM134B)
RETREG2	Reticulophagy Regulator family, member 2 (also known as FAM134A)
RETREG3	Reticulophagy Regulator family, member 3 (also known as FAM134C)
Rev	Reversine
RFP	Red Fluorescent Protein
RLU	Relative Light Unit
RNA	Ribonucleic Acid
RNase	Ribonuclease
RNF10	Ring Finger Protein 10, E3-Ligase
ROS	Reactive Oxygen Species
RPE1	human hTERT Retinal Pigment Epithelia cell line (hTERT RPE-1)
RPL26	Ribosomal Protein L26 (large subunit)
RPL28	Ribosomal Protein L28 (large subunit)
RPS3	Ribosomal Protein S3 (small subunit)
RPS6	Ribosomal Protein S6 (small subunit)
RQC	Ribosome-associated Quality Control
RRub	Regulatory Ribosomal ubiquitylations
RT-qPCR	Real Time quantitative Polymerase Chain Reaction
SAC	Spindle Assembly Checkpoint

SAR405	PI3K / VPS34 selective inhibitor
SASP	Senescence-Associated Secretory Phenotype
SD	Standard Deviation
SDS-PAGE	Sodium Dodecyl Sulphate - PolyAcrylamide Gel Electrophoresis
SEM	Standard Error of the Mean
SILAC	Stable Isotope Labelling by Amino acids in Cell culture
siRNA	Small interfering RNA
SG	Stress Granules
SQSTM1	Sequestosome 1 (also known as p62)
STING	Stimulator of Interferon Genes
SunSET	Surface Sensing of Translation
TBS	Tris-Buffered Saline
TCA	Trichloroacetic Acid
TCGA	The Cancer Genome Atlas
TFEB	Transcription Factor EB
TIA1	T cell Internal Antigen 1
TMI	Tetraphenylethene Maleimide (TPE-MI)
Torin1	mTOR selective inhibitor
tpm	Transcript per million
tRNA	Transfer RNA
Ub	Ubiquitin
UBA	Ubiquitin-Associated domain
UBE2O	Ubiquitin-conjugating Enzyme 2 O
Ubp3	Ubiquitin-specific proteases 3 (yeast homologue of human USP10)
ULK1	Unc-51-Like Kinase 1
UPR	Unfolded Protein Response
UPS	Ubiquitin Proteasome System
USP10	Ubiquitin-specific peptidase 10 (human homologue of yeast Ubp3)
USP21	Ubiquitin-specific peptidase 21
VER	VER-155008
VPS34	Vacuolar Protein Sorting 34
WB	Western Blot
Wt	Wild-type
XBP1	X-box Binding Protein 1
XRN1	5′-3′ exoribonuclease 1
ZNF598	Zinc Finger Protein 598, E3-Ligase

Abstract

Chromosome segregation errors lead to the generation of aneuploid daughter cells with unbalanced karyotypes. This condition has a profound impact on cell physiology, causing a plethora of cellular stresses. One of the most prominent effects of abnormal karyotypes is the development of proteotoxic stress, which is characterised by the aggregation of aberrant proteins in the cytoplasm. The disruption of protein homeostasis correlates with and depends on gene copy number changes and occurs at multiple levels in aneuploid cells. Protein folding, for instance, is known to be compromised and this feature together with the overwhelming of quality control mechanisms leads to the accumulation and aggregation of not-properly folded proteins in the cytoplasm. The pathway that is in charge for the degradation of extra, misfolded or defective proteins is autophagy, which, accordingly, is close to saturation in aneuploid cells.

Unlike other aspects of aneuploidy, how exactly cells respond to the onset of proteotoxic stress is yet to be explored. The studies conducted within my PhD project revealed that, in aneuploid cells with random chromosome gains and losses, an impaired protein folding is strictly connected to the lysosome-mediated degradation of ribosomes. In detail, with my work I showed that, right after chromosome mis-segregation, cells face an increasing folding demand that challenges Hsp90 and Hsp70 chaperone families. The lack of an efficient folding machinery, in turn, causes the attenuation of the synthesis of new polypeptides, which is further exacerbated by the activation of the unfolded protein response (UPR). By addressing the molecular mechanisms that aneuploid cells activate to cope with folding and translation deficiencies, I have found that ribosomes are recognised by the E3-ligase ZNF598 and tagged for degradation. Their clearance is carried out by the autophagic pathway, in particular by their selective degradation mediated by lysosomes. This is indicated by the increased ribophagy I observed in aneuploid cells, right after chromosome mis-segregation.

On the other hand, aneuploidy-driven genomic instability is known to fuel a vicious cycle leading to the generation of complex karyotypes. Accumulation of such chromosomal aberrations, in turn, exacerbate the aneuploidy-associated stresses and I demonstrated that this is also the case with proteotoxic stress. Importantly, I showed that ribosome degradation is increased under this condition, but the initial selectivity mediated by ZNF598 is lost, due to the uncontrolled increase in bulk autophagy. As a matter of fact, the accumulation of toxic aggregates and extra proteins boost bulk autophagy, leading to the random engulfment of cytosolic cargo in the autophagic structures, including ribosomes.

Interestingly, by stratifying aneuploid human cancers by their aneuploidy score, I found that the highly aneuploid ones are negatively associated with ribosomal signatures and tend to overexpress ZNF598, which might enable them to keep under control the proteotoxic stress.

Overall, this study shed light on a previously uncharacterised chain of events activated by aneuploid cells in response to the onset of proteotoxic stress. My results have the potential to indicate specific targets for cancer therapy, in contexts in which modulation of protein translation can be selectively targeted with the goal to interfere with cell proliferation.

Introduction

The research I am going to present in this PhD thesis focuses on dissecting how chromosome segregation errors affect cell physiology and, in particular, it addresses the consequences of proteotoxic stress in aneuploid cells. By using cell biology, molecular biology, genome editing approaches and imaging techniques, I am describing a series of processes that aneuploid cells employ to manage proteome imbalances, giving a novel glance on the molecular mechanisms involved.
Hence, the introduction below will provide an up-to-date overview of aneuploidy with its associated stresses, as well as a description of the already-known quality control pathways.

1. Chromosome mis-segregation and aneuploidy

Aneuploidy is a condition in which a cell has an incorrect chromosome number (Täckholm, 1922) and it is a consequence of chromosome mis-segregation events (Pfau & Amon, 2012).

1.1 Cell division

Chromosome segregation is a critical step to maintain a balanced euploid genome throughout cell division and, in general, for the fitness of a multicellular organism (Levine & Holland, 2018). Cells get ready for the segregation of chromosomes through a series of events that define the eukaryotic **cell cycle** (Alberts et al., 2015). Considering its two main stages (interphase and mitosis), interphase is composed of G1 phase (or gap-phase between mitosis and S phase), in which the cell grows and duplicates its organelles; by S phase (S for DNA synthesis), in which the duplication of DNA strands takes place and, before arriving in mitosis, by a second gap-phase (G2 phase) (Figure 1). Cells spend most of their time in interphase, although the duration of cell cycle varies considerably across different cell types. For example, in a typical proliferating mammalian cell, with a total cell cycle of 24 hours, G1 phase can proceed for about 11 hours, S phase takes around 8 hours and G2 about 4 hours. Mitosis, instead, lasts only 1 hour, but it is during this phase that duplicated chromosomes are segregated into two distinct nuclei and the mother cell accomplishes to divide into two identical daughter cells (Alberts et al., 2015).

The fascinating events that allow the cell to achieve the segregation of chromosomes are mirrored by the succession of the five steps of **mitosis**: prophase, prometaphase, metaphase, anaphase and telophase (Alberts et al., 2015) (Figure 1). M phase, then, ends followed by cytokinesis. During prophase, chromatin condensates to form mitotic chromosomes, where sister chromatids are still linked together by cohesins (Nasmyth & Haering, 2009), and cell cytoskeleton disassembles to be replaced by mitotic spindle. The end of prophase and the beginning of prometaphase are identified by the progressive nuclear envelope breakdown (Alberts et al., 2015). In prometaphase, the attachment of

each sister chromatid to microtubules emanating from opposite spindle poles takes place (Alberts et al., 2015). This is possible thanks to specialised proteins in the centromeric region of chromosomes that are collectively known as kinetochore (Santaguida & Musacchio, 2009). At this point, mitotic chromosomes start moving towards the spindle centre. Metaphase is identified by the alignment of all the chromosomes on the so-called metaphase plate, where they are bi-oriented, a status guaranteed by the tension generated by the pulling forces of microtubules and the resistance of cohesins to these forces (Tanaka et al., 2000). The metaphase-to-anaphase transition represents a crucial part of mitosis and therefore it is tightly controlled to ensure the correct segregation of chromosomes, as I will detail in the next paragraph. With anaphase, in fact, sister chromatids evenly separate while the spindle poles move outward, to finally organise two sets of daughter chromosomes (Alberts et al., 2015). At the last stage of mitosis, in telophase, the spindle disassembles and the nuclear envelope reassembles to form two distinct nuclei, that will be divided during cytokinesis into two daughter cells, with further division of cytoplasm thanks to the cleavage furrow activity (Alberts et al., 2015) (Figure 1).

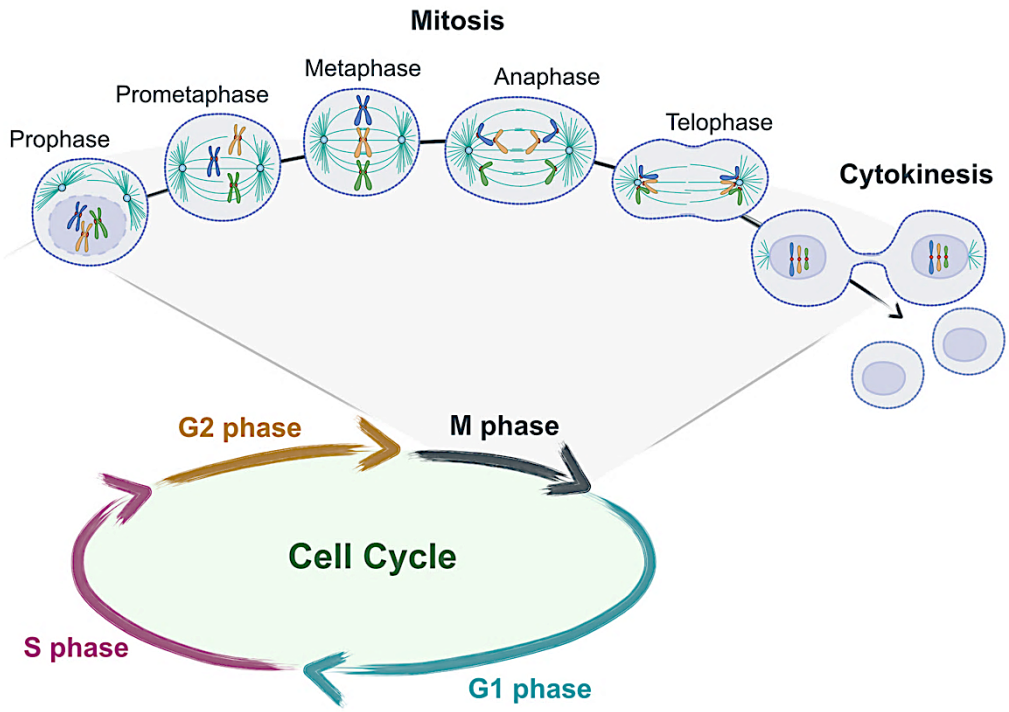

Figure 1: Eukaryotic cell cycle and mitosis.
Interphase is composed of G1 phase, where the cell grows and duplicates organelles; S phase, where DNA duplication takes place; a second gap-phase, G2 phase. M phase starts with mitosis, a succession of five steps that leads to chromosome segregation; and it ends with cell division during cytokinesis.

Cell cycle is tightly regulated by control systems that ensure both progression through its major phases and accuracy of cell division. The central components of the cell-cycle control system are the cyclin-dependent kinases (CDKs): they promote specific cell-cycle events only when their phosphorylation activity is triggered by binding with cyclins, whose

concentration oscillates during cell cycle (Pines & Hunter, 1991). To proceed with mitosis, the master mitotic kinase CDK1 must bind cyclin B and securin binds and keeps inactive the protease separase, which is in charge of cohesin cleavage to begin chromosome segregation (Peters, 2006). The metaphase-to-anaphase transition is triggered by the anaphase-promoting complex/cyclosome (APC/C) and its activator CDC20 (APC/C^{CDC20}) (Acquaviva & Pines, 2006). APC/C^{CDC20} initiates sister chromatids separation by ubiquitylating cyclin B and securin (Hagting et al., 2002), leading to their degradation by the proteasome, thus allowing anaphase to proceed and complete the exit from mitosis (Peters, 2006). The fidelity of chromosome segregation is ensured by an evolutionary conserved mechanism known as **spindle assembly checkpoint** (SAC), that prevent errors by ensuring that cells do not enter anaphase until all chromosomes are bi-oriented on the metaphase plate (Musacchio & Salmon, 2007). SAC depends on a mechanism that senses the decrease in tension of unattached kinetochores and/or the lack of attachment to the mitotic spindle (Taylor et al., 2004) (Figure 2). Indeed, mitotic chromosomes that are not accurately attached to microtubules emanating from opposite spindle poles promote APC/C^{CDC20} inhibition through the incorporation of CDC20 into the mitotic checkpoint complex effector, MCC (Izawa & Pines, 2015), which contains three SAC proteins: BUBR1, BUB3 and MAD2 (Mapelli et al., 2007; Musacchio & Salmon, 2007). Other SAC core components are MAD1 (mitotic arrest deficient 1) and the checkpoint kinases Mps1 (monopolar spindle protein 1), BUB1 and Aurora B (Musacchio & Salmon, 2007; Santaguida et al., 2011). These kinases phosphorylate kinetochore components involved in incorrect microtubule attachments, destabilizing and converting them into correct amphitelic attachments (Musacchio & Salmon, 2007). SAC is normally silenced when all the faulty attachments are resolved, letting the cell progress into the cell cycle (London & Biggins, 2014). By delaying cell division until a faithful chromosome segregation takes place, SAC plays a key role in maintaining genome stability (Lara-Gonzalez et al., 2012).

1.2 Causes and outcomes of chromosome mis-segregation

Although the spindle assembly checkpoint generally ensures the fidelity of mitosis reducing the rate of aneuploidy, there are several circumstances that give rise to unfaithful chromosome segregation, escaping the controls. The origin of mitotic errors can be identified both in pre-mitotic events, such as abnormal DNA structures or erroneous DNA duplication and repair, and in post-mitotic events (Garribba & Santaguida, 2022). The latter comprises defects in structural components of the mitotic machinery, for example spindle aberrations due to centrosome amplification (Basto et al., 2008) and multipolar spindles (Maiato & Logarinho, 2014), or weak sister chromatids cohesion (Barber et al., 2008).

Importantly, **incorrect kinetochore-microtubule attachments** account for a big part of these mitotic defects (Soto et al., 2019) and they are strictly connected with microtubule dynamics and SAC function (Figure 2). Indeed, hyperstable kinetochore-microtubule

interactions are suggested to drive faulty chromosome segregation, as well as a reduced interaction may protect against errors (Bakhoum et al., 2009). In this context, an abnormal SAC function can have catastrophic effects on the fidelity of chromosome segregation, due to the non-identification and resolution of aberrant kinetochore-microtubule attachments (Levine & Holland, 2018). The nature of faulty attachments can vary. As mentioned above, the correct connection between microtubules and kinetochores of both sister chromatids, that lead to a bi-oriented mitotic chromosome, is known as amphitelic attachment (Figure 2a). Variations in this connection inevitably cause the mis-segregation of the involved chromosomes. Among these, the condition where only one sister chromatid is attached to microtubules is defined as monotelic attachment (Figure 2b), while a syntelic attachment is determined when both sister kinetochores are pulled from the same spindle pole (Santaguida & Amon, 2015b) (Figure 2c). Merotelic attachments are also of note, as they interfere with the correct segregation of chromosomes, in particular leading to the "lag" of the sister chromatid involved (Cimini et al., 2001). They are, in fact, defined when one sister kinetochore is linked to microtubules emanating from both poles (Figure 2d).

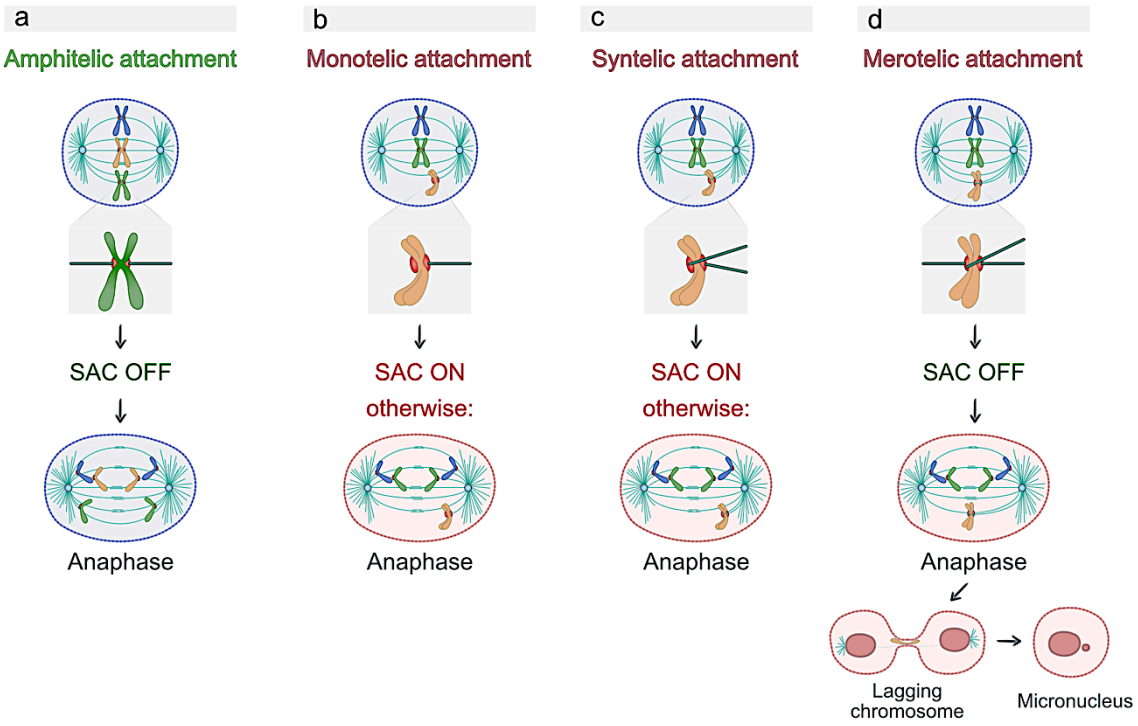

Figure 2: Kinetochore-microtubule attachments and chromosome (mis)segregation.
Correct microtubule-kinetochore attachment, known as amphitelic attachment, generates a bi-oriented mitotic chromosome (**a**). Monotelic attachment, defined as only one kinetochore anchored to microtubules (**b**), and syntelic attachment, when both kinetochores attach microtubules from the same pole (**c**), activate SAC, that senses the decreased tension of unattached kinetochores; if in these conditions SAC is inhibited or defective, chromosome mis-segregation events occur. Merotelic attachments are determined when one (or both) kinetochore(s) attach to microtubules emanating from both poles, resulting in the lag of the chromosome involved, which is one of the leading causes of micronuclei formation(**d**).

Lagging chromosomes are left behind during anaphase in the mid-zone of the mitotic spindle and have been identified as a major cause of aneuploidy (Cimini et al., 2001) (Figure 2d). If they do not catch-up with the rest of chromosomes before cytokinesis, they risk being damaged and physically broken by the forces exerted by the cleavage furrow. This results in high levels of DNA damage on the genetic material involved and, likely, in structural chromosome aberrations (Janssen et al., 2011). Another possible fate of lagging chromosomes is their extreme "stretch" between the two daughter nuclei, generating anaphase bridges first and, then, chromosome bridges (Martin & Santaguida, 2020). In this case as well, the outcome is a breakage that occurs later (Maciejowski et al., 2015), and that may even lead to catastrophic genome rearrangements in the subsequent cell divisions (a process known as chromothripsis) (Umbreit et al., 2020). Chromothripsis is also tightly associated with **micronuclei** (MNi) (C. Z. Zhang et al., 2015), which are by-products of mis-segregated chromosomes that have been confined in a nuclear-ish structure different from the primary nucleus. DNA in MNi accumulates damage, further exacerbated by dysfunctional replication and repair mechanisms, which lead to multiple chromosomal rearrangements (Crasta et al., 2012). These defects have been demonstrated to delay the reincorporation of MNi in primary nuclei (Soto et al., 2018). But, once MNi are re-incorporated, further DNA damage seems to be overcome (Soto et al., 2018). This, however, fuels the transfer and the propagation of the already-arisen mutations from MNi to the cell genome, with dramatic implications in genomic instability and tumorigenesis (Ly et al., 2019). The high level of genomic instability triggered by the previously mentioned chromosome segregation errors is, therefore, strictly connected with the increased rate of structural and numerical chromosomal aberrations, widely known as chromosomal instability (CIN) (Garribba & Santaguida, 2022).

1.3 Chromosomal instability and the aneuploid state

While "aneuploidy" refers to an unbalanced genomic state, "chromosomal instability" (CIN) is a condition with high rate of chromosome mis-segregation that invariably leads to aneuploidy (Levine & Holland, 2018). **CIN** is commonly described as a form of genomic instability in which cells dynamically gain or lose whole- or part-of- chromosomes (Geigl et al., 2008). Gains or losses of whole chromosomes at elevated rates are classified as numerical CIN; while the continuous formation and re-assembly of structurally abnormal chromosomes due to translocations, inversions, deletions or amplifications of chromosome portions are known as structural CIN (McGranahan et al., 2012).

A similar distinction can also be made for the aneuploid state, despite the strict meaning of **aneuploidy** refers only to the number of chromosomes that is not a multiple of the haploid complement. Nowadays, aneuploidy is comprehensive of both numerical (whole chromosome) aneuploidies and segmental aneuploidies, which result from sub-chromosomal imbalances (Pfau & Amon, 2012). Polyploidy, instead, indicates a different

status, where a cell contains an exact multiple number of its entire genome, which, therefore, is balanced. Since aneuploid karyotypes can show a grey-scale of imbalances, it is useful to describe as “highly aneuploid” the karyotypes with a deviation of many chromosomes from the euploid counterpart, and as “low aneuploid” the karyotypes that deviate just for one or two chromosomes from the euploid number (Pfau & Amon, 2012). Importantly, aneuploid cells do not necessarily exhibit CIN, as they can be stable in their aneuploid state.

2. Aneuploidy is a hallmark of cancer

One of the widely recognised characteristics of cancer cells is their aneuploidy. Indeed, 90% of solid tumours and the vast majority of blood cancers have aneuploid karyotypes (Beroukhim et al., 2010; Campbell et al., 2020). Accordingly, human health is dramatically affected by aneuploidy, as this condition is implicated in several diseases (Siegel & Amon, 2012).

2.1 Aneuploidy is rare in normal tissues

At the organismal level, both somatic and constitutional aneuploidies are **rare**. The former are generated by random mitotic errors and their frequency rates are very low, pointing out how aneuploidy can’t provide any advantage to tissues and organs (Knouse et al., 2014). The latter are the result of errors during meiosis and generally lead to embryonic lethality. In the infrequent exceptions, constitutional aneuploidies cause growth and developmental defects in almost all the organisms studied (Torres et al., 2008). In humans, only three trisomies are compatible with life and they involve the chromosomes with the least number of encoding genes, while all other autosomal trisomies and monosomies are not vital. Trisomy 13 and trisomy 18 cause respectively Patau syndrome and Edward syndrome and the patients can survive birth, but die in the first months of life. Down syndrome (DS), which is characterised by an extra copy of chromosome 21, is more frequent. DS patients can live to adulthood, although they share a wide number of defects and abnormalities in growth and development and have an increased risk of specific pathologies and childhood cancer onset, compared to the rest of the population (Pfau & Amon, 2012).

2.2 Aneuploidy and cancer

The majority of aneuploid cells generated via faulty cell divisions are eliminated, but this does not happen in a tumour context. In mammals, the alteration of karyotype for functional adaptation is known to occur only in **cancer** (Knouse et al., 2014). Whether aneuploidy plays an active role in tumorigenesis or it is only a by-product of it is still widely debated. In fact, cancer cells often show inactivating mutations of cell cycle and cell division master genes and display deregulation of genome stability (Schvartzman et al., 2011). On the other

hand, in several mouse models, aneuploidy-driven CIN can increase tumorigenesis (Gordon et al., 2012). The karyotype heterogeneity and reshuffling that aneuploidy and CIN generate in tissues can be exploited by cancer cells to better adapt to challenging conditions (Hanahan & Weinberg, 2011; Holland & Cleveland, 2012). Indeed, increasing aneuploidy and karyotype complexity correlates with tumour evolution from benign to invasive and metastatic (Siegel & Amon, 2012). The cancer-promoting aneuploid karyotypes that confer proliferative advantage to survive under challenging circumstances are particularly important in chemotherapy. Cancer cells can become chemo-resistant thanks to their ability to find a useful karyotypic landscape to survive (Ippolito et al., 2021; Lukow et al., 2021). It is, therefore, not surprising that aneuploidy strongly associates with poor prognosis; in particular, the higher the levels of aneuploidy, the poorer the prognosis (Ben-David & Amon, 2020). It is also crucial to take into account that many different aneuploidies and chromosomal abnormalities can be found in distinct cancer contexts, as well as each of them can present various grades of intratumour heterogeneity (Ben-David & Amon, 2020). These factors highlight the difficulty of generalizing the relationship between aneuploidy, CIN and cancer but, bearing in mind the context-dependent role of aneuploidy, this hallmark can be definitely considered as a therapeutic target.

3. Detrimental effects of aneuploidy in untransformed cells

Although aneuploidy is a hallmark of cancer - a disease characterised by uncontrolled proliferation - the condition of having an abnormal karyotype is also associated with a number of detrimental effects on cellular fitness. This dichotomy of the aneuploid state is commonly recognised as the “paradox of aneuploidy” (Weaver & Cleveland, 2008). The efforts that have been done in the last decade to explain the paradox pointed out that imbalanced karyotypes impact cell proliferation in stress-free contexts, while aneuploid cells can survive better in sub-optimal environments (Sheltzer & Amon, 2011).

3.1 Immediate consequences of aneuploidy

One of the first outcomes of chromosome mis-segregation is the formation of micronuclei (MNi), which is a feature detectable even at the microscope at low magnification, and can help the researcher to spot highly-probable aneuploid cells. As previously mentioned in this introduction, MNi are not-fully-functional organelles that cannot properly replicate their genetic material (a chromosome or a piece of a chromosome) (Crasta et al., 2012; Hatch & Hetzer, 2015; C. Z. Zhang et al., 2015). Consequently, MNi show high levels of **DNA damage** and low efficiency in DNA damage repair, fuelling genomic instability (Garribba & Santaguida, 2022) (Figure 3a). Another important MNi feature that is worth mentioning is their often-ruptured membrane. This leads to the spillage of micronuclear DNA into the cytoplasm with the consequent activation of cGAS, the master nucleic acid sensor, which,

in turn, triggers the immune surveillance mechanism mediated by STING (Bakhoum et al., 2018; MacKenzie et al., 2017) (Figure 3a).

In various model systems and contexts, chromosome mis-segregation and aneuploidy have been shown to activate p53 (Figure 3). Since cells with constitutional aneuploidies do not trigger this control pathway (Tang et al., 2011), **p53 activation** seems to be an acute effect of aneuploidy (Santaguida & Amon, 2015b). What exactly causes p53 activation is debated, and multiple mechanisms can be responsible. For example, lagging chromosomes during cell division and broken chromosomes in daughter cells can activate DNA damage response mediated by ATM/Chk2 and, consequently, p53 (Janssen et al., 2011) (Figure 3a). Another possible feature of aneuploid cells that might be involved is their altered metabolism that leads to the generation of reactive oxygen species (ROS), which in turn trigger DNA damage response and p53. More in general, aneuploid cells inevitably spend more time in mitosis and, if this worsens to mitotic arrest, these cells undergo apoptosis or G1-arrest mediated by p53 (Uetake & Sluder, 2010) (Figure 3b).

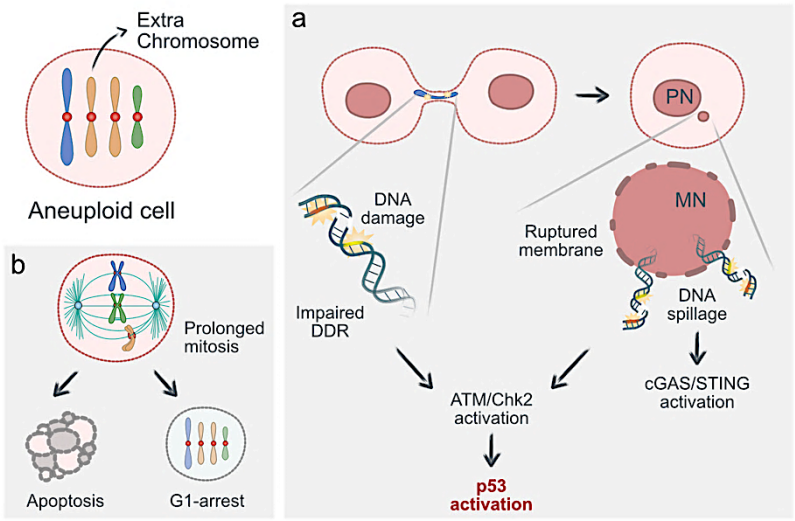

Figure 3: Immediate consequences of aneuploidy.
Lagging chromosomes can accumulate DNA damage (**a**, left) and generate micronuclei (MNi). MNi ruptured membrane leads to DNA spillage in the cytoplasm, which in turn activates cGAS pathway (**a**, right). High levels of DNA damage activate p53. Aneuploid cells spend more time in mitosis than euploid ones, and this can cause mitotic arrest. Prolonged arrest can lead to p53-mediated apoptosis (**b**, left) or p53-mediated G1 arrest (**b**, right). PN = primary nucleus

3.2 Long-term alteration of cell physiology

Given the fact that cells can tolerate much better polyploidy than aneuploidy (see paragraph 1.3), it is easy to infer that gene dosage plays an important role in cell physiology. Moreover, the majority of phenotypes related to aneuploidy are not associated with specific karyotypes, suggesting that these traits simply depend on an unbalanced chromosome composition (Figure 4).

Many **gene-specific effects** are studied and are associated with various diseases (F. Zhang et al., 2009), but when even a single whole chromosome is gained or lost, a massive deregulation of gene expression can occur. While the alteration of a single gene copy number leads to a specific phenotype, the concomitant change in dosage of many genes cause a plethora of phenotypes that are identified as aneuploidy-associated stresses. These stresses are shared by aneuploid cells regardless of their karyotype and contribute to cell fitness decrease (Santaguida & Amon, 2015b).

As already mentioned, the impact of aneuploidy on cell **proliferation** is dramatic (Figure 4a). *In vitro*, aneuploid cells proliferate slower (Thompson & Compton, 2010); but, also in more complex models, aneuploidy leads to growth defects that are strictly linked to low proliferation rates (Williams et al., 2008). This is further confirmed by transcriptomic studies that showed how genes involved in cell growth, proliferation and nucleic acid metabolism are downregulated in aneuploid cells of diverse model organisms, while stress-response genes are consistently upregulated (Sheltzer et al., 2012) (Figure 4a).

Genome instability is another significant long-term effect of aneuploidy, and it is strictly linked to the DNA damage increase that occurs right after chromosome mis-segregation (see paragraph 3.1) (Figure 4b). A recent study in the lab demonstrated that aneuploid cells experience DNA replication stress in the first S-phase and complete DNA synthesis in the following mitosis (Garribba et al., 2023), a process referred to as MiDAS (mitotic DNA synthesis) (Garribba et al., 2018). The redistribution of DNA damage in the following daughter cells fuels further genomic instability and the continuous genomic instability triggers increased rate of mis-segregation, ultimately leading to the accumulation of cells with aberrant complex karyotypes (Santaguida et al., 2017) (Figure 4b). The ongoing re-shuffling of karyotypes and acquisition of mutations might eventually promote cancer evolution. In fact, these mechanisms play a crucial role in improving cellular fitness through the search for optimal karyotypes able to adapt and overcome aneuploidy-associated stresses (Rutledge et al., 2016). *In vitro*, cells with complex karyotypes show senescence-associated gene expression signature (SASP) and eventually cease to divide, by arresting in G1 (Santaguida et al., 2017). Another important signature of the arrested cells with complex karyotype (ArCK) is the upregulation of pro-inflammatory genes and immune response activation that leads to the elimination of such cells by natural killer cells (NK) (Santaguida et al., 2017) (Figure 4b). In the first part of my PhD, I have participated in a study aimed at dissecting the mechanisms involved in the immune clearance of aneuploid cells. We demonstrated that untransformed aneuploid senescent cells, enriched and isolated from the cycling ones (Wang et al., 2018), activate both canonical and non-canonical NF-kB (nuclear factor-kappa B) pathways to elicit their NK-mediated clearance (Wang et al., 2021).

In addition, aneuploid cells also experience **metabolic stress**, which is developed in different manners, depending on the cell type and complexity. Since metabolic homeostasis is normally maintained by the synergistic effects of multiple metabolic pathways, the observed alterations in aneuploid cells span from glucose uptake, lactate production to accumulation of reactive oxygen species (ROS) (Siegel & Amon, 2012) (Figure 4c). The resulting oxidative and energy stresses are among the causes of the already-mentioned slowdown in proliferation and activation of p53-mediated cell cycle arrest and apoptosis (Li et al., 2010). Interestingly, recent studies in *Drosophila melanogaster* showed that ROS are produced massively also in epithelial CIN models, leading to JNK-dependent cell death (Clemente-Ruiz et al., 2016) or JNK-induced cell senescence (Joy et al., 2021). However, the ROS-activated JNK pathway is also recognised as a tumour promoter in contexts where apoptosis is inhibited and this represents a relevant link between aneuploidy-driven energy stress and tumorigenesis (Muzzopappa et al., 2017).

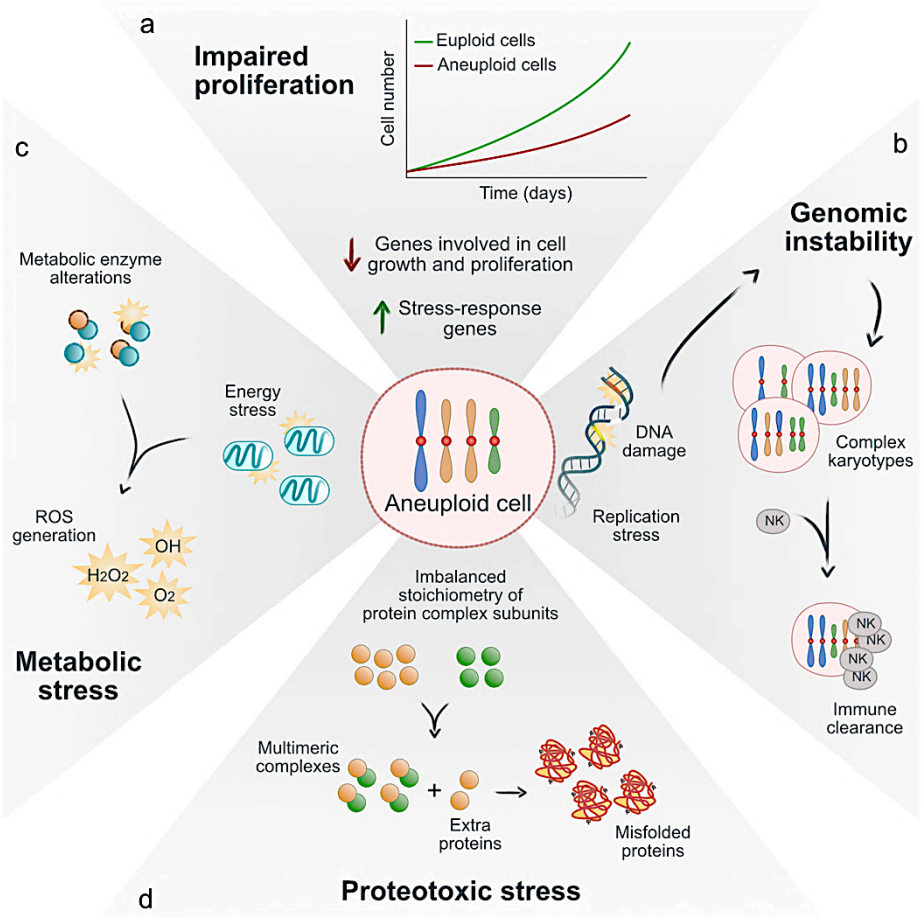

Figure 4: Aneuploidy-associated stresses.

Aneuploidy causes different stresses and long-term deleterious effects. The upregulation of stress-response signatures and the downregulation of genes involved in cell growth and metabolism have a major impact on aneuploid cell proliferation (**a**). High levels of DNA damage and replication stress result in genome instability, also associated with the evolution of complex aberrant karyotypes (**b**, top). Aneuploid cells with complex karyotypes elicit immune response and promote their own clearance mediated by natural killer cells (NK) (**b**, bottom). Energy stress and imbalanced metabolic enzyme activities trigger the generation of toxic reactive

oxygen species (ROS), characteristic of metabolic stress (**c**). Aneuploid cells also present high levels of proteotoxic stress. This is due to the imbalanced stoichiometry of multimeric complex subunits and the consequent accumulation of damaged and misfolded proteins that overwhelm quality control pathways (**d**).

Among the aneuploidy-associated stresses, **proteotoxic stress** is one of the most prominent. This stress is induced by the accumulation in the cell cytoplasm of misfolded polypeptides or proteins lacking interacting partners (Oromendia et al., 2012) (Figure 4d). Considering the central dogma of molecular biology, *DNA makes RNA and RNA makes protein*, it is easy to understand that aneuploid cells may suffer proteome imbalances. The presence of extra chromosome/s, as well as the loss of chromosome/s, inevitably alters the cell's protein composition. However, between theory and practice there are mechanisms and processes to be considered. In aneuploid cells, changes in the relative ratio of proteins include also an imbalanced stoichiometry of heteromeric complex subunits (Chunduri & Storchová, 2019; Oromendia & Amon, 2014; Santaguida & Amon, 2015b; Stingele et al., 2012), since subunits can be encoded by genes on different chromosomes (Figure 4d). If the expression of subunits of the same complex is not coordinated or if their ratio is not maintained, orphan subunits end up crowding the cytoplasm (Juszkiewicz & Hegde, 2018; Siegel & Amon, 2012). Therefore, protein aggregation and promiscuous interaction of orphan proteins are the main outcomes of cytoplasm overcrowding (Figure 4d). Interestingly, protein aggregation is also thought to be a characteristic that helps cells to manage the excess of proteins with long half-life (Brennan et al., 2019). An example is represented by ribosomes and ribosomal subunits, whose homeostasis is crucial for the cell. When their stoichiometry is disrupted, excess subunits tend to aggregate and compromise cellular fitness (Tye et al., 2019). Under physiological conditions, cells maintain a regulated protein stoichiometry through the activation of a broad regulatory proteostatic network (Pechmann et al., 2013). This involves chaperone-mediated folding mechanisms and quality control pathways that promptly degrade extra or misfolded proteins via the ubiquitin-proteasome system and, alternatively, through the autophagic pathway (Harper & Bennett, 2016). The critical levels of proteotoxic stress in aneuploid cells challenges the capacity of all these mechanisms, resulting in overwhelmed protein quality control (Donnelly et al., 2014; Oromendia & Amon, 2014; Santaguida & Amon, 2015b). Proteotoxicity is considered a common feature of aneuploid cells, since similar conditions and overloading have been observed in all aneuploid models, from yeast (Oromendia et al., 2012) to *Drosophila* (Joy et al., 2021). The paragraphs below will detail these processes and will deal thoroughly with proteome imbalances induced by aneuploidy.

4. Aneuploidy-induced proteome imbalances

Protein homeostasis is crucial for cell and organism health and it is, therefore, guaranteed by the fine balance between protein synthesis, protein folding and protein degradation (Pechmann et al., 2013). In the first part of this section (Introduction paragraph 4.1), I will present the principal components of the regulatory network, while in the second one (Introduction paragraph 4.2) I will describe what is known so far about the impact of aneuploidy on cell proteostasis.

4.1 Translation and protein quality control network overview

The regulatory network that ensures cell **proteostasis** is, at first, organised around ribosomes (Pechmann et al., 2013), and, later, relies on mechanisms that control quality and degradation of transcripts, proteins and ribosomes themselves (Harper & Bennett, 2016).

4.1.1 Chaperone-mediated protein folding

The production of proteins in eukaryotic cells is continuously carried out by their 10^6 - 10^7 ribosomes and protein synthesis is spatially and temporally related to protein folding (Pechmann et al., 2013) (Figure 5a). Folding is necessary to confer the nascent polypeptides the right structure and function, but this process is intrinsically error-prone, due to the vast conformation possibilities (Balchin et al., 2016). In fact, to fulfil protein demand, protein folding normally starts as soon as the N-terminal of the nascent protein emerges from the ribosome, while the rest of the polypeptide is still being synthesised. Polypeptide length and the number of protein domains are determinant for a fast and successful folding. That's why both ribosomes and co-translational folding are crucial to ensure translational fidelity and reduce aggregation rates (Pechmann et al., 2013).

Together with ribosomes, **chaperones** are the core of the folding regulatory network (Figure 5a). Chaperones are highly conserved molecular families that assist protein folding at different stages (Balchin et al., 2016). In eukaryotes, protein folding starts co-translationally, with chaperones operating on the ribosome. At this level, the Hsp70 (heat shock protein 70) system plays important roles, with its ribosome-binding isoforms. Hsp70 assists also proteins that are not fully folded at the ribosome level, thanks to its interactions with chaperonins and other downstream players (Balchin et al., 2016). This function is crucial to prevent promiscuous contacts between misfolded peptides and their consequent aggregation. Among the highly specialised downstream chaperones that operate post-translationally, Hsp90 (heat shock protein 90) is the most characterised and counts numerous clients (Taipale et al., 2010). As a matter of fact, Hsp90 and its cofactors coordinate also the structural regulation and conformational maturation of a wide range of oligomeric complexes (Taipale et al., 2010). Hsp90 client functions span from those of receptors or transcription factors, to transduction of clinically relevant pathways (Young et

al., 2001). Although the chaperone-mediated folding network has evolved to be dynamic and redundant to minimise faulty folding, it is easy to understand how detrimental could be the impairment of chaperone functions for cell proteostasis.

4.1.2 Cellular stress responses: UPR, ISR and stress granule assembly

Failure of proper protein folding leads to the aggregation of misfolded and unfolded proteins (Figure 5b). The toxicity of these aggregates is exerted by their interference with the normal function of other proteins and cellular mechanisms, as well as triggering of stress responses (Balchin et al., 2016).

The increase in unfolded and misfolded polypeptides in the endoplasmic reticulum (ER) lumen (a condition known as ER stress) is sensed by cells and, in particular, by three ER-localised sensors, namely the activating transcription factor 6 (ATF6), the inositol requiring enzyme 1(IRE1) and the PKR-like ER kinase (PERK) (Walter & Ron, 2011) (Figure 5b, bottom-left). Each of them is in charge of the activation of a specific branch of the so-called **unfolded protein response** (UPR), the signalling network that cells trigger upon ER stress (Vitale et al., 2019). The ultimate goal of this stress response is to alleviate ER stress by inducing the transcription of genes involved in protein folding or by a transient attenuation of protein synthesis to reduce ER folding load (Walter & Ron, 2011) (Figure 5b, bottom-left). The transduction of the signal resulting from the presence of unfolded proteins has different bases in the three UPR branches. ATF6 signal is mediated by the specific proteolysis of its luminal and transmembrane domain, which leads to the translocation of the N-terminal portion of ATF6 into the nucleus, where it can induce its target genes. Among these, there are those encoding for chaperones of the Hsp70 family (such as BiP, also known as GRP78) or belonging to the Hsp90 family (as GRP94) which, in turn, enhance ER folding capacity (Ye et al., 2000). The IRE1 branch is the most conserved from yeast to mammals and it is mediated by non-conventional mRNA splicing. IRE1 has the double function of kinase and endoribonuclease (RNase) and the latter can cleave XBP1 in $XBP1^{S}$, the active form of the transcription factor that induces UPR gene activation. As well as with transcriptional response, IRE1 branch further mitigates ER stress by inducing mRNA decay of the transcripts bound on the ER (Maurel et al., 2014). The third UPR branch is triggered by the ER kinase PERK which, once activated, dimerises and auto-phosphorylates to transduce the signal. Apart from itself, PERK phosphorylates the alpha subunit of the eukaryotic translation initiation factor eIF2 (eIF2α). Phosphorylated eIF2α cannot form the ternary complex eIF2-GTP-Met-tRNA, which is normally in charge of recognizing the start codon to initiate mRNA translation. This, in turn, leads to a decrease in global protein synthesis and it helps to reduce the load of protein in the ER (Walter & Ron, 2011). On the other hand, if ER stress is too severe, PERK can induce the transcription factor ATF4 and its target gene *CHOP*, which controls the transcription of apoptotic pathway components (Yang et al., 2017) (Figure 5b, bottom).

Serine 51 phosphorylation of eIF2α is also part of a wider stress response, known as **integrated stress response** (ISR), which temporarily suspends protein synthesis to allow the resolution of cytotoxic stress and the restoration of proteostasis (Figure 5b, bottom-right). In eukaryotes, ISR is regulated by four distinct kinases, HRI (heme- regulated inhibitor), PKR (protein kinase R), PERK (already described above as UPR mediator) and GCN2 (general control non-depressible 2), whose activation can vary according to the type of stress (Taniuchi et al., 2016). Interestingly, a recent study proposed that prolonged activation of the PKR branch in Down syndrome (trisomy 21) models has detrimental effects on neurophysiological functions and long-term memory (Zhu et al., 2019). This represents evidence of the activation of translational stress response as a consequence of the presence of extra chromosomes.

When protein synthesis is suppressed following the abovementioned stress responses, non-translating RNAs together with pre-initiation factors, 40S ribosome subunits and other RNA-binding proteins (RBPs) can assemble and mediate **stress granule** condensation (Panas et al., 2016). Stress granule (SG) formation is, therefore, tightly linked to the activity of eIF2 and its phosphorylation on the alpha subunit represents a major trigger of the nucleation of SGs (Kedersha et al., 2002) (Figure 5b, bottom-right). Two other main components of SGs are the RNA-binding proteins G3BP1 and TIA1, which are recruited by the stalled pre-initiation complex, composed among others of the cap-binding system factor eIF4G (Panas et al., 2016). SGs play the important role of transient “storage” that protect specific mRNAs from degradation, following stress-mediated translation stalling (Decker & Parker, 2012). If cells cannot recover from their stress, mRNA fate is modulated by the dynamic relationship between SGs and the processing-bodies (P-bodies) that contain the mRNA decay machinery, including the exoribonuclease Xrn1 (Decker & Parker, 2012).

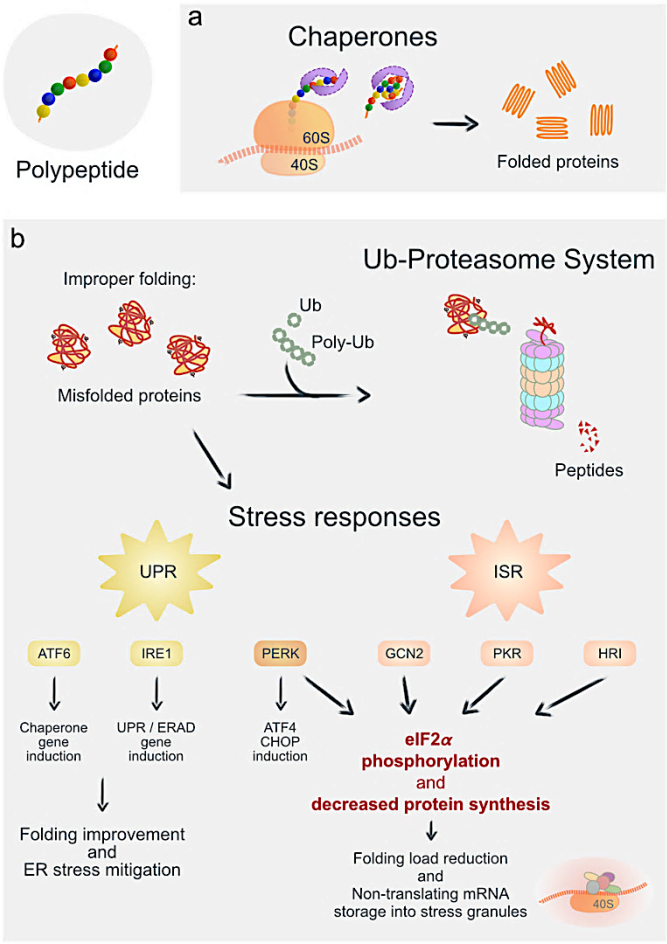

Figure 5: Protein quality control network.

Protein folding mediated by chaperones is at the core of quality control to prevent promiscuous interaction and aggregation of unfolded polypeptides (**a**). Misfolded proteins are ubiquitylated (Ub) first, and then degraded via the ubiquitin-proteasome system (UPS) (**b**, top). If the amount of misfolded proteins exceeds UPS capacity, ATF6, IRE1 and PERK activates the unfolded protein response (UPR), aiming at folding promotion and transient protein synthesis reduction (**b**, bottom-left). Unbalanced proteostasis also triggers the integrated stress response (ISR), mediated by eIF2α phosphorylation by four sensor kinases, to temporarily reduce protein synthesis. Here, non-translating mRNAs can be stored into stress granules (**b**, bottom-right).

4.1.3 Ubiquitin-proteasome system

In the context of protein folding failure and, more in general, disrupted protein homeostasis, the **ubiquitin-proteasome system** (UPS) plays a key role (Figure 5b, top). The quality control exerted by UPS is directed towards the proteasome-mediated clearance of misfolded and damaged proteins (Ding & Yin, 2008; Goldberg, 2003), as well as nascent polypeptides that are stuck when ribosomes stall on aberrant mRNAs (Brandman & Hegde, 2016; Joazeiro, 2019). Of course, proteasome-mediated degradation can also be physiologically functional with the purpose of cellular regulation. Ubiquitylation is the modification that allows the recognition of the substrate through the protein ubiquitin (Ub) (Figure 5b, top). There are either mono-ubiquitylations, often associated with non-degradative processes, or poly-ubiquitylations, where the first Ub can be extended to form

a Ub-chain (H. Meyer & Weihl, 2014). As general definition, UPS is in charge of the degradation of short-lived proteins and it is widely accepted that the degradation is specific, since target proteins must be ubiquitylated (Ding & Yin, 2008), mostly with a K48-linked poly-ubiquitin chain (Kirkin et al., 2009). Further specificity is conferred to the system by the ubiquitin-protein ligases, the enzymes known as E3-ligases, which are specific for their substrates and mediate Ub transfer to the target protein by recruiting an E2 Ub-conjugating enzyme which, in turn, has been loaded with Ub by an E1 Ub-activating enzyme (Goldberg, 2003). In the case of protein misfolding, aberrant polypeptides are recognised by heat-shock chaperones which, while promoting proper refolding, can interact with specific E3-ligases to foster ubiquitylation (Ding & Yin, 2008). The poly-Ub signal tags proteins to degradation through the 26S proteasome, a complex of proteins and enzymes that processes and digests target proteins via proteolysis (Figure 5b, top). As discussed at the beginning of the paragraph, UPS-mediated degradation has a crucial function in the clearance of misfolded proteins, both the cytoplasmic ones and the ER-luminal ones responsible for ER stress. In the latter case, improperly folded proteins in the ER can be retro-translocated into the cytosol to undergo proteasomal degradation with a process known as ER-associated degradation (ERAD) (Ding & Yin, 2008). ERAD pathway acquires further importance to maintain protein homeostasis in contexts where UPR induction is not the cell first choice (Walter & Ron, 2011).

4.1.4 Autophagic pathway

UPS is not the only machinery responsible for protein degradation in eukaryotic cells. The other main evolutionarily conserved system is based on the hydrolytic function of the lysosomes and depends on the **autophagic pathway** (Ding & Yin, 2008) (Figure 6). The principal cargoes of autophagy are composed of long-lived proteins, macromolecular complexes and insoluble aggregates, which are too hard to be degraded by the 26S proteasome (Kirkin et al., 2009). Since the autophagic pathway sequesters cytosolic portions, it is not considered as selective as the UPS, with some exceptions (discussed below) (Beese et al., 2020). In physiological conditions, the principal role of autophagy is to maintain the pool of amino acids during starvation, through the degradation of macromolecules. Thus, autophagy can be massively induced by drugs that simulate starvation, such as Rapamycin (natural compound) and Torin1 (synthetic compound) (Klionsky et al., 2021; Mizushima et al., 2010). They both interfere with mTOR, the kinase responsible for the inhibitory phosphorylation of TFEB, the transcription factor downstream of the pathway that integrates the signalling of nutrient and amino acid shortage (Settembre et al., 2011, 2012). When autophagy is triggered, a chain of events takes place, each of them characterised by different structures and different sets of regulatory proteins. The first step is the formation of the isolation membrane, also known as phagophore, which is mediated by the ULK1 protein kinase complex and the VPS34-Beclin1 PI3 kinase complex

that start membrane nucleation, and by ATG-complex, which monitors membrane elongation and expansion when it begins to enclose a portion of cytoplasm (Mizushima et al., 2010). In this phase, the cytosolic microtubule-associated protein light chain 3 (LC3-I) is incorporated into the isolation membrane after being lipidated (LC3-II) (Figure 6). Besides monitoring phagophore expansion and sealing into autophagosome, LC3-II role is to interact with autophagic receptors that bind various cargoes for selective autophagy (Lee & Lee, 2016). These initial steps of the autophagic pathway can be blocked using PI3K inhibitors, such as the chemical inhibitor of VPS34, SAR405 (Mizushima et al., 2010). After the formation of a double-membraned autophagosome, the outer membrane assembles an autolysosome by fusing with a lysosome. At this stage, the sequestered cargo starts to be degraded by the lysosomal hydrolases (Settembre et al., 2013), and the by-products of this step can be recycled as new sources of nutrients, which is the main purpose of bulk autophagy (Ding & Yin, 2008) (Figure 6). It is possible to interfere with the last step of the autophagic pathway with Bafilomycin A_1, which is known to inhibit the acidification of the lysosome and the fusion of autophagosomes with lysosomes (Mizushima et al., 2010). A certain degree of autophagy specificity is achieved when it aims to degrade misfolded protein and aggregates. In this case, targets to be degraded are ubiquitylated and interact with specific autophagic adaptors, such as p62 (also known as SQSTM1/sequestosome-1) (Ding & Yin, 2008). As a matter of fact, p62 presents a ubiquitin-associated (UBA) domain, as well as a LC3 interacting region (LIR), in addition to the other structural and functional domains (Lin et al., 2013). Through the former, p62 binds polyubiquitylated proteins and aggregates (with higher affinity for K63-Ub chains (W. J. Liu et al., 2016)) and, interacting with LC3 II on the phagophore, it drives the engulfment of these substrates into the forming autophagosomes (Lin et al., 2013). For all these reasons, p62 is widely used as a marker to monitor the autophagic flux. Its accumulation is observed when the lysosomal activity is inhibited, and therefore mirrors an accumulation of autophagosomes and early autophagic structures. On the other hand, if the degradation step is properly completed, p62 levels tend to decrease. LC3 II levels also follow the same trend (Klionsky et al., 2021; Mizushima et al., 2010). It is worth mentioning that autophagy and UPS are not mutually exclusive degradative pathways. First of all, p62 is also involved in UPS, as it can bind K48-Ub chains as well, even if with lower affinity (W. J. Liu et al., 2016). Secondly, upon defective proteostasis the relationship between autophagy and UPS become tighter, since proteotoxic stress and inhibition of proteasomal degradation further enhance autophagy (W. J. Liu et al., 2016).

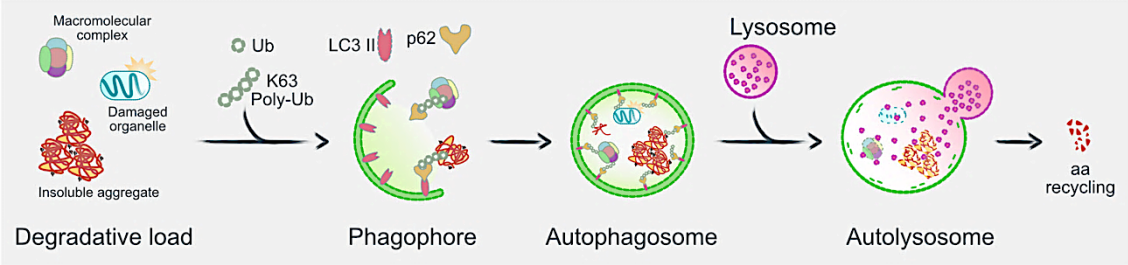

Figure 6: Autophagic pathway.
Macromolecular complexes, damaged organelles and insoluble aggregates of misfolded proteins are degraded through autophagy. First step is the formation of the phagophore, which incorporates the lipidated form of LC3 (LC3 II). This isolation membrane encloses the ubiquitylated degradative cargo, recognised by the autophagic receptor p62. After the formation of the closed autophagosome, its outer membrane fuses with the lysosome, an organelle containing acid hydrolases. This step proceeds with the degradation of the autophagosome content and the recycling of its by-products, including amino acids (aa).

Analysis of the autophagic cargo highlighted the presence of organelles and large protein complexes that are normally involved in protein homeostasis, but are themselves susceptible to homeostatic regulation (Kirkin et al., 2009). Recent studies in this direction have shown how mitochondria, but also proteasomes, ER and ribosomes can be targeted for selective degradation, in particular for **selective autophagy** (Beese et al., 2020). These are often stress-related programs and play significant roles in the clearance of damaged organelles/structures potentially dangerous for the cell. The selectivity of the process must be mediated by adaptors and autophagic receptors, but their identification is not always trivial. For instance, depolarised mitochondria or those that are no more functional are actively eliminated via autophagy (mitophagy) in a Ub-dependent manner (Le Guerroué et al., 2017). Similarly, it has been observed that proteasomes can be ubiquitylated upon starvation, a signal that allows their recognition by p62 and the following degradation by autophagy (proteaphagy). This mechanism seems to be conserved across plants, yeast and mammals (Beese et al., 2020). The endoplasmic reticulum (ER), as well, is an organelle strictly linked to protein dynamics. ER-phagy, the autophagic removal of ER portions, can occur both physiologically to re-shape ER volume depending on the cellular demand for protein, and as a stress-mediated quality control (Beese et al., 2020). In conditions where cells are not eligible for ERAD (see paragraph 4.1.3) to exert quality control of ER-stress, lysosomal degradation of ER portions represent a valid alternative (De Leonibus et al., 2019). Selective ER-phagy is mainly mediated by a family of receptors called FAM134 (FAM134A, FAM134B, FAM134C), which are ER membrane proteins and present a conserved LIR domain, crucial to mediate the engulfment into autophagosomes (Iavarone et al., 2022). The identification of different ER-phagy receptors with nonredundant functions and activated by different modifications suggests the high levels of specificity of this process (Di Lorenzo et al., 2022; Iavarone et al., 2022). As mentioned before, also the central hub

of protein synthesis, the ribosome, can be targeted for selective autophagy. Normal turnover of ribosomes is carried out by proteasomal degradation of the single excess ribosomal proteins, while the first evidence of entire 80S ribosome clearance has been described in yeast (Kraft et al., 2008). In this model organism, **ribophagy** seems to be mediated by an antagonistic interaction of the E3-ligase listerin (Ltn1) and the de-ubiquitylating enzyme Ubp3-Bre5. In particular, Ltn1, which is involved in the ribosome-associated quality control (RQC, see next paragraph), is shown to protect ribosomes from degradation, while their de-ubiquitylation by Ubp3-Bre5 target them for ribophagy (Kraft et al., 2008; Ossareh-Nazari et al., 2014). Recent evidence suggests that also human cells can induce ribophagy in particular stress conditions, but we still lack a thorough analysis of the triggering stimuli and the molecular mechanisms involved. So far, we know that both the small and the large subunits of ribosomes can undergo autophagy-mediated selective degradation, even if the responsible pathways are not the same (An & Harper, 2018). VPS34-Beclin1 complex is involved in small and large subunit clearance, but only the large subunit seems to be degraded also in an ATG5-dependent manner (An & Harper, 2018). Furthermore, whether this mechanism is mediated by the NUFIP1 receptor, as little evidence suggests, is still controversial (Beese et al., 2020). Since a trigger mechanism for selective ribophagy has not been identified yet, there are several theories about the engulfment of ribosomes in autophagic structures (An & Harper, 2020). In the first place, cytosolic ribosomes can end up in autolysosomes randomly during the sequestration of cytosolic portions in bulk autophagy, for example upon starvation. Secondly, due to the high density of ribosomes on ER, ribophagy can occur as a bystander flux during ER-phagy (An & Harper, 2020). Another hypothesis takes into account the overall inventory of ribosomes in response to nutrient stress, suggesting that ribophagy *per se* has a minor role in the production of amino acids, compared to other degradative and proteome remodelling mechanisms (An et al., 2020). Nevertheless, the previously mentioned evidence of a selective mechanism that induces lysosome-mediated removal of ribosomes, upon specific stress, triggers further studies in this fascinating field.

A limitation in the field of autophagy is the lack of a reliable method to monitor cargo degradation. Nowadays, many techniques are employed for this purpose (Klionsky et al., 2021), but it is worth mentioning a compelling recent approach that takes advantage of the fluorescent coral protein **Keima** (Figure 7). The main advantage is that Keima is not susceptible to hydrolases, and therefore it is stable in lysosomes, unlike other proteins that are degraded. Keima can be fused with target proteins, such as cytosolic (An & Harper, 2018), ER (Di Lorenzo et al., 2022), mitochondrial (Sun et al., 2017), or ribosomal proteins (An & Harper, 2018) and it allows to follow their fate in the autophagic structures. In particular, if fusion protein ends up in autolysosomes, target protein is cleaved and degraded, while Keima alone is stable and can be detected by Western Blot with an anti-

Keima antibody, at 25KDa (increasing processed-Keima band corresponds to the delivery of target protein to lysosomal degradation) (Klionsky et al., 2021) (Figure 7). Keima also has another advantage: its pH-sensitive dual-excitation. In neutral pH (cytosol, phagophore and autophagosomes), Keima excitation peak is at 440nm, while at acidic pH (autolysosomes and lysosomes) excitation shifts at 550nm. Therefore, with live-cell imaging it is possible to analyse the accumulation of red Keima puncta as a proxy of lysosomal degradation of the target protein (An & Harper, 2018) (Figure 7). An interesting application of this reporter is the comparison of the autophagic degradation of organelle-specific protein (namely the respective processed-Keima signal) with the autophagic degradation of a cytosolic protein, such as LDHB, to assess the degree of selectivity of an organelle degradation, compared to aspecific bulk autophagy (which randomly sequesters cytosolic portions with cytosolic proteins) (Klionsky et al., 2021).

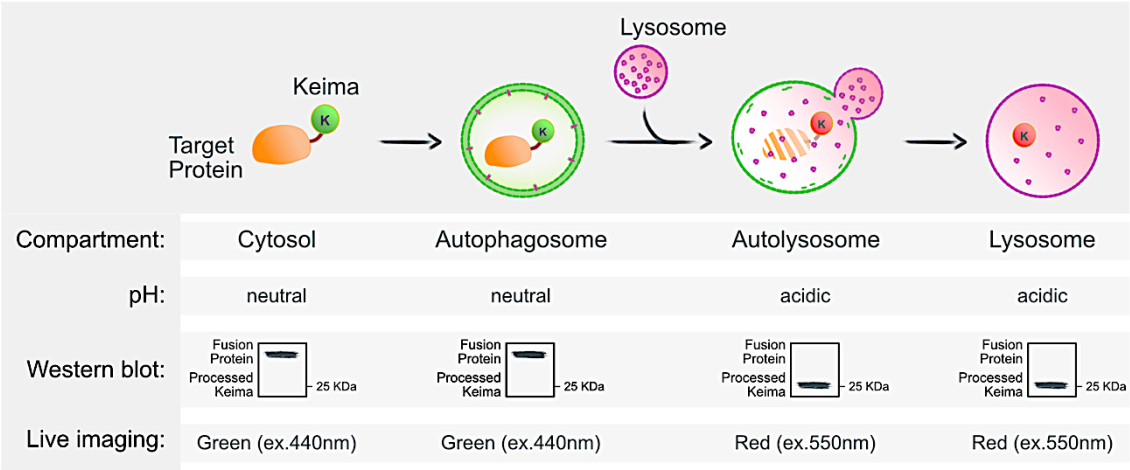

Figure 7: Keima reporter.

The fluorescent protein Keima can be fused to a target protein to follow the degradation of the latter via autophagy. Keima is stable to lysosomal hydrolases and can be detected at 25KDa (via Western blot) when the target protein is cleaved and degraded in autolysosomes/lysosomes. Keima has also a dual excitation depending on the pH: in compartments with neutral pH the excitation peak is at 440nm, while in acidic pH the excitation shifts at 550nm.

4.1.5 Players in the eukaryotic ribosome-associated quality control

Proteome quality control represents a demanding, but necessary, challenge for the cell. It is crucial to develop different mechanisms able to recognise, target and solve problems that can occur at various levels and in many compartments of the cell (Shao & Hegde, 2016). Of course, surveillance cannot be directed just towards proteins, it should address as well the other factors involved in proteostasis, primarily mRNAs and ribosomes (Lykke-Andersen & Bennett, 2014). Since in the previous paragraphs I dealt with mechanisms that orchestrate the quality control of misfolded and aggregated proteins, in this section I will focus on the players that act during the ribosome-associated quality control.

Ribosome-associated quality control (RQC) is mainly triggered by ribosome stalling during protein synthesis (Figure 8, top). Translation normally requires an initiation step, followed by an elongation step along the coding region and a termination step, which is coupled with the release of newly synthesised polypeptide and ribosome recycling (Schuller & Green, 2018). During the elongation step several problems may occur, which result in the stalling of ribosomes before reaching the mRNA stop codon. This can happen in limiting conditions, such as tRNA insufficiency or damaged mRNAs and tRNAs or defective ribosome subunit biogenesis (Schuller & Green, 2018). Instead, transcript truncation within the coding region or mRNA secondary structures that impede ribosome travelling can physically interrupt translation. These types of translation stalling are relatively easy to recognise. Conversely, other scenarios are less "black-and-white" and are more difficult to be discriminated. The presence of a premature polyadenylation (poly(A)) in the open reading frame (ORF), for example, generates a non-stop mRNA. Here, the ribosome doesn't stop necessarily, but continues to translate the poly(A) into a poly-lysine sequence (AAA encodes for lysine residue), eventually slowing down (Chandrasekaran et al., 2019; Joazeiro, 2019). Translation slowdown on polysomes is likely to cause **ribosome collisions** between properly-trailing ribosomes and stalled ones (Collart & Weiss, 2019) (Figure 8, top). Conditions of proteotoxic stress or impairment of chaperone-mediated co-translational folding are known to slow down global protein synthesis and induce pausing of ribosomes at the beginning of the elongation step. This highlights, once more, the central role of the ribosome in tuning translation, considering the availability of chaperones and the global protein homeostasis (B. Liu et al., 2013). Moreover, mounting evidence suggests that widespread ribosome pausing can occur to help co-translational protein folding (Zhao et al., 2019), even if this stratagem can be risky, as it possibly ends in collision events (Collart & Weiss, 2019). Importantly, ribosome stalling and collisions don't go unnoticed and cells respond triggering protein and mRNA quality control pathways. When collisions happen in large-scale and overwhelm quality control, cells can activate a broader stress response, the GCN2-mediated integrated stress response (ISR) (see paragraph 4.1.2), promoting cell survival, or, alternatively, JNK-mediated apoptosis (Wu et al., 2020). Basal collision levels, instead, can initiate RQC that will degrade the truncated nascent polypeptide, drive the floating mRNA decay and process 80S stalled ribosomes (Joazeiro, 2019).

Recently, EDF1 (the endothelial differentiation-related factor 1) has been identified as a general sensor for collided ribosomes (Sinha et al., 2020). In particular, it recognises collisions on transcripts where the density of ribosomes is excessive and inhibits translation initiation to temporarily and locally reduce ribosome loading (Juszkiewicz, Slodkowicz, et al., 2020). Indeed, inter-ribosome distance and translation speed are two important factors in defining collision probability (Juszkiewicz et al., 2018). If collision persists, the induction of downstream events of RQC is committed to the **E3-ligase ZNF598** (Sitron & Brandman,

2020). ZNF598 recognises the interface between the two collided ribosomes (*i.e.* disome), which adopt a rotated conformation due to the impact, where the two 40S small subunits are in contact (Juszkiewicz et al., 2018). This interface generated by the collided ribosome and the stalled one presents the sites for ZNF598 ubiquitylation (Juszkiewicz et al., 2018), and this modification is required for the initiation of RQC (Juszkiewicz & Hegde, 2017) (Figure 8a). The interface between the two 40S ribosomal subunits is stabilised by the ribosome-associated protein RACK1 which, therefore, facilitates ZNF598 ubiquitylation of 40S proteins. These regulatory ubiquitylations are believed to function as a scaffold for downstream factors that have roles in subsequent ribosome splitting, nascent polypeptide degradation and mRNA decay (Sundaramoorthy et al., 2017). Ribosome splitting is the next necessary step to proceed with RQC (Figure 8b). The separation of stalled ribosome subunits is carried out by other factors compared to those of the splitting during canonical translation termination. The most evident difference is that the nascent -stalled- polypeptide is not cleaved and remains attached to the 60S subunit, an intermediate structure that needs further processing (Sitron & Brandman, 2020).

Aberrant nascent polypeptide degradation is fundamental to re-establish proper translation and homeostasis after the recognition of ribosome stalling. First of all, the atypical structure composed of the 60S subunit and the stuck polypeptide chain should be resolved and the latter needs to be extracted from the ribosome, to be finally degraded (Brandman & Hegde, 2016). After 40S splitting, the inter-subunit interface on the 60S and the peptidyl-tRNA are exposed and allow the binding of RQC components (Brandman & Hegde, 2016). A major role at this point is played by the ubiquitin ligase listerin (Ltn1), which adds a poly-Ub chain to the emerging nascent protein, therefore recruiting the extraction complex (Figure 8d). Ltn1 is highly specialised in the recognition of the 60S-nascent chain complex and this increases the selectivity of its ubiquitylation (Shao et al., 2013). Furthermore, since steric hindrance prevents the association of Ltn1 to 60S and 40S simultaneously, Ltn1 is specifically active to resolve stalled 60S-nascent chain structures, while it cannot interfere with polypeptides on properly translating ribosomes (Lyumkis et al., 2014). After the extraction, RQC factors and undamaged 60S subunits are recycled, while the nascent polypeptide is degraded via 26S proteasome (Joazeiro, 2019) (Figure 8d). The importance of a properly functioning RQC is highlighted by the fact that failure of this quality control leads to proteotoxicity (Choe et al., 2016; Joazeiro, 2019).

Stalled ribosomes also coordinate the fate of the floating mRNA, since they initiate mRNA decay concurrently with RQC-mediated degradation of stalled nascent polypeptide (Simms et al., 2017). Specifically, mRNA degradation is performed by the **no-go decay** (NGD) surveillance pathway, through the XRN1-mediated exonucleolytic cleavage (Figure 8c). In yeast, this canonical branch of NGD is also supported by a secondary one, mediated by the endonuclease Cue2 (homologue of human N4BP2) (D'Orazio et al., 2019). This synergistic

contribution of two pathways highlights the importance of recognizing and promptly degrading error-prone mRNAs, to avoid the re-translation of aberrant transcripts. Indeed, if NGD is compromised and collisions are not resolved, deleterious +1 frameshift events can occur with high frequencies (Simms et al., 2019).

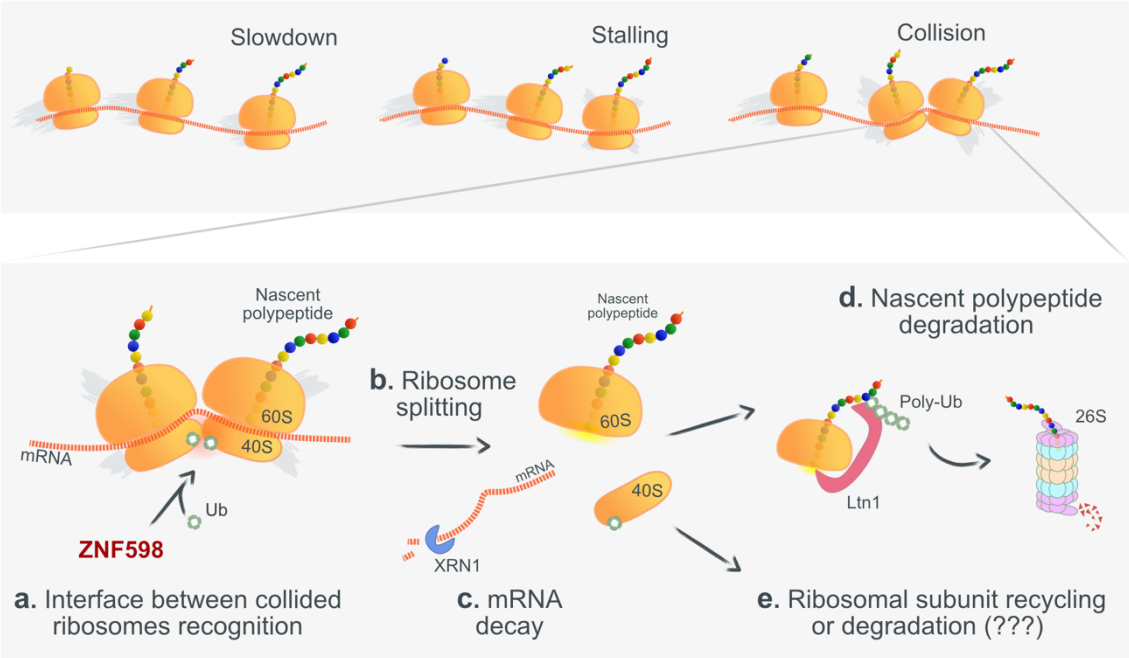

Figure 8: Ribosome-associated quality control (RQC).

RQC is triggered by collision between a stalled ribosome and a trailing one, as a consequence of translation slowdown (top). Collision persistence is sensed by ZNF598, an E3-ligase that ubiquitylates the interface between the collided 40S subunits, driving the subsequent events (**a**). Ribosome splitting separates the two ribosomal subunits and releases the mRNA from the stalled complex (**b**). Floating mRNA is then degraded by the no-go-decay surveillance pathway, mediated by the exonuclease XRN1 (**c**). In the meanwhile, the stalled nascent polypeptide is ubiquitylated by listerin (Ltn1) and extracted from the 60S subunit, in order to be degraded via the 26S proteasome (**d**). Undamaged ribosomal subunits are recycled, but emerging evidence suggests that specific regulatory ubiquitylations can be responsible for their degradation (**e**).

While nascent polypeptide and stalled mRNA fates have been extensively characterised, what happens to ribosomes, in particular the 40S subunits, involved in stalling and collisions is not yet crystal clear. Bennett's group showed that ribosomal subunits are subjected to specific regulatory ubiquitylations (RRub) upon the induction of specific stresses, in the first place UPR (see paragraph 4.1.2) (Higgins et al., 2015). RRubs on 40S subunits, for example, can prevent the assembly of pre-initiation complexes, hence downregulating protein synthesis, besides their best-known role of mediating the downstream RQC components nucleation (Higgins et al., 2015). More recently, few de-ubiquitylating enzymes (Dubs) - involved in the removal of Ub from 40S - have been identified: OTUD3 (ovarian tumour family) and USP21 (ubiquitin-specific peptidase family) (Garshott et al., 2020), but also G3BP1-Family-USP10 Dub complex (C. Meyer et al., 2020). These findings indicate that RRubs are reversible and suggest their dynamic role in shaping translational quality

control (Figure 8e). The growing interest in dissecting RRub roles and codes led to the recognition of a distinct branch of the ribosome-associated surveillance pathway. This has lots in common with canonical RQC, but it controls translation initiation and mediates RRubs that ultimately lead to the degradation of 40S subunits of ribosomes stalled in deficient translation initiation (Garshott et al., 2021). Altogether, these clues show how important and fine-tuned is the surveillance of translation and the control of its central hub -the ribosome- at every step, in order to maintain cell proteostasis.

4.2 Impact of aneuploidy on cell proteostasis

As already mentioned, the presence of extra chromosome(s) or a chromosome number that diverge from the euploid one inevitably has a profound impact on cell proteostasis (Oromendia & Amon, 2014). As a matter of fact, the aneuploid state confers high levels of proteotoxic stress, exacerbated by deregulated stoichiometry of complex subunits (Stingele et al., 2012), impaired chaperone-mediated folding (Donnelly et al., 2014) and eventually lysosomal stress (Santaguida et al., 2015) (Figure 9).

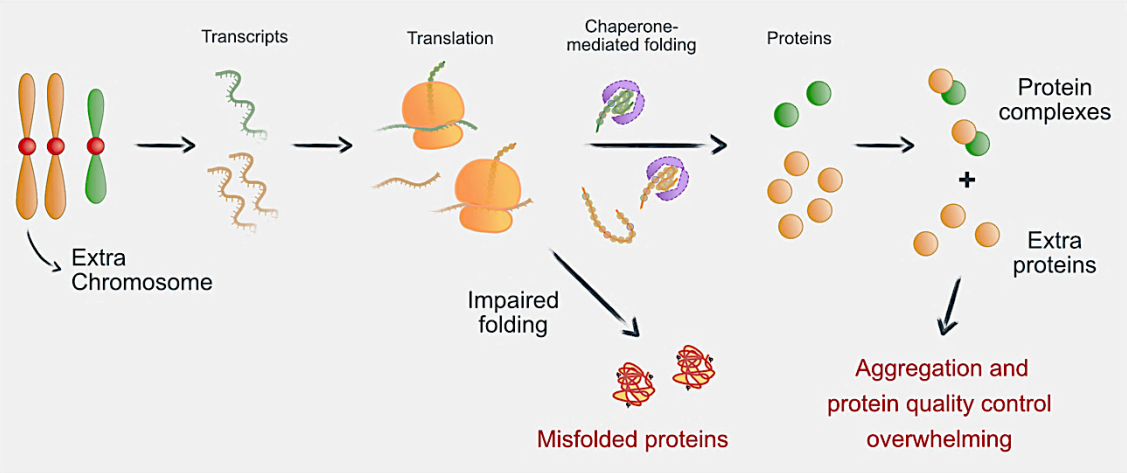

Figure 9: Impact of aneuploidy on cell proteostasis.
The presence of extra chromosome(s) is mirrored by increased transcription and translation demand. Chaperone-mediated folding is the first quality control that prevents the accumulation of misfolded proteins, but in aneuploid cells it is impaired and limiting, due to the increased folding request (top). This results in the accumulation of unfolded and misfolded proteins in the cell cytoplasm (bottom). Furthermore, the translation of extra genetic material causes the alteration of protein complex subunits stoichiometry (top-right), which exacerbates the aggregation of extra proteins. The toxicity derived from these aberrant structures cannot be efficiently counteracted by quality control and degradation pathways, since they are overwhelmed by increased burden (bottom-right).

4.2.1 Imbalanced protein composition and deregulated stoichiometry of protein complex subunits in aneuploid cells

First evidence of proteotoxic stress in aneuploid controlled model systems was found in **yeast** (Torres et al., 2007). Aneuploid yeast strains harbouring an extra copy of a single chromosome, in fact, are prone to endogenous protein aggregation (Oromendia et al.,

2012). Similarly, aneuploid yeast cells with random chromosome gains and losses, generated through faulty mitosis and meiosis, show similar phenotypes (Oromendia et al., 2012), suggesting that increased aggregate burden is karyotype-independent. It is also demonstrated that a considerable part of proteins encoded by genes on extra chromosome(s) is attenuated by post-translational mechanisms (Dephoure et al., 2014). This dosage-compensation is of particular interest to subunits of macromolecular complexes, which also represent the vast majority of the aggregate-prone proteins in aneuploid cells (Brennan et al., 2019). Together, these works indicate that the uncoordinated production of protein complex subunits and their altered stoichiometry is a prime cause of proteotoxic stress in aneuploid cells (Figure 9). Besides degradation, aggregation can be a tool to lower the levels of excess subunits of protein complexes, serving as an alternative mechanism for dosage-compensation (Brennan et al., 2019), although risky for the cytotoxicity of aggregates. Recently, a study in yeast showed that strains with specific karyotypes and particular genetic backgrounds are more predisposed to tolerate proteotoxic stress and its derivatives (Larrimore et al., 2020). This could represent the first step to shed light on the so-called “paradox of aneuploidy”, whereby aneuploidy at the same time leads to detrimental consequences, but it is also a hallmark of cancer, a disease characterised by uncontrolled proliferation (Weaver & Cleveland, 2008). Importantly, abundance of mRNAs and proteins do not scale linearly with ploidy in budding yeast (Yahya et al., 2022), implying, again, some type of compensation.

Drosophila larval epithelium primordia (wing disc or eye primordia) are widely used as model systems to address aneuploidy-associated phenotypes. Mechanisms of dosage compensation have been identified in these models as well, where chromosome-wide gene dosage imbalances have detrimental effects and drive tumorigenic behaviour of highly aneuploid cells (Clemente-Ruiz et al., 2016). Another important consequence of aneuploidy recently highlighted in *Drosophila* model is the alteration of ribosomal protein amount. Since ribosomal protein genes are located on every chromosome and aneuploidy alters the number of chromosomes, it is straightforward that ribosomal protein dosage is compromised (Ji et al., 2021). Interestingly, it is also suggested that this feature of aneuploid cells is responsible for a cell competition mechanism with neighbouring euploid cells, which eventually results in the elimination of the aneuploid ones (Ji et al., 2021). The loser status in cell competition, indeed, is driven by impaired proteostasis, ribosome mutations and proteotoxic stress (Baumgartner et al., 2021). Contextually, CIN *Drosophila* model generated through the depletion of SAC genes, which causes the delamination of highly aneuploid cells from the wing primordium epithelium, shows high levels of proteotoxic stress (Joy et al., 2021). In particular, proteotoxic aggregates, caused by gene dosage imbalances, are associated with polyubiquitin, indicating that in CIN contexts both UPS and autophagy work near saturation (Joy et al., 2021).

The cellular models to study aneuploidy in **human** system can be aneuploid lines with chromosome gains mainly generated from hTERT RPE-1 and HCT-116 cells, which derive from retinal pigmental epithelium and colorectal cancer, respectively. First study that addressed transcriptome and proteome homeostasis revealed that, while transcript levels mirror the chromosome number changes, proteome behaves differently (Stingele et al., 2012). Notably, in a karyotype-independent manner, the abundance of protein complex subunits and protein kinases tends to be regulated to resemble the euploid one (Stingele et al., 2012). Recently, also the impact of monosomies on cell transcriptome and proteome has been investigated (Chunduri et al., 2022). In particular, monosomic lines adjust transcriptionally and post-transcriptionally the expression levels of genes encoded on monosomes, to mitigate the effects of reduced gene copy numbers (Chunduri et al., 2021). Importantly, among the protein families commonly altered in all the monosomic lines, large and small ribosomal subunit proteins were particularly affected by downregulation (Chunduri et al., 2021). This highlights their haploinsufficiency, which is in line with what is observed in yeast and *Drosophila*. The downregulation of ribosomal proteins and, consequently, the reduction in translation occur also in human tetraploid cells that underwent whole-genome duplication (Yahya et al., 2022). Global proteome adjustments imply their usefulness to enhance cell survival to otherwise detrimental events, such as whole-genome duplication.

Of particular interest for human health is the investigation of consequences of aneuploidy in **Down syndrome** (DS) models. DS mice, but also human CH21 trisomic iPS and post-mortem brain cells from DS individuals present reduced translation rates and lower global protein synthesis (Zhu et al., 2019). The activation of the integrated stress response (ISR) and phosphorylation of eIF2α, which point out defective proteostasis (see paragraph 4.1.2), contribute to cognitive defects associated with DS (Zhu et al., 2019). This confirms that extra copy of a single chromosome, even the smallest one, can cause deleterious effects to the organism. Altered proteostasis is an aneuploidy-driven consequence observed also in the other two vital autosomal trisomies in humans, trisomy 13 and trisomy 18 (see paragraph 2.1) (Hwang et al., 2021). Analysis of the transcriptome and proteome of DS patient-derived fibroblasts, showed an increase quite proportional to copy number, with the exception of macromolecular complex subunits (Hwang et al., 2021). As demonstrated also in yeast and other mammalian aneuploid models (Brennan et al., 2019; Stingele et al., 2012), the expression of subunits of protein complexes is attenuated post-transcriptionally to preserve the cell from further proteotoxic damages (Hwang et al., 2021).

Given the universality of the aneuploidy-driven **disrupted stoichiometry** of protein complex subunits (Figure 9), it is interesting to understand how aneuploid cells can tolerate these issues, most of all in the context of aneuploid cancers. An important role in alleviating proteotoxic stress is played by the proteasome (see paragraph 4.1.3) (Padovani et al.,

2022) and by the yeast de-ubiquitinase Ubp3 (Dodgson et al., 2016). Another enzyme involved in ubiquitylation and important for the clearance of orphan subunits of multiprotein complexes is human UBE2O. This E2 enzyme can also act without an E3-ligase for the recognition and ubiquitylation of cytosolic unassembled subunits, including orphan ribosomal proteins (Yanagitani et al., 2017). Interestingly, this enzyme is amplified in several aneuploid human cancers, suggesting its role in proteotoxicity tolerance (Yanagitani et al., 2017). The upregulation of these and other key mechanisms that help maintain proteostasis, indeed, is crucial for aneuploid cancer cell survival (Brancolini & Iuliano, 2020) and, therefore, these processes represent attractive targets for cancer therapies.

4.2.2 Chaperone-mediated protein folding is impaired in aneuploid cells

Under physiological conditions, quality control mechanisms prevent cellular toxicity by reducing aggregation and promiscuous interactions among proteins (see paragraph 4.1). Conversely, the aneuploid state is known to limit and impair these processes, causing proteostasis alteration and cellular overcrowding (Choe et al., 2016; Padovani et al., 2022) (Figure 9). The observation that proliferation in aneuploid yeast strains is negatively impacted by the interference with protein folding (Torres et al., 2007) suggests that this process is indeed essential for aneuploid cell viability. As a matter of fact, the inhibitor of Hsp90 chaperone 17-AAG has been identified as proteotoxic stress-inducing compound able to antagonise aneuploid cell proliferation, as well as to foster apoptosis of trisomic lines (Tang et al., 2011). Importantly, also highly aneuploid human cancer lines are more sensitive to this compound, compared to pseudo-diploid ones (Tang et al., 2011), indicating that antiproliferative compounds that inhibit protein folding can be promising in therapy. Chromosomal instability in *Drosophila* model, as well, causes increased sensitivity to folding stress (Khan et al., 2018), in line with what was previously observed. A deeper analysis of the molecular mechanisms underlying impaired folding in human cells showed that aneuploidy compromises the HSF1-mediated heat shock response (Donnelly et al., 2014). This, in turn, impairs Hsp90 chaperone folding activity, therefore impacting numerous clients with crucial roles in maintaining cellular fitness (Donnelly et al., 2014). Thus, the **impaired protein folding machinery** in aneuploid cells is directly involved in proteostasis disruption, since cells rely on chaperone functions to fold extra proteins and to maintain soluble the ones that lack a binding partner (Figure 9). Importantly, the partial restoring of HSF1 activities can alleviate folding defects and proteotoxic stress (Donnelly et al., 2014). HSF1 has been found to have a pivotal role also for restoring folding in conditions of disrupted ribosome biogenesis and ribosomal subunit aggregation, ultimately ameliorating aneuploid cell growth (Tye et al., 2019). As already mentioned, this factor is one of the most commonly overexpressed in aneuploid cancer cells, probably conferring an advantage to convive with proteotoxic stress (Brancolini & Iuliano, 2020).

4.2.3 Aneuploidy saturates autophagic degradation and leads to lysosomal stress

Protein folding stress and impaired quality control pathways cause aneuploid cells to accumulate misfolded protein aggregates and excessive degradative load (Santaguida & Amon, 2015a) (Figure 10, left). In particular, the persistence of LC3-II signal in cytoplasm of cycling aneuploid cells indicates that autophagic structures accumulate after a few cell cycles from chromosome mis-segregation (Santaguida et al., 2015; Stingele et al., 2013). The colocalization of the poly-ubiquitin receptor p62 with LC3-II represents further evidence of the increased autophagic cargo within aneuploid cells (Santaguida et al., 2015). Interestingly, while the formation of autophagosomes and the consequent fusion with lysosomes are carried out correctly, the degradation of their content is less efficient, highlighting an overloading of lysosomes (Santaguida et al., 2015) (Figure 10). Importantly, lysosomal function *per se* is not impaired, but the degradation machinery cannot keep up with the increased cargo present in aneuploid cell cytoplasm. The **autophagic pathway saturation** and resulting **lysosomal stress** trigger a cellular response mediated by TFEB (Santaguida et al., 2015; Santaguida & Amon, 2015a), which translocates into the nucleus and ultimately induces the expression of its target genes involved in autophagy and lysosomal degradation (Settembre et al., 2011) (Figure 10, right). Since proteotoxic by-products are continuously produced by aneuploid cells, the TFEB-mediated response is not sufficient to restore the efficiency of lysosome-mediated degradation, thus leaving cells in a state of altered proteostasis. On the other hand, several aneuploid cancer cells do not present the same autophagic overwhelming, suggesting that they might have found ways to enhance lysosomal clearance, increasing their fitness (Santaguida et al., 2015).

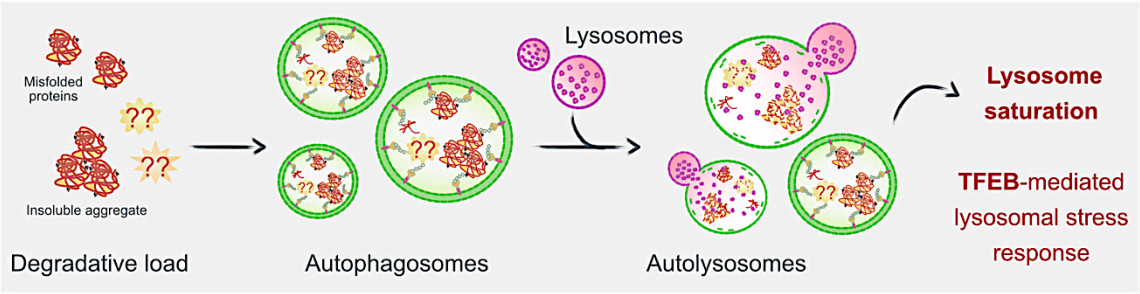

Figure 10: Aneuploidy-driven autophagy saturation and lysosomal stress.
The increased proteotoxic load in aneuploid cells challenges the capacity of the autophagic degradation pathway. In particular, lysosomes become limiting and the degradation step reaches saturation. This, in turn, triggers a lysosomal stress response mediated by the transcription factor TFEB, to stimulate further expression of autophagic genes.

Aim of the project

The presence of extra chromosome(s) or the loss of chromosome(s) have a profound impact on cell physiology, from every point of view. Over the past years, the aneuploidy field has made many efforts - with success - to dissect the consequences of chromosome mis-segregation and the stresses associated with the aneuploid state. Importantly, aneuploidy is also considered a hallmark of cancer, but it is still not clear how transformed cells overcome or are able to cope with the mentioned aneuploidy-associated stresses.

Among the long-term effects of an unbalanced karyotype, the increasing proteotoxic stress is particularly interesting, since the disruption of protein homeostasis represents a major challenge for cell survival. Previous works highlighted that multiple protein quality control pathways are impaired in aneuploid cells (see paragraph 4.2). Yet, so far, the field lacks direct evidence of the accumulation of misfolded and unfolded proteins in mammals, as well as proof of the onset of associated responses. In particular, the accumulation of autophagic structures within aneuploid cells and the saturation of the degradation step suggest that lysosomes cannot keep up with the excessive amount of degradative load produced. However, it is still not clear which structures are encapsulated within autophagosomes, the reason for why those cargoes are encapsulated and why they are hard to degrade. Moreover, given the detrimental impact of aneuploidy on cell proteome, the hypothesis that, in this condition, organelles involved in proteostasis become partially or completely dysfunctional still remains to be addressed.

Considering these open questions, my project has the goal to shed light on the mechanisms activated by aneuploid cells in response to the onset of proteotoxic stress. In particular, the project aims at dissecting the molecular basis of the cellular events and pathways involved in buffering aneuploidy-driven proteome imbalances. Given the plethora of processes responsible for the organization and maintenance of proteostasis, this work would provide crucial insights into the events in charge of dealing with proteotoxicity. A thorough analysis of what happens in an aneuploid background, irrespectively of the karyotype, can highlight common features relevant for basic cell biology, but also crucial for cancer biology. Importantly, the identification of novel roles and molecular players that manage proteotoxicity has the potential to suggest specific targets for cancer therapy, in contexts in which protein translation machinery can be interfered with to disturb cell proliferation.

Materials and Methods

1. Cell culture conditions

hTERT RPE-1 cells (RPE1, Prof. Santaguida group internal stock), including those stably expressing RPS3-Keima, RPL28-Keima, LDHB-Keima, RAMP4-Keima, MT-Keima or RPS3-RFP-GFP (all generated in house, see Materials and Methods paragraph 3) and those transiently transfected for MAD2 or BUB1 siRNA-mediated knock-down (see Materials and Methods paragraph 5), were cultured in Dulbecco's modified Eagle's High Glucose medium (DME/HIGH with stable L-Glutamine and Sodium Pyruvate; Cat# ECM0103L, EuroClone) supplied with 10% FBS (South America origin) and 100U/mL Penicillin/Streptomycin.

HCT-116 cells (HCT116, IEO internal stock), including those stably expressing RPS3-Keima, RPL28-Keima (kindly provided by Prof. Wade Harper) or LDHB-Keima, RAMP4-Keima or MT-Keima (all generated in house, see Materials and Methods paragraph 3) and those transiently transfected for the over-expression of HSF1ca, HA-Hsp90 or GFP-ZNF598 (see Materials and Methods paragraph 4) or for MAD2, BUB1, p62 or ZNF598 siRNA-mediated knock-down (see Materials and Methods paragraph 5), were cultured in Mc Coy's 5A medium (Cat# M8403, Sigma-Aldrich) supplied with 10% FBS (South America origin), 2mM L-Glutamine and 100U/mL Penicillin/Streptomycin.

HEK-293T (Human Embryonic Kidney) cells (IEO internal stock) were cultured in Dulbecco's modified Eagle's High Glucose medium (DME/HIGH with stable L-Glutamine and Sodium Pyruvate; Cat# ECM0103L, EuroClone) supplied with 10% FBS (South America origin) and 100U/mL Penicillin/Streptomycin.

All cell lines were previously tested free of mycoplasma contamination using Myco Alert kit (Lonza) according to manufacturer's instructions, followed by PCR confirmation with previously reported oligonucleotides of different mycoplasma species (Uphoff & Drexler, 2002). Cells were cultured for no more than 20 passages after new thawing. RPE1 and HCT116 cell passage was performed as follow: cells were washed with 1X PBS (Dulbecco's Phosphate-Buffered Saline without calcium and magnesium, Cat# TL1006-500ML, Microgem); then, cell detaching was obtained through trypsinization by adding 1X Trypsin-EDTA in PBS without phenol red, calcium and magnesium (Cat# ECB30529, Euroclone). HEK-293T cell passage was performed by detaching cells from the dish mechanically, after washing them with 1X PBS without calcium and magnesium. All cell lines were grown at 37°C with 5% CO_2 in a humidified incubator (Thermo Forma 3140 IR 2 Water Jacketed CO_2 Incubator, Cat. #3110, ThermoFisher Scientific).

2. Cell treatments

To induce random aneuploidy, cells were seeded in 10cm dishes or in six-well plates and pulsed with the Mps1 inhibitor reversine (500nM, Cat# 656820-32-5, Cayman Chemical) for 24 hours (see Figure 11 and ref. (Santaguida et al., 2010)); while to generate the relative controls (Ctrl) cells were pulsed with the vehicle dimethyl sulfoxide (DMSO) for 24 hours. Sample analysis were performed either immediately after the pulse ("24 hours" samples) or after 1 o 2 cell cycles ("48 hours" or "72 hours" samples, in these cases Mps1i/DMSO were washed-out), as reported in figure legends. To evaluate the effects of the increasing aneuploidy degree on the ribophagic phenotype or on the global protein synthesis rate, cells were treated with increasing concentrations of the Mps1 inhibitor reversine (125nM, 250nM or 500nM) as reported in figure legends.

To induce the aggregation of misfolded proteins, cells were treated with L-azetidine-2-carboxylic acid (AZC, 10mM, Cat# A0760, Sigma-Aldrich), as indicated in the corresponding figure legend.

To inhibit PERK kinase, cells were treated with increasing concentrations (0-0,05-0,1-0,5-1-5-10-50-100-500μM) of PERK inhibitor I (GSK2606414, Cat# 516535, Sigma-Aldrich) for 72 hours. Then, a cell viability and EC_{50} assay was performed as described below (see Materials and Methods paragraph 6).

To modulate autophagy, cells were treated either with Torin1 (250nM, Cat# 4247, Tocris), SAR405 (1μM, Cat# 16979, Cayman Chemical) or Bafilomycin A_1 (BafiloA_1, 100nM, Cat# B1793, Sigma-Aldrich), as indicated in figure legends.

To inhibit Hsp90 chaperone family, cells were treated either with Geldanamycin (Geld, 1μM, Cat# 1368, Tocris) or 17-allylamino-17-demethoxy-geldanamycin (17-AAG, 1μM, Cat# 1515, Tocris) as indicated in figure legends. Instead, to inhibit Hsp70 chaperone family, cells were treated with VER-155008 (VER, 50μM, Cat# SML0271, Sigma-Aldrich) as indicated in the corresponding figure legend.

To inhibit translation elongation, cells were treated with Cycloheximide (CHX, 10μg/mL, Cat# C4859, Sigma-Aldrich) as indicated in the corresponding figure legend.

To induce stress granules assembly, cells were treated with sodium arsenite ($NaAsO_2$, 500μM, Cat# S7400, Sigma-Aldrich) as indicated in the corresponding figure legend.

3. Stable cell line generation

The following lentiviral plasmids (kindly provided by the indicated laboratories, see Table 1) were used to generate stable cell lines derived by either RPE1 or HCT116 cell lines:

Construct	Vector name	Source	Bacterial growth strain	Bacterial resistance	Eukaryotic resistance
LDHB-Keima	pHAGE LDHB-mKEIMA	Prof. Wade Harper	Stbl3	Ampicillin	Puromycin
MT-Keima	pHAGE MT-mKEIMA	Prof. Wade Harper	Stbl3	Ampicillin	Puromycin
RAMP4-Keima	pDEST mKEIMA-RAMP4	Prof. Carmine Settembre	Stbl3	Ampicillin	Blasticidin
RPL28-Keima	pHAGE RPL28 mKEIMA	Prof. Wade Harper	Stbl3	Ampicillin	Puromycin
RPS3-Keima	pHAGE RPS3-mKEIMA	Prof. Wade Harper	Stbl3	Ampicillin	Puromycin
RPS3-RFP-GFP	pHAGE RSP3 RFP-GFP	Prof. Carmine Settembre	Stbl3	Ampicillin	Puromycin

Table 1: List of the plasmids used to generate stable cell lines.

3.1 Bacteria transformation and DNA extraction

To obtain a sufficient amount of each plasmid, competent Stbl3 *E. coli* cells were used for the heat shock transformation. Around 10ng of each plasmid were incubated into one aliquot of competent Stbl3 *E. coli* cells for 10 minutes on ice. The heat shock was given for 40 seconds at 42°C, and cells were then incubated on ice for 2 minutes. Lysogeny Broth (LB) culture media was then added to the competent cells and the culture was kept in agitation (300rpm) in a thermomixer at 37°C for 1 hour, to favour cell recovery. 150µL of liquid culture were plated onto a pre-warmed LB agar plate containing the specific antibiotic for bacterial resistance (see Table 1, for ampicillin: 100µg/mL) to allow overnight colony growth at 37°C. The day after, an over-day pre-inoculation of one individual picked colony was performed in 5mL of LB culture media with the specific antibiotic for bacterial resistance (see Table 1) and kept in agitation (300rpm) at 37°C. Then, the maxi-inoculation was performed mixing the 5mL-pre-inoculation with 300mL of LB culture media with the specific antibiotic for bacterial resistance (see Table 1) and kept in agitation (300rpm) overnight at 37°C. Bacterial cells were isolated from the culture media through centrifugation at 5000xg (6000rpm) for 20 minutes at 4°C. Plasmid DNA was extracted using NucleoBond Xtra Maxi kit (Cat# 740414.50, Macherey-Nagel) according to manufacturer's instructions. Plasmid DNA was quantified using NanoDrop 2000 Spectrophotometer (Cat# ND-2000, ThermoFisher Scientific).

3.2 Virus production and target cell infection

Plasmid DNA for each construct was independently used to transfect HEK-293T cells. Viral particles produced by HEK-293T containing the constructs were used to infect the target cells (either RPE1 or HCT116). The protocol I followed is detailed below:

Day 1: HEK-293T cells were plated in 10cm dishes at 20-25% confluence (two 10cm dishes per construct were considered).

Day 2: HEK-293T medium was changed (9mL/dish) 8 hours before transfection. Transfection was then performed preparing a mixture containing 10µg plasmid DNA, 3µg VSVG (lentiviral packaging plasmid, internal stock), 6µg pAX2G (lentiviral packaging plasmid, internal stock), $CaCl_2$ 2M and H_2O up to 500µL (reagents per dish). The DNA/$CaCl_2$ mixture was added dropwise in 500µL 2X HEPES-Buffered Saline (HBS) bubbling solution and incubated for 15 minutes at room temperature. Chloroquine was added to a final concentration of 20µM to each HEK-293T dish, to improve cell transfection. The DNA/$CaCl_2$/HBS mixture was then added to HEK-293T cells and the formation of evenly distributed small black particles was checked under the microscope. Cells were incubated overnight.

Day 3: transfected HEK-293T medium was changed with 5,5mL fresh medium per dish, to concentrate the produced viral particles. Target cells (either RPE1 or HCT116) were split to have 50% confluence on the day after.

Day 4: the medium containing the viral particles was collected from one of the two HEK-293T dishes transfected for each construct, filtered (0,45µm filter) and added to target cells, adding also polybrene to a final concentration of 8µg/mL to improve target cell infection. After 3 hours incubation, target media was replaced with fresh one to allow for a 2-hour recovery. Then the infection cycle was repeated for another 3 hours, using the medium from the second HEK-293T dish. At the end of this second infection cycle fresh media was added to the target cells.

Day 5: infected target cells (either RPE1 or HCT116) were split at different ratios and the antibiotic for eukaryotic resistance specific for each construct was added (see Table 1). In particular, for puromycin-resistant constructs puromycin (Puromycin Dihydrochloride, Cat# P8833, Sigma-Aldrich) was added to RPE1 to a final concentration of 10µg/mL, while for HCT116 a final concentration of 3µg/mL was used. For blasticidin-resistant constructs, instead, blasticidin (Blasticidin S, Cat# SC-495389, Santa Cruz Biotechnology) was added to a final concentration of 5µg/mL or 6µg/mL to RPE1 or HCT116, respectively.

Selection of cell lines expressing puromycin resistance lasted 5 days (media with antibiotic refreshed every other day), while selection of cells blasticidin resistant lasted around 8 days (media with antibiotic refreshed every other day).

Once the stable cell lines in which the constructs have been individually incorporated were obtained, cells were either used for further analysis (as indicated in the figure legends) or frozen in liquid nitrogen for future experiments.

4. Transient construct over-expression

The following constructs (either purchased from the indicated companies or kindly provided by the indicated laboratories, see Table 2) were used to transiently transfect HCT116 RPS3-Keima or HCT116 RPL28-Keima cell lines with Lipofectamine 3000:

Construct	Vector name	Source	Cat. #	Bacterial growth strain	Bacterial resistance
Empty pcDNA 3.1	pcDNA3.1	Prof. Zuzana Storchová	BZ474	DH5α	Ampicillin
HA-Hsp90	pcDNA3/HA-Hsp90	Addgene	22487	DH5α	Ampicillin
HSF1ca	pcDNA3.1/HSF1ca	Prof. Zuzana Storchová	BZ539	DH5α	Ampicillin
ZNF598	pcDNA4/TO/GFP-ZNF598	Addgene	141191	DH5α	Ampicillin

Table 2: List of the constructs used to transiently transfect HCT116 RPS3-Keima or HCT116 RPL28-Keima cell lines.

Sufficient amount of constructs was obtained through DH5α competent cell transformation, as previously described (see Materials and Methods paragraph 3.1). DNA was then extracted and quantified as previously described (see Materials and Methods paragraph 3.1).

To transiently transfect HCT116 RPS3-Keima or HCT116 RPL28-Keima cells, Lipofectamine 3000 transfection reagent (Cat# L3000015, Invitrogen) was used by optimizing the manufacturer's instructions. Briefly, cells were plated at 30-40% confluence in a six-well plate, in 2mL medium. 24 hours later, cells were transfected as follow (indicated quantities are for one well): 6µL Lipofectamine 3000 transfection reagent were diluted in 150µL Opti-MEM reduced serum medium (Cat# 31985070, Gibco) and 2µg HSF1ca (as previously reported (Donnelly et al., 2014)) or 2 µg HA-Hsp90 or 0,5µg ZNF598 (or the corresponding empty vectors) were diluted in 150µL Opti-MEM together with P3000 reagent (2µL/µg DNA); then, the DNA master mix was added to the diluted Lipofectamine 3000 mix and incubated for 10 minutes at room temperature. Afterwards 300µL of the mix containing the DNA-lipid complexes were added to the target cells to allow for their transfection. 8 hours later, medium was changed to avoid Lipofectamine toxicity. 500nM Mps1i (or DMSO) was added for 24 hours (or otherwise indicated in the figure legends) before sample collection (72h after transfection) to proceed with further analysis.

5. Transient knock-down through RNA interference

The following small interfering RNAs (siRNA) were used to transiently knock-down the indicated targets in HCT116 RPS3-Keima or HCT116 RPL28-Keima cell lines, upon transfection with Lipofectamine RNAiMAX:

Target	siRNA identifier	Source	Cat. #	Sequence
BUB1	BUB1 siRNA	(Johnson et al., 2004)	-	AUACCACAAUGACCCAAGA
MAD2	MAD2 siRNA	(Sigoillot et al., 2012)	-	GGAACAACUGAAAGAUUGG
Non-targeting	ON-TARGET Plus Non-targeting Pool	Dharmacon	D-001810-10	N/A
Non-targeting	Silencer Select Negative Control #1	Invitrogen	4390843	N/A
p62/SQSTM1	ON-TARGET Plus Human SQSTM1 siRNA SMARTpool	Dharmacon	L-010230-00-0010	GAACAGAUGGAGUCGGAUA GCAUUGAAGUUGAUAUCGA CCACAGGGCUGAAGGAAGC GGACCCAUCUGUCUUCAAA
ZNF598	Silencer Select against ZNF598	Invitrogen	s40509	GCAGCAAGAAGGUAGCACA

Table 3: List of the siRNA sequences used to transiently knock-down the indicated targets in HCT116 RPS3-Keima or HCT116 RPL28-Keima cell lines.

To transiently knock-down the targets of interest in HCT116 RPS3-Keima or HCT116 RPL28-Keima cells, Lipofectamine RNAiMAX transfection reagent (Cat# 13778150, Invitrogen) was used by optimizing the manufacturer's instructions. Briefly, cells were plated at 30% confluence in a six-well plate, in 2mL medium. 24 hours later, cells were transfected as follow (indicated quantities are for one well): 9µL Lipofectamine RNAiMAX transfection reagent were diluted in 150µL Opti-MEM reduced serum medium (Cat# 31985070, Gibco) and 3µL of MAD2 siRNA or BUB1 siRNA (20µM stock) or 3µL of p62 siRNA (20µM stock) or 3µL of ZNF598 siRNA (10µM stock) (or the corresponding non-targeting siRNA controls) were diluted in 150µL Opti-MEM; then, the diluted siRNA mix was added to the diluted Lipofectamine RNAiMAX mix and incubated for 15 minutes at room temperature. Afterwards, 250µL of the mix containing the siRNA-lipid complexes were added to the target cells to allow for their transfection. 8 hours later, medium was changed to avoid Lipofectamine toxicity. 500nM Mps1i (or DMSO) was added for 24 hours (or otherwise indicated in the figure legends) before sample collection (72h after transfection) to proceed with further analysis.

6. Cell viability and EC_{50} assay

To determine the amount of viable cells in culture in the presence of PERK inhibitor and to calculate its half maximal effective concentration (EC_{50}), the CellTiter-Glo Luminescent Cell Viability Assay (Cat# G7570, Promega) was used, following manufacturer's instructions. The assay is based on the quantitation of ATP in the cell culture, as an indicator of metabolically active cells (viable cells). An ATP-dependent luciferase reaction produces a luminescent signal proportional to the number of viable cells. In brief, $3*10^3$ RPE1 cells were plated in a 96-well plate (white flat bottom; Cat# 165306, ThermoFisher Scientific) in 50µL

of culture medium /well, each condition in triplicate. After cell attachment, either Mps1i or DMSO were added to the respective wells diluted in 50µL of medium (final working concentration 500nM). 24 hours later, Mps1i/DMSO were washed out and cells were cultured for 48 more hours. 100µL culture medium was then changed adding PERKi at increasing concentrations (see Materials and Methods paragraph 2).

After 72-hour incubation, the 96-well plate was equilibrated at room temperature and 100µL of CellTiter-Glo reagent was added to each well. Cell lysis was performed with 2 minutes shaking in the presence of the mixture and, after another 10-minute incubation, the luminescence signal was measured with a GloMax Discover microplate reader (Cat# GM300, Promega). The relative luminescence unit (RLU) was represented on the graph and EC_{50} values were calculated using GraphPad PRISM (version 9.3.1).

7. RNA extraction and quantitative Real-Time PCR

The expression levels of the mRNA of PERK target genes were calculated by quantitative real-time PCR technique.

RNA was extracted from cells using RNeasy Plus Mini Kit (Cat# 74136, QIAGEN), following manufacturer's instructions.

Then, 500ng of the extracted RNA were retro-transcribed in 20µL DEPC-treated water (Cat# AM9916, Invitrogen) using OneScript Plus cDNA Synthesis Kit (Cat# G236, abm), according to the manufacturer's protocol.

The reverse-transcribed cDNA was diluted to 6,25ng/µL and 2µL were used to perform quantitative real-time PCR. RT-qPCR reactions were carried out using Fast SYBR Green Master Mix (Cat# 4385617, ThermoFisher Scientific) as follow (indicated quantities are for one sample-gene reaction): 10µL of Fast SYBR Green Master Mix were mixed with 0,5µL of 10µM forward primer, 10µM reverse primer and 7µL of DEPC-treated water. Then, the 18µL-SYBR-primer mix was added to 2µL diluted cDNA, to a final 20µL mix volume per well. The following primers were used:

Gene	Forward primer	Reverse primer	Source
ATF3	CTCGGGGTGTCCATCACAAAAG	AGCTTCTCCGACTCTTTCTGC	Prof. Giuliana Pelicci Laboratory
CHOP/DDIT3	GGAAACAGAGTGGTCATTC	CTGCTTGAGCCGTTCATTCT	Prof. Giuliana Pelicci Laboratory
GAPDH	CAACTACATGGTTTACATGTTC	GCCAGTGGACTCCACGAC	Merk

Table 4: List of the primers used for quantitative Real-Time PCR.

Quantitative Real-Time PCR reactions were run on a CFX 96 Real-Time PCR system (Bio-Rad). mRNA relative expression levels were calculated with the $2^{-\Delta\Delta Ct}$ method and were shown on the graphs as fold changes: data normalization was performed on *GAPDH* housekeeping gene expression and then compared to the pseudo-diploid control samples.

8. Western blot analysis

8.1 Cell lysis and protein quantification

To detect proteins by Western blot, cells were washed in 1X PBS, scraped and lysed directly in the plate on ice with cold RIPA Buffer (Cat# 9806, Cell Signaling Technology) diluted in ddH_2O and supplemented with Protease Inhibitor Cocktail Ser III (Cat# 539134, Millipore) and phosphatase inhibitor cocktail (PhosSTOP, Cat# 4906837001, Roche). Cell lysates were kept on ice for 10 minutes and centrifuged for 15 minutes at 13000rpm at 4°C to precipitate and discard cellular debris. Proteins were quantified with a Bradford method-based colorimetric assay, using Bio-Rad Protein Assay Dye Reagent Concentrate (Cat# 5000006, Bio-Rad) diluted 1:5 in ddH_2O to a final volume of 1mL per 2µL sample. Absorbances were measured at λ=595nm using a Ultrospec 2100 pro spectrophotometer (Amersham Biosciences). The calibration curve used to calculate sample protein concentrations was generated with BSA (Bovine Serum Albumin) standard samples and was described by the following function: Y= 0,0454X + 0,0135 where Y is the absorbance (at 595nm) and X is the protein concentration (µg/µL). Samples were then diluted with a 4X loading buffer (250mM TRIS HCl pH 6.8, 8% SDS and 40% Glycerol), 0,1M DTT and heated at 96°C for 5 minutes.

8.2 SDS-PAGE and protein transfer

Around 30µg of samples were loaded on 4-20% Criterion TGX Stain-Free Protein Gel (18 well, Cat# 5678094, Bio-Rad) or 4–15% Mini-PROTEAN TGX Stain-Free Protein Gel (10 well, Cat# 4568083, Bio-Rad), together with pre-stained protein standard marker (Precision Plus Protein Dual Color Standards, Cat# 1610374, Bio-Rad). Denatured protein electrophoretic separation was performed in Criterion Cell (midi, Cat# 1656001, Bio-Rad) or in standard electrophoresis apparatus, filled with running buffer (Tris 3%, Glycine 14,4% and SDS 1% in ddH_2O), by applying 90V-200V voltage. Around 1 hour of electrophoretic run was performed for each experiment.

At the end of the electrophoretic run, proteins were transferred to 0,2µm nitrocellulose membranes (Trans-Blot Turbo Midi 0.2µm Nitrocellulose Transfer Packs Cat# 1704159, Bio-Rad; or Trans-Blot Turbo Mini 0.2µm Nitrocellulose Transfer Packs Cat# 1704158, Bio-

Rad, depending on gel size), using 7- or 10-minutes, 25V transfer protocol on Trans-Blot Turbo Transfer System (Cat# 1704150, Bio-Rad).

8.3 Immunoblot

Nitrocellulose membranes with transferred proteins were stained with Ponceau S staining solution (Ponceau 0.2% and acetic acid 1% in ddH_2O) to verify transfer efficiency and loading balance. After membrane wash with TBS-T 0,1% (TBS: 3% Tris base 25mM, 8.7% of NaCl 150mM and 0.2% KCl 2.7mM + 0,1% TWEEN 20, Cat# P1379, Sigma-Aldrich, in ddH_2O), membrane blocking was performed with a 30-minutes incubation with either 5% BSA or 5% milk (Nonfat dried milk powder, Cat# A0830, AppliChem GmbH) in TBS-T 0,1% at room temperature. Membranes were then incubated overnight at 4°C with primary antibodies diluted in 5% BSA or 5% milk in TBS-T 0,1% (according to antibody datasheets). The following primary antibodies were used for immunoblot analysis, as reported:

Antibody	Source	Cat. #	Dilution
anti-BUB1	Abcam	ab54893	1:1000
anti-EGFR	Kindly provided by Prof. Di Fiore Lab	in-house polyclonal ab against human EGFR aa 1172–1186	1:500
anti-eIF2α	Cell Signaling Technology	9722S	1:1000
anti-GAPDH	Santa Cruz Biotechnology	sc-32233	1:500
anti-HA	BioLegend	MMS-101P	1:2000
anti-HSF1	Cell Signaling Technology	4356S	1:1000
anti-Hsp27	Enzo Life Science	ADI-SPA-800-D	1:1000
anti-Hsp70/72	Enzo Life Science	ADI-SPA-810-D	1:1000
anti-Hsp90	Cell Signaling Technology	4877S	1:1000
anti-Keima-red	MBL	M182-3M	1:1000
anti-MAD2	Bethyl Laboratories	A300-301A	1:500
anti-MET	Santa Cruz Biotechnology	sc-162	1:250
anti-mTOR	Cell Signaling Technology	2983S	1:1000
anti-p62/SQSTM1	Santa Cruz Biotechnology	sc-28359	1:1000
anti-PDGFRβ	Cell Signaling Technology	3169S	1:1000
anti-Phospho eIF2α Ser 51	Cell Signaling Technology	3398S	1:1000
anti-Puromycin	Merk	MABE343	1:25000
anti-Tubulin	Sigma-Aldrich	T9026	1:1000
anti-Vinculin	Sigma-Aldrich	V9131	1:2000
anti-ZNF598	Abcam	ab241092	1:10000

Table 5: List of the primary antibodies used for Western blot analysis.

After primary antibodies incubation, membranes were washed in TBS-T 0,1% three times, for 10 minutes each and incubated for 30 minutes at room temperature with secondary horseradish peroxidase (HRP)-conjugated antibodies (either anti-mouse Cat# P0447, Agilent or anti-rabbit Cat# P0448, Agilent, depending on the primary antibody species) diluted 1:10000 in TBS-T 0,1%. After another three washes in TBS-T 0,1% (10 minutes each), membranes were incubated with Clarity Western ECL Substrate (Cat# 1705061, Bio-Rad) or Clarity Max ECL Substrate (Cat# 1705062, Bio-Rad), according to manufacturer's instructions, to detect chemiluminescence by an HRP-mediated enhanced chemiluminescence (ECL) reaction. Protein bands were imaged using a ChemiDoc XRS+ system (Cat# 1708265, Bio-Rad) and the ImageLab Software (Bio-Rad). The latter was also used to quantify band intensities, through "Lane and Bands" and "Quantity tool" tools, while smear intensities derived by anti-puromycin immunoblots where quantified with "Volume tool". Raw data corresponding to each band/smear value were firstly normalised on the respective loading control value, then a second normalization was performed comparing each sample to the relative control sample (*e.g.* DMSO-treated sample, Ctrl) and values were expressed as ratios sample/Ctrl (see corresponding figure legends for more details).

9. Puromycin incorporation and WB-SunSET assay

To evaluate protein synthesis rates, the SunSET (Surface Sensing of Translation) assay was used, which consists in the incorporation of puromycin into newly synthesised polypeptides (Goodman & Hornberger, 2013). Cells were plated in order to be 70-80% confluent at the time of the assay, and the same confluence was maintained among the samples, to exclude any related bias in the puromycin incorporation rates. 24 hours (HCT116) or 72 hours (RPE1) after aneuploidy induction with 500nM Mps1i treatment (or otherwise reported in figure legend) (or DMSO for pseudo-diploid controls) or 6 hours after Cycloheximide treatment, puromycin (Puromycin Dihydrochloride, Cat# P8833, Sigma-Aldrich) was diluted in cell culture medium to 10µg/mL final concentration and cells were incubated for 30 minutes at 37°C. All samples from the same experimental set were processed together. After this time window, medium was removed, cells were washed twice with 1X PBS and lysed with 1X RIPA lysis buffer supplemented with protease and phosphatase inhibitors, before proceeding with Western blot analysis as described above (see Materials and Methods paragraph 8), loading 30µg of each sample. The truncated proteins generated via puromycin incorporation into newly synthesised polypeptides produced a "smear" between 10KDa and 110KDa, after immunoblot detection with anti-puromycin antibody (clone 12D10, Cat# MABE343, Merk). The upper part of the nitrocellulose membrane was then cut and Vinculin (around 120KDa) was blotted to be used as loading control. Puromycin incorporation detection was carried out as previously described (see Materials and Methods paragraph 8.3).

10. Microscopy techniques

10.1 Immunofluorescence analysis

To analyse p62 (autophagic receptor) or G3BP1 (stress granule component) proteins with an imaging technique, $2,5*10^5$ RPE1 cells were plated on 10cm dish containing glass coverslips previously coated with 5µg/mL fibronectin (Cat# F1141, Sigma-Aldrich). 72 hours after the induction of aneuploidy with 500nM Mps1i treatment (or DMSO for pseudo-diploid controls) and, for stress granules experiment only, after 10- or 30-minutes treatment with $NaAsO_2$ (as reported in the corresponding figure legend), cells were washed in 1X PBS and then fixed in 4% paraformaldehyde (PFA Solution 4% In PBS, Cat# sc-281692, Santa Cruz Biotechnology) for 15 minutes at room temperature. After three washes in 1X PBS, cells were permeabilised with 0,5% TRITON X-100 (Cat# 108603, Merk) in PBS for 10 minutes at room temperature. Cells were blocked in 3% BSA in PBS for 30 minutes and then incubated with primary antibodies diluted in the same blocking buffer for 90 minutes at room temperature in a wet chamber. The following primary antibodies were used for immunofluorescent analysis, as reported:

Antibody	Source	Cat. #	Dilution
G3BP1	BD Science	611126	1:250
p62/SQSTM1	Enzo Life Science	BML-PW9860	1:250

Table 6: List of the primary antibodies used for immunofluorescence analysis.

After three washes in 1X PBS, cells were incubated with fluorophore-labelled secondary antibodies (either Alexa Cy3-anti-mouse or Alexa 488-anti-rabbit, Invitrogen, depending on the primary antibody species) diluted 1:400 in the same blocking buffer and mixed with 0,5µg/mL DAPI (solution in ddH2O, Cat# 32670, Sigma-Aldrich), for 45 minutes at room temperature in a wet and dark chamber. After three washes in 1X PBS and a 5-minutes wash in ddH_2O, coverslips were mounted on glass slides using 4µL Mowiol-DABCO mounting medium (12% glycerol, 9,6% Mowiol Sigma-Aldrich, 50% TrisHCl 0,2M pH7.4, 1,5% DABCO in ddH_2O), which was let to polymerise overnight at room temperature. Cells were imaged using a Leica SP8 AOBS confocal microscope with a 63X magnification objective and LasX software with Navigator (version 3.1.5.16308). Images were processed after acquisition with Fiji software (version 2.0.0-rc-59/1.51n).

In p62 immunofluorescence experiment, images were processed with Fiji software as follows: brightness and contrast levels were adjusted equally among samples and DAPI (blue LUT) channel was then merged with p62 channel (green LUT).

For stress granule experiment, images were acquired as Z stacks (4 steps, 0,3µm each) and analysed with Fiji software as follow: Z stacks were projected in 2D with Maximum Intensity Projection method, brightness and contrast levels were adjusted equally among the samples and DAPI channel (blue LUT) was then merged with G3BP1 channel (grey LUT). The percentage of cells with stress granules was obtained by manual count. To quantify the number of stress granules per cell and to analyse the distribution of stress granule areas, images were further analysed with Fiji software as follow (macro script implemented by Dr. Chiara Soriani, IEO imaging facility, Milan, Italy): the Z stacks of G3BP1 channel were projected in 2D with Maximum Intensity Projection method, background was subtracted (rolling factor=20), gaussian blur (σ=1) and OTSU Dark auto-threshold were applied to segment the objects (stress granules). Objects with an area >0,03µm^2, a circularity factor ≥0,3 (where 1.0 is referred to a circle) and a mean fluorescence intensity >60 were considered for the analysis. To count nuclei, the Z stacks of DAPI channel were projected in 2D with Maximum Intensity Projection method and nuclei were segmented as ROI (region of interest, Huang and Watershed algorithms were applied to individuate and separate two adjacent nuclei) with sizes between 60-700µm^2 and circularity factor ≥0,5 (where 1.0 is referred to a circle). The results obtained for stress granules object analysis were used to produce graphs with GraphPad PRISM (version 9.3.1).

10.2 Live-cell imaging analysis

To monitor red-Keima puncta as a proxy of ribophagy (Keima is excited at around 550nm in lysosomal structures), cells were imaged live in order to maintain the pH of cellular compartments. Keima cannot be used with fixed cells, as its fluorescence relies on lysosomal acidity. HCT116 RPS3-Keima and HCT116 RPL28-Keima cells were plated (7*10^4/well) onto a 12-well glass-bottom plate (Cat# P12G-1.5-14-F, MatTek) previously coated with 5µg/mL fibronectin, cultured for 24 hours in presence of 500nM Mps1i (aneuploid samples) or DMSO (ctrl samples) and treated as indicated in figure legend (with Bafilomycin A_1 or Torin1); for ZNF598 knock- down samples, see the protocol above (Materials and Methods paragraph 5). After the corresponding treatments, cells were stained with 2µg/mL hoechst 33342 (solution in ddH2O, Cat# 4082, Cell Signaling Technology) for 10 minutes. Cells were then imaged with a Leica SP8 AOBS confocal microscope with incubator (Okolab, 37°C with 5% CO_2), using 63X magnification objective, 561nm laser excitation and 630/750nm emission collection (red-Keima channel), 405nm laser excitation and 415/480nm emission collection (hoechst channel) and LasX software with Navigator (version 3.1.5.16308). 9 fields were acquired per sample, with 10µm Z size (6 stacks). Acquired images were displayed as maximal intensity Z projections, brightness and contrast levels were adjusted equally among the samples and hoechst channel (blue LUT) was then merged with red-Keima channel (red LUT) using Fiji software (version 2.0.0-rc-59/1.51n).

The experiments with the fluorescent tandem construct RPS3-RFP-GFP were performed on RPE1 cells stably expressing the construct (generated as reported in Materials and Methods paragraph 3). Cells were imaged live, as RFP-GFP fluorescence ratio depends on cell compartment pH. RPE1 RPS3-RFP-GRP cells were plated in 10cm dishes at 30% confluence and treated with 500nM Mps1i or DMSO to generate aneuploid and control samples, respectively (72-hour time-point). 24 hours later, drugs were washed out and cells were trypsinised and re-plated ($5*10^4$/well) together with other not-treated samples onto a 12-well glass-bottom plate previously coated with 5µg/mL fibronectin and cultured for another 48 hours before live-cell imaging. 24 hours before imaging, either Mps1i or DMSO were added to the not-treated samples, to generate aneuploid and control samples respectively (24-hour time-point) and then cells were treated as indicated in figure legend (with Bafilomycin A_1 or Torin1). After the corresponding treatments, cells were stained with 2µg/mL hoechst 33342 for 10 minutes. Cells were then imaged with a Leica SP8 AOBS confocal microscope with incubator (37°C with 5% CO_2), using 63X magnification objective, 561nm laser excitation (RFP channel), 488nm laser excitation (GFP channel), 405nm laser excitation (hoechst channel) and LasX software with Navigator and Autofocus tools. 30 fields were acquired per sample, with 2µm Z size (5 stacks) each and BIT depth factor =12. Acquired images were then analysed with Fiji software as follow (macro script implemented by Dr. Mattia Marenda, IEO imaging facility, Milan, Italy): the Z stacks of the acquired images were projected in 2D with Maximum Intensity Projection method and, using the Image Calculator tool, RFP channel was divided by GFP channel, to obtain an RFP/GFP ratio per pixel. Ratios with denominator equal to zero (*e.g.* outside the cells) were considered equal to zero. Nuclei were segmented with Otsu algorithm, and ratio inside nuclei was considered equal to 0. A Bin 2X2 pixel binning and a rainbow LUT were applied to improve RFP/GFP ratio visualization. Warmer colours indicate a higher ratio, *i.e.* lysosomal structures in which RPS3 protein and GFP have been degraded and RFP is still detectable. To the obtained ratio values, a threshold of ratio ≥ 2 was applied to eliminate background noise. The resulting data were used to produce graphs with GraphPad PRISM (version 9.3.1). Relative distributions of average RFP/GFP ratios (above the threshold) per field per sample were represented on the graphs, by normalizing each intensity value to the mean value of the respective Ctrl (pseudo-diploid) samples. Representative images were produced with the described analysis and blue borders, based on hoechst staining, were added to highlight nuclei.

10.3 Correlative Light Electron Microscopy

To directly visualise ribosomes in the lysosomal structures of aneuploid cells, correlative light electron microscopy (CLEM) technique was used. RPE1 Keima cells were plated in a 10cm dish at 30% confluence and treated with 500nM Mps1i and after 24 hours drug was washed-out. After another 24-hours, cells were trypsinised and re-plated ($1,5*10^4$/dish) onto

35mm gridded MatTek dishes (Cat# P35G-1.5-14-C-GRD, MatTek) previously coated with 5µg/mL fibronectin and cultured for another 24 hours (to reach the end 72-hour time-point). Before live-cell acquisitions, cells were stained with 2µg/mL hoechst 33342 for 10 minutes. Cells were then imaged with a Leica SP5 confocal microscope with incubator (37°C with 5% CO_2) and LasAF software (version 3.1.5.16308), firstly using 20X magnification objective to visualise the grid coordinates and select the cell to acquire at a higher magnification. Then, using the Mark and Find tool, the selected cell was acquired again with 63X magnification objective, 561nm laser excitation (red-Keima channel) and 405nm laser excitation (hoechst channel), around 8µm Z size (around 26 stacks with 0,3µm step size each). Right after acquisition, cells were fixed adding a pre-heated fixative buffer (2,5% Gluteraldehyde Cat# G765, Sigma-Aldrich in 0,1M cacodylate Cat# C4945, Sigma-Aldrich buffer pH=7.4) for 1 hour at room temperature. After three washes in 0,1M cacodylate buffer (5 minutes each), cells were stored in the same buffer at 4°C until electron microscopy analysis (performed by Dr. Alessia Loffreda at the Advanced Light and Electron Microscopy BioImaging Center, I.R.C.C.S. San Raffaele Hospital, Milan, Italy).

Cells were post-fixed in 1% OsO_4 (Cat# 75632, Sigma-Aldrich), 1.5% $K_4Fe(CN)_6$ (potassium ferricyanide, 702587), 0,1M sodium cacodylate for 1 hour at 4C° protected from light. After post-fixation, samples were washed three times with 0,1M Cacodylate Buffer and washed five times with ddH_2O. Then, samples were stained with Uranyl acetate 0,5% at 4C° overnight, protected from light. After five washing steps with ddH_2O, samples were dehydrated using the following concentration of ethanol (5 minutes per step) 30% - 50% - 70% - 80% - 90% - 96%, then three steps in 100% ethanol. Samples were covered with a mixture of ethanol and epoxy resin 1:1 and left for 2 hours on a shaker at room temperature. Then, after two changes of pure epoxy resin (1 hour per step), samples were embedded in fresh epoxy resin and polymerization took place in two steps: overnight at 45°C and then 24 hours at 60°C. Once embedding is complete, the cells of interest identified by fluorescence microscopy were found back in the EM. The reference coordinate system on the MatTek chamber ensured that the previously-imaged cells were maintained in the resin small block for sectioning the pyramide. Ultrathin sectioning (70nm) was performed on a Leica EM UC6 ultramicro-tome; then, sections were picked up and positioned on a 300 Mesh grid. Thin sections were contrasted with 2% aqueous uranyl acetate for 5 minutes and washed three times (1 minute each) in filtered ddH_2O. Subsequently, the grids were placed in a drop of Sato's lead stain and incubated for 2 minutes. Then grids were rinsed for 3 times with pure water and dried with Whatman filter paper. Images were collected using a FEI Tecnai-12 transmission electron microscope. TEM and confocal images were aligned and merged to identify the objects highlighted by the red-Keima signal using Fiji software (version 2.0.0-rc-59/1.51n).

11. TMI staining and FACS analysis

To measure the amount of misfolded and unfolded proteins in aneuploid cells, the cell-permeable fluorescent dye tetraphenylethene maleimide (TMI (Chen et al., 2017), kindly provided by Prof. Yuning Hong and Prof. Danny Hatters, La Trobe University and University of Melbourne, Melbourne, Australia) was used. RPE1 cells were plated in order to be 70-80% confluent at the time of sample collection and 500nM Mps1i (or DMSO) was added for 24 hours. After drug wash-out and 48 hours of culturing (or 24h hours after AZC treatment), cells were trypsinised, resuspended in TMI (50μM in PBS) and incubated for 45 minutes at 37°C. For Flow cytometry (FACS) analysis, cells were then washed in 1X PBS and resuspended $1*10^6$ cells/mL in FACS tubes. Cells were analysed in a FACS Celesta 2 B-V-YG flow cytometer (BD Bioscences). 50.000 events per sample were collected with 405nm laser and BV421 450/40nm bandpass filter. 2,5ug/mL propidium Iodide (Cat# P4864, Sigma-Aldrich) were used to select live cells. Data were analysed with FlowJo software (version 10.5.3). The same gate was applied to all samples to identify singlets and the threshold for TMI fluorescence was set on the negative control (not stained), to select cells containing higher than background TMI signal. The obtained results were used to quantify the relative mean fluorescent intensity (MFI) of TMI per each sample and data were represented on a graph as the ratio aneuploid/ctrl, using GraphPad PRISM (version 9.3.1).

12. Autophagosome isolation and MS/MS analysis

Autophagosome isolation from aneuploid and pseudo-diploid cells was performed after about 3 cell cycles from drug treatments (500nM Mps1i or DMSO). The isolation protocol and the following mass spectrometry analysis on autophagosome content was carried out in collaboration with Dr. Laura Pontano Vaites and Prof. Wade Harper at Harvard Medical School (Boston, USA), as previously described (Mancias et al., 2014). For this study, data derived from the most enriched functional annotations were considered as hints to proceed with further *in vitro* analysis.

13. *In vivo* experiments with *Drosophila melanogaster*

The experiments *in vivo* with the *Drosophila melanogaster* CIN model were used to evaluate aneuploid cell sensitivity to the depletion of Hsp70 chaperone and were carried out in collaboration with Prof. Marco Milán and Dr. Lara Barrio at the Institut de Recerca Biomèdica de Barcelona (IRB, Barcelona, Spain).

13.1 Fly models and strains

Wing imaginal disc and eye-antennal imaginal disc were used to induce CIN and perform the following screenings. Discs are useful to experimentally address how cells and tissues respond to over-expression or depletion of specific genes. Strains of *Drosophila melanogaster* were maintained on standard medium (4% glucose, 55 g/L yeast, 0.65% agar, 28 g/L wheat flour, 4 ml/L propionic acid and 1.1 g/L nipagin) at 25°C in light/dark cycles of 12 hours.

For CIN eye experiments, females carrying either the ey-gal4 driver alone (5535, Bloomington Drosophila Stock Center) (control) or the ey-gal4 driver together with the UAS-bub3-RNAi transgene (21037, Vienna Drosophila RNAi Center) (CIN) were crossed with males of the indicated genotypes (UAS-GFP-RNAi, UAS-Hsp70A-RNAi, UAS-Hsp70B-RNAi or UAS-Hsp70A) and allowed to lay eggs on standard fly food for 24 hours at 25°C. Progeny was kept at 25°C until they enclosed. Experimental flies and control individuals were grown in parallel. The eye phenotype was monitored in adult males. The following transgenes were used: UAS-GFP-RNAi (9331, Bloomington Drosophila Stock Center), UAS-Hsp70A-RNAi (42639, Bloomington Drosophila Stock Center), UAS-Hsp70B-RNAi (32997, Bloomington Drosophila Stock Center), UAS-Hsp70A (17624, Bloomington Drosophila Stock Center). The eye phenotypes observed in each condition were represented on a graph as percentage of weak/strong, using GraphPad PRISM (version 9.3.1).

To monitor cell death in wing imaginal disc, females carrying either the ap-gal4-myristoylated-Tomato driver alone (ap-gal4-myrT, 32221, Bloomington Drosophila Stock Center) (control) or the ap-gal4-myrT driver together with the UAS-bub3-RNAi transgene (21037, Vienna Drosophila RNAi Center) (CIN) were crossed with males of the indicated genotypes (GFPi, Hsp70A-i, Hsp70B-i or Hsp70A) and allowed to lay eggs on standard fly food for 24 hours at 25°C and kept at 25°C for another 24 hours. Then, larvae were switched to 29°C and maintained for 3 days before dissection. Experimental flies and control individuals were grown in parallel. The same transgenes reported in the previous paragraph were used. To quantify cell death, immunostaining and imaging analysis were performed as described in the following section (Materials and Methods paragraph 13.2).

13.2 Immunostaining and imaging analysis

Wing imaginal discs of third instar larvae were dissected in cold PBS, fixed with formaldehyde 4% for 20 minutes, rinsed three times in PBT (PBS + 0.1% Triton) and blocked for 1 hour in BBT (PBS + 0.1% Triton+ 0,3% BSA + 250mM NaCl). Then discs were incubated with primary antibodies overnight, rinsed with BBT and incubated with secondary antibodies for 2 hours. After 3 PBT washes, discs were kept on mounting media (80ml

glycerol + 10ml PBS 10x + 0,8 ml N-propyl-gallate 50%). The following antibodies were used: anti-cleaved-Dcp1 (1:100, Cat# 9578, Cell Signaling Technology), Alexa 488-anti-rabbit secondary antibody (Jackson Immunoresearch). DAPI (Cat# D1306, ThermoFisher Scientific) was used to stain DNA, Zeiss LSM780 confocal microscope was used to image disc samples. Since the apterous transgene (ap-gal4 driver) expressing domain is the dorsal (D) region, size of the Dorsal (D) compartment in the wing primordia was measured using Fiji software. Given that dying cells delaminate basally in the epithelium, images from basal planes were considered to determine the area positively labelled by the number of Dcp-1 positive cells, and those values were normalised to the area of the dorsal region (D). Data were represented on a graph as cDcp1 signal / D area ratios, all of them normalised to the value obtained in the control (UAS-GFP-RNAi), using GraphPad PRISM (version 9.3.1).

14. Polysome profiling analysis

To evaluate translation efficiency, polysome profiles from aneuploid and control cells were analysed. Cells (either RPE1 or HCT116) were plated in order to be 70-80% confluent at the time of sample collection. For RPE1 samples, 24 hours after the treatment with 500nM Mps1i (or DMSO), drug was washed out and 48 hours later (72-hour time-point) cells were treated with 10µg/mL Cycloheximide for 3,5 minutes. For HCT116 samples, instead, the 3,5-minute treatment with 10µg/mL Cycloheximide Samples was performed right after the 24-hour treatment with Mps1i (or DMSO). Then, cells were rinsed in 1X PBS supplemented with 10µg/mL cycloheximide and lysed directly in the dish with 300µL of ice-cold lysis buffer (10mM NaCl, 10mM MgCl2, 10mM Tris-HCl pH 7.5, 1% Triton-X100, 1% NaDeoxycholate, 0.2U/µL Rnase inhibitor, 1mM dithiothreitol, 10µg/ml cycloheximide, 0.005U/ µL DNAse I). Cell lysates were cleared with a 5-minute centrifugation at 13000rpm at 4°C and, then, stored at -80°C. The following passages were performed by Dr. Gabriella Viero at the Institute of Biophysics (CNR Unit, Trento, Italy).

10%–40% sucrose gradient was prepared in polyallomer ultracentrifuge tubes in cold room, and cell lysate was carefully added over the gradient. Tubes were filled with Buffer A (10X in DEPC-treated water: 300mM Tris-HCl pH 7.5, 1M NaCl, 100mM $MgCl_2$). Samples in sucrose gradient were ultracentrifuged in a SW41Ti rotor (Beckman) for 1 hour and 40 minutes at 180,000xg at 4°C in a Beckman Optima LE-80K Ultracentrifuge. After stabilization (20 minutes on ice), gradients were fractionated in 1mL volume fractions with continuous monitoring absorbance at 254nm using a Teledyne ISCO UA-6 UV/VIS detector. Proteins were isolated from the fractions using the TCA/acetone overnight protein precipitation method, with 100µL of 100% TCA 6M and 1mL of cold acetone (-20°C). After sample centrifugation (14000rpm, 10 minutes, 4°C), protein pellet isolation with three

washes in cold acetone and 5-minutes centrifugation (14000rpm, 4°C) each, proteins were resuspended in 50µL of SDS-PAGE loading buffer, loaded on a 4%-12% gradient gel (Novex) and blotted on nitrocellulose or PVDF membranes, for Western blot analysis. Western blots were performed using the following primary antibodies: anti-RPL26 (1:2000, Cat# ab5956, Abcam), anti-RPS6 (1:1000, Cat# 2217, Cell Signaling Techonology), anti-ZNF598 (as reported in Table 5) and the appropriate HRP-conjugated secondary antibodies (1:5000, Santa Cruz Biotechnology). Detection was performed using the ECL Prime Western Blotting Detection Reagent (Cat# RPN2232, Amersham Biosciences). Co-sedimentation profile signals were acquired and analysed as previously described (Lauria et al., 2020).

The fraction of ribosomes in polysomes (FRP) was calculated from polysomal profiles as the ratio between the area under the curve of polysomes and the area under the curve of polysomes plus the area of the 80S peak, as reported in the corresponding figure legend and as previously described (Bernabò et al., 2017). Polysome profiles from at least three different biological replicates were considered for each sample. The profiles of each biological replicate were obtained from three technical replicates.

15. Data analysis for cancer cells

A bioinformatic approach was used to assess how aneuploid cancer cells correlate with ribosome- and translation-related pathways and ZNF598-mediated quality control. Data analyses were performed by Dr. Uri Ben-David and Yonatan Eliezer at Tel Aviv University (Tel Aviv, Israel).

15.1 CCLE data analysis

Gene expression data were obtained from the CCLE using the Dependency Map (DepMap) 22Q1 release (www.DepMap.org). Single sample gene set enrichment analysis (ssGSEA) was performed using GenePatterns (Reich et al., 2006; Subramanian et al., 2005) and calculated for the following signatures: “GOBP_RIBOSOME_BIOGENESIS”,“GOBP_RIBOSOME_ASSEMBLY”,“KEGG_RIBOSOME”,“GOBP_DE_NOVO_PROTEIN_FOLDING”,“GOBP_PROTEIN_FOLDING”,”GOBP_REGULATION_OF_ENDOPLASMIC_RETICULUM_UNFOLDED_PROTEIN_RESPONSE”, “GOBP_MITOCHONDRIAL_EXPRESSION”,”GOBP_MITOCHONDRIAL_TRANSCRIPTION”,“REACTOME_MITOCHONDRIAL_BIOGENESIS”,“BIOCARTA_MITOCHONDRIA_PATHWAY”. Aneuploidy scores were obtained from (Cohen-Sharir et al., 2021) and cancer cells were divided into “high aneuploidy”, defined as the top-quartile of the number of arm-level events (either chromosome gains and losses), and “low aneuploidy”, as the bottom-quartile of the number of arm-level events. Data were represented on graphs with ssGSEA

expression scores on Y-axes and aneuploidy scores on X-axes, using GraphPad PRISM (version 9.3.1). Significance was calculated by unpaired t test.

To correlate gene expression data with ZNF598 expression in human cancer cell lines, data from DepMap 22Q1were used. Pathway enrichment analysis was performed using PreRanked GSEA and the MsigDB platform (https://www.gsea-msigdb.org/gsea/msigdb/) on the top 200 positively and negatively correlated genes with ZNF598 expression (TOP 200 and BOT 200, respectively). Data were represented on graphs with signatures on the Y-axes and -log1o(q value) on X-axes, using GraphPad PRISM (version 9.3.1).

15.2 TCGA data analysis

To correlate ZNF598 expression in patient primary cancer samples, data from TCGA were analysed. The correlation between ZNF598 mRNA expression (in RSEM) and the aneuploidy score of the tumours was assessed by linear regression (Y=0,02X+9,66; Spearman's coefficient ρ=0.2524, Pearson coefficient=0.22, R^2=0.05), using GraphPad PRISM (version 9.3.1). Data were also represented on a dot-plot with cancer types on the Y-axis and Spearman's correlation coefficient between aneuploidy score and ZNF598 expression (where ρ=0 indicates no correlation, ρ=1 perfect positive correlation and ρ=-1 perfect negative correlation) per each cancer type on the X-axis, using GraphPad PRISM (version 9.3.1).

16. Quantification and statistical analysis

To test statistical significance, the biological replicates (at least 3) indicated in each figure legend were considered. The statistical analysis was performed using GraphPad PRISM (version 9.3.1). Details of the statistical tests were reported in figure legends. Error bars are shown if n>2 and represent SEMs or SDs. P-value is shown in the graphs where it applies (P < 0.05 was considered significant), as follow: * for P < 0,05, ** for P < 0,01, *** for P < 0,001 or **** for P < 0,0001.

Results

To study aneuploidy and uncover its acute consequences on cell physiology and homeostasis it is crucial to identify the right approach. In particular, it is of foremost importance to consider the corresponding euploid counterpart as a control, to correctly evaluate the impact of aneuploidy on a given phenotype. To this aim, the aneuploidy field has identified hTERT RPE-1 and HCT-116 cell lines as optimal cellular models, as they are two different human near-diploid and chromosomally stable cell lines. hTERT RPE-1 (henceforth RPE1) are human untransformed hTERT-immortalised retinal pigment epithelial cells, with known clonal gains of chromosome 10q arm and chromosome 12 (C. Z. Zhang et al., 2015). HCT-116 (henceforth HCT116) are human colorectal carcinoma cells with an epithelial morphology and with only four structural chromosomal rearrangements (Miao et al., 2007). Both cell lines, in basal conditions, cycle in about 24 hours.

Starting from these near-diploid lines, I generated the aneuploid system by inducing chromosome mis-segregation. To do this, I took advantage of a well-established protocol (Santaguida et al., 2015) to inhibit the function of the spindle assembly checkpoint (see Introduction paragraph 1.1 and ref. (Musacchio & Salmon, 2007)) by interfering with its key components. Specifically, I used the small molecule reversine (Rev or Mps1i), a chemical inhibitor of the catalytic activity of Mps1 kinase, to allow for mitotic progression even in the presence of chromosome misalignments and improper attachments (Santaguida et al., 2010). Importantly, at sub-micromolar concentrations, reversine does not affect cytokinesis (Santaguida et al., 2010), therefore minimizing the presence of polyploid cells in the treated populations and excluding effects related to polyploidization from the subsequent analysis. In parallel, I also treated cells with the vehicle dimethyl sulfoxide (DMSO) to obtain the control samples. I added either Mps1i 500nM or DMSO to cell cultures for 24 hours, to allow cells to transit through one mitosis in the presence of the drug. After the incubation, drugs were washed out to avoid prolonged chromosome mis-segregation driven by continuous SAC inhibition. As a result, I obtained heterogeneous populations of aneuploid cells with random chromosome gains and losses. For the majority of my experiments, I collected samples either 24, 48 or 72 hours after drug addition, reflecting approximately 1, 2 or 3 cell cycles (Figure 11). As mentioned before, for the time-points after 24 hours I washed-out the drugs and cultured the cells for more cell cycle(s). The collection of aneuploid populations at different time-points allows for the analysis of aneuploid cells harbouring increasing levels of aneuploidy-associated stresses. On the other hand, this time-frame grants as well the study of the immediate cellular responses to chromosome mis-segregation. To confirm the key results with an orthogonal approach, I also depleted -individually- two additional SAC components, namely MAD2 and BUB1, with small interfering RNAs. Also in this case, I obtained populations of aneuploid cells with random karyotypes that are useful to address the acute response to aneuploidy (Santaguida et al., 2015).

Hence, heterogeneous aneuploid populations are suitable for the analysis of common features and common mechanisms that cells exploit to cope with aneuploidy-related acute stresses. On the downside, however, the exact karyotypes remain unknown, as well as the contribution of a specific chromosome alteration to the phenotype of interest. On the other hand, an approach that uses isogenic, stable aneuploid cells with given karyotypes would allow the study of chronic effects of the aneuploid state, losing important information about the immediate consequences, which does not match the purpose of my project.

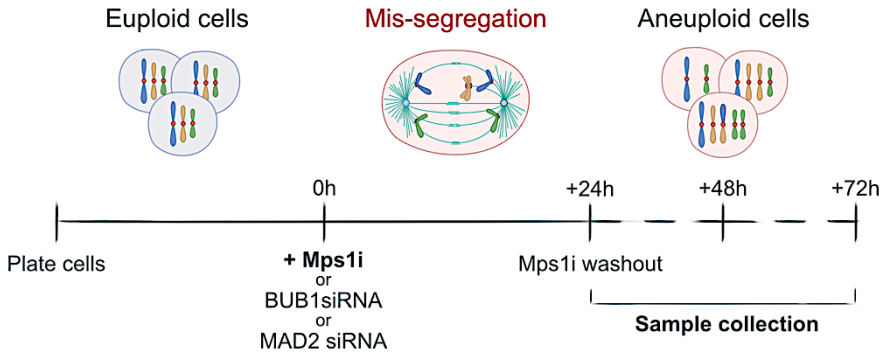

Figure 11: Experimental set-up for the generation of a heterogeneous aneuploid population.
Schematic representation for the generation of a heterogeneous population of aneuploid cells with random chromosome gains and losses. Time 0 is defined by the addition of the Mps1 inhibitor (Mps1i), or by MAD2 or BUB1 depletion with siRNA. Samples are collected about 1, 2 or 3 cell cycles (+24h, +48h or +72h) after chromosome mis-segregation. DMSO or non-targeting siRNA are used to generate pseudo-diploid controls. For time-points after 24 hours, drugs are washed out and cells are grown for another 24 hours (for samples hereafter called 48h) or another 48 hours (for samples hereafter called 72h).

1. Aneuploidy causes the accumulation of misfolded and unfolded proteins

As described in the introduction of this thesis, proteotoxic stress is one of the widely recognised stresses that aneuploid cells experience (see Introduction paragraph 4.2). The negative impact of aneuploidy on cell proteome has been thoroughly analysed in yeast (Brennan et al., 2019; Oromendia et al., 2012; Oromendia & Amon, 2014; Torres et al., 2007), but so far human aneuploid cell models provided just indirect clues that suggest the presence of misfolded aggregates (Santaguida et al., 2015). Ubiquitylated proteins and presence of ubiquitin receptors (*e.g.* p62) have been widely used as surrogates to detect unfolded or misfolded proteins; however, not all protein ubiquitylations are triggered by misfolding events. To start investigating the impact of aneuploidy on protein homeostasis, it was crucial to prove, once for all, that aneuploid cell cytoplasm accumulates misfolded and unfolded proteins.

1.1 Misfolded and unfolded protein accumulation in aneuploid cells

A direct strategy to identify misfolded and unfolded proteins is provided by the recently-described fluorescent dye tetraphenylethene maleimide (TPE-MI or, henceforth, TMI) (Chen et al., 2017). TMI is a cell-permeable probe that fluoresces when it interacts with cysteine thiols (Figure 12a, right). Cysteines present free thiols only when they are not engaged in disulphide bonds, and this condition rarely occurs on protein surface, since they are normally buried within the folded protein structure (Marino & Gladyshev, 2010). Thus, exposed cysteine abundance increases with increasing levels of misfolded/unfolded proteins (Figure 12a, left). The fluorescent dye tetraphenylethene is quenched by the conjugated maleimide, until the latter interacts with a free thiol, hence enabling emission at around 480nm (Chen et al., 2017). These characteristics confer TMI a high reliability in detecting unfolded and misfolded proteins in various contexts and models (Chen et al., 2017; Hidalgo San Jose et al., 2020).

I adapted TMI for the purpose of evaluating the accumulation of not-properly folded proteins in aneuploid cells, compared to the pseudo-diploid counterparts. To do this, I measured TMI fluorescence by flow cytometry (FACS) in RPE1 samples treated with Mps1i (Aneu) or DMSO (Ctrl) and collected after 72 hours. This time-point allowed aneuploid cells to accumulate sufficient proteotoxic stress to be detected with this technique. Indeed, the aneuploid sample showed a higher TMI mean fluorescence intensity (MFI) than the pseudo-diploid counterpart (Figure 12b, orange peak *vs* green peak), which reflects higher TMI binding to exposed cysteines. I then quantified the relative MFI of TMI in aneuploid samples, as the ratio between aneuploid and pseudo-diploid TMI MFI (Aneu/Ctrl) in six independent biological replicates (Figure 12c). To test that TMI was effectively measuring unfolded and misfolded proteins in my experimental set-up, I produced a positive control treating cells with L-azetidine-2-carboxylic acid (AZC), which is a proline analogue that is systematically mis-incorporated into nascent polypeptides. Thus, AZC treatment leads to high rates of unfolding and to the aggregation of aberrant polypeptides in cell cytoplasm. As expected, AZC-treated samples showed the highest TMI MFI (Figure 12b, red peak). Not stained samples (NS) were used as negative controls (Figure 12b, light-blue peak).

In summary, TMI dye provided a useful approach to prove that aneuploid cells have an altered proteostasis, which is exacerbated by an increased load of unfolded proteins.

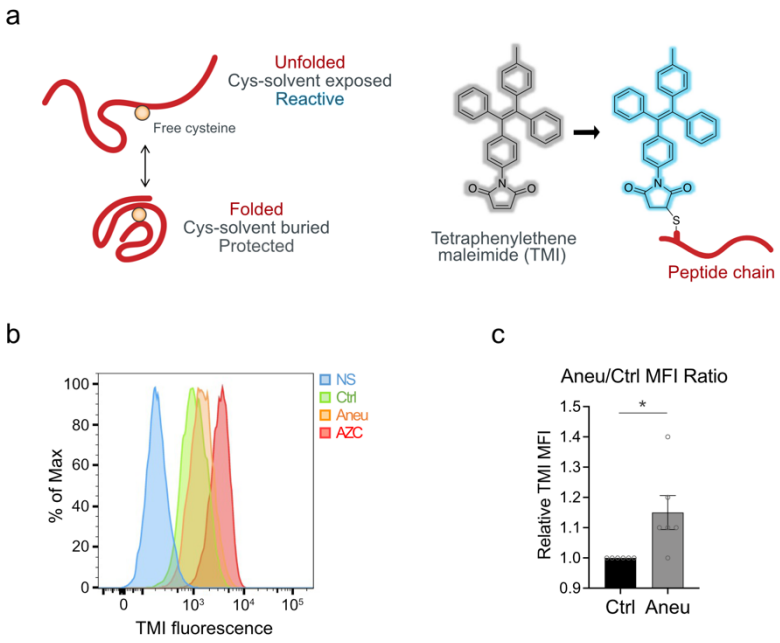

Figure 12: Misfolded and unfolded protein accumulation in aneuploid cells.
(a) Strategy for the identification of misfolding/unfolding events and structure of tetraphenylethene conjugated to a maleimide. TMI dye fluoresces (light-blue contour) upon the interaction with an exposed cysteine of unfolded polypeptide chain. *Adapted from (Chen et al., 2017)*. **(b)** Representative histogram showing tetraphenylethene maleimide (TMI) fluorescence in the indicated samples, obtained by FACS analysis. RPE1 cells were treated with Mps1 inhibitor (Aneu) or DMSO (Ctrl) and collected after about 3 cell cycles (72 hours); L-azetidine-2-carboxylic acid (AZC, red) (10mM, 24h) was used as positive control; not-stained sample (NS, blue) was used as negative control. **(c)** Quantitation of the relative mean fluorescence intensity (MFI) of TMI in aneuploid cells, obtained as in (b) and expressed as the ratio between aneuploid and pseudo-diploid TMI MFI. Mean ± SEM; n=6; one sample t test.

1.2 Evidence of PERK-mediated UPR activation in aneuploid cells

To further characterise the impaired proteostasis of aneuploid cells, I considered also a mechanism that cells are known to activate to mitigate folding stress. The unfolded protein response (UPR), as suggested by the name, is triggered when cells sense a decrease in the folding capacity of the endoplasmic reticulum (ER, see Introduction paragraph 4.1.2 and ref. (Walter & Ron, 2011)). Firstly, I checked the phosphorylation status of the eukaryotic transcription factor 2 (phopsho-eIF2α) on serine 51, as a readout for the activation of the PERK kinase branch of UPR (Walter & Ron, 2011). At the same time-point in which aneuploid cells showed increased misfolding (72 hours after Mps1i treatment), there was a corresponding increase in eIF2α phosphorylation, compared to the pseudo-diploid samples (Figure 13a-b).

Importantly, PERK-mediated phosphorylation of eIF2α is a key event also in a broader stress response, known as the integrated stress response (ISR, see Introduction paragraph 4.1.2 and ref. (Taniuchi et al., 2016)). Together with Dr. Elena Morelli, a previous postdoc in the lab, we therefore looked at other downstream effectors of PERK that are specifically

activated in the context of UPR (Jiang et al., 2004; Marciniak et al., 2004). *CHOP* and *ATF3* expression levels in aneuploid cells were evaluated for this purpose (Figure 13c). Their higher mRNA levels, compared to the euploid samples, further confirmed that aneuploid cells activate the pathway to cope with the folding stress.

Lastly, I tested whether aneuploid cells rely on UPR PERK branch activation to survive and for this I performed a viability assay. I used increasing concentrations of PERK inhibitor (PERKi) and compared the behaviour of aneuploid and pseudo-diploid cells in the presence of this drug. The results, obtained from two independent biological replicates, showed a higher sensitivity of aneuploid cells to the inhibition of PERK, highlighted by the values of the half maximal effective concentration (EC_{50}) of PERKi (Figure 13d). PERKi EC_{50} calculated for control cells was, in fact, almost 2-fold over the aneuploid sample.

Together, these data suggest that aneuploid cells activate UPR, at least the PERK branch of this stress response, to buffer the proteotoxicity derived from misfolded and unfolded protein accumulation.

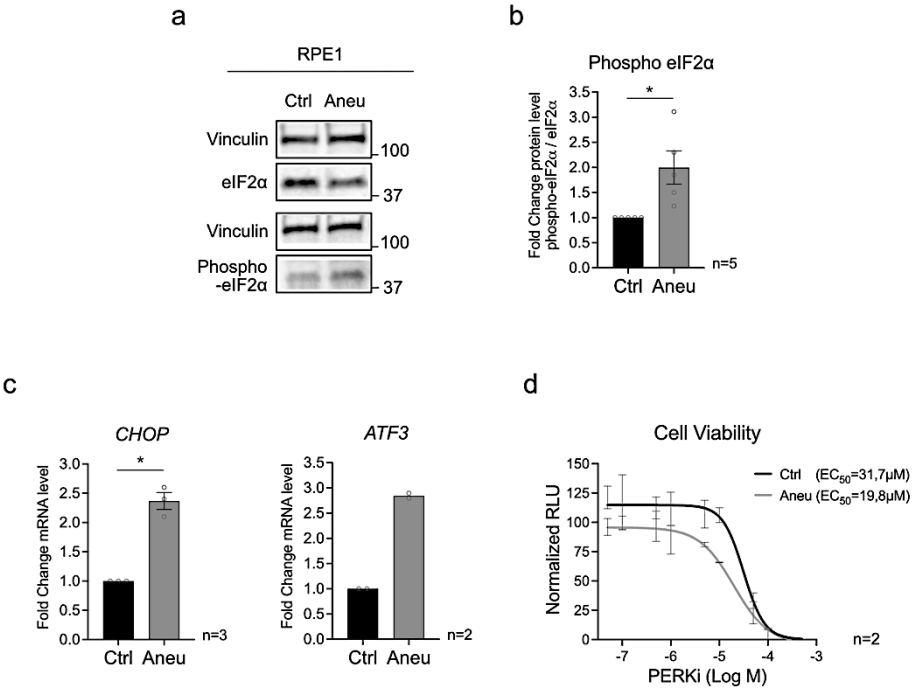

Figure 13: PERK-mediated UPR activation in aneuploid cells.
(a) Representative immunoblot of eIF2α phosphorylation (Phospho- eIF2α) and total eIF2α in RPE1 cells treated with Mps1 inhibitor (Aneu) or DMSO (Ctrl) and collected after about 3 cell cycles (72 hours). Vinculin was used as loading control. **(b)** Quantitation of phospho- eIF2α immunoblots obtained as in (a), from the indicated biological replicates. Band values are normalised to the respective loading controls and to total eIF2α; values are expressed as fold changes Aneu/Ctrl. Mean ± SEM; n=5; one sample t test. **(c)** *CHOP* and *ATF3* expression levels from quantitative Real-Time PCR performed on aneuploid (Aneu) and pseudo-diploid (Ctrl) samples at 72 hours from drug treatments. *GAPDH* was used as a housekeeping gene to normalise expression data. Expression levels are shown as fold changes Aneu/Ctrl. Mean ± SEM (where it applies); n=3 (*CHOP*) or n=2 (*ATF3*); one sample t test (where it applies). **(d)** Comparison of viability assay profiles of aneuploid cells (Aneu)

and pseudo-diploid counterpart (Ctrl), treated with increasing concentrations (0-500μM) of PERK inhibitor (PERKi) for 72 hours. Values of the respective half maximal-effective concentration (EC_{50}) are shown. Relative Light Unit (RLU) values, a proxy of cell viability obtained with CellTiter Glo assay, are expressed as percentage to compare the two samples. Mean ± SD; n=2.

2. Analysis of the autophagic cargo in aneuploid cells

Considering that impaired protein folding challenges cell proteostasis, it has been proposed that proteotoxic stress is responsible for the increase in the degradative load in aneuploid cells (Santaguida et al., 2015; Stingele et al., 2013). Furthermore, the accumulation of autophagic structures, such as autophagosomes, within the aneuploid cell cytoplasm indicates that the degradation step is likely to be saturated by the excessive degradative demand (Santaguida et al., 2015). To follow-up on this previous work and to start deciphering the nature of the hard-to-degrade cargo engulfed in autophagosomes of aneuploid cells, I firstly evaluated the degree of autophagy overwhelming in my cellular systems and, then, I exploited a proteomic approach already performed in the lab.

2.1 Aneuploid cells increase and saturate bulk autophagy

As mentioned, I checked the bulk autophagy increase in both RPE1 and HCT116 cell lines, in order to confirm that this feature was generalised in the aneuploid systems I was using. To do this, I monitored the levels of the autophagic receptor p62 as a proxy of the autophagic flux. p62 is incorporated into early autophagic structures (phagophores and autophagosomes) through the interaction with LC3 II, which is integrated in their membranes. Proceeding with the degradation step, upon fusion with lysosomes, both LC3 and p62 are efficiently degraded (see Introduction paragraph 4.1.4 and ref. (Mizushima et al., 2010)). Thus, the analysis of their cellular levels, either by immunoblot or fluorescence microscopy, is a reliable tool to monitor the autophagic flux. Specifically, p62 levels inversely correlates with autophagic degradation, since increased p62 indicates autophagy activation on one side, but also impaired degradation on the other (Mizushima et al., 2010). The western blot analysis on p62 protein levels in aneuploid samples (compared to the respective pseudo-diploid ones), indeed, showed an increased accumulation of this autophagic receptor, both in RPE1 and HCT116 cellular models. In particular, p62 protein levels correlated with the increased accumulation of aneuploidy-associated stresses, as shown by the time-course analysis on aneuploid samples collected after 24, 48 and 72 hours from Mps1 inhibition (Figure 14a-b).

Saturation of the autophagic pathway in aneuploid cells at the latest time-point (72 hours from Mps1 inhibition) was further confirmed at the single-cell level with a qualitative immunofluorescence analysis. RPE1 aneuploid samples (Aneu) and the respective pseudo-diploid controls (Ctrl) were immunostained with p62 antibody and DAPI (DNA) (Figure 14c).

Although p62 level assay is widely used for this purpose, it is also highly sensitive to the various stresses of cell culture conditions (Mizushima et al., 2010). To overcome this possible drawback and confirm the increased bulk autophagy in aneuploid cells, I moved towards a different approach. I took advantage of the monomeric form of the fluorescent tag mKeima (henceforth Keima, see Introduction Figure 7 and ref. (Klionsky et al., 2021)) fused with LDHB, used as a cytosolic marker, to monitor the aspecific bulk autophagic flux. As previously described in the introduction, the western blot analysis of Keima-tagged proteins allows for the evaluation of their presence in the autophagic structures. In particular, using an anti-Keima antibody, it is possible to spot Keima alone at 25KDa, since it is unaffected by lysosomal hydrolases, in contrast with the tagged protein that is degraded in autolysosomes. Therefore, here, a higher processed-Keima signal at 25KDa reflects a higher LDHB autophagic trafficking (*i.e.* a greater bulk autophagy). After the generation of stable cell lines (from both RPE1 and HC116) expressing LDHB-Keima, I have performed the experiment on aneuploid samples in a time-course of 24, 48 and 72 hours after Mps1i treatment, comparing the results with the corresponding pseudo-diploid controls. As expected, when the aneuploidy-associated stresses were more serious (at late time-points), the bulk autophagic flux was higher (Figure 14d-e).

These results are in line with previous works (Santaguida et al., 2015; Stingele et al., 2012) and, together, point out that aneuploid cells tend to activate and boost the autophagic pathway to cope with their increasing proteotoxic stress, but also saturate the degradation step, because of the excessive amount of cargoes.

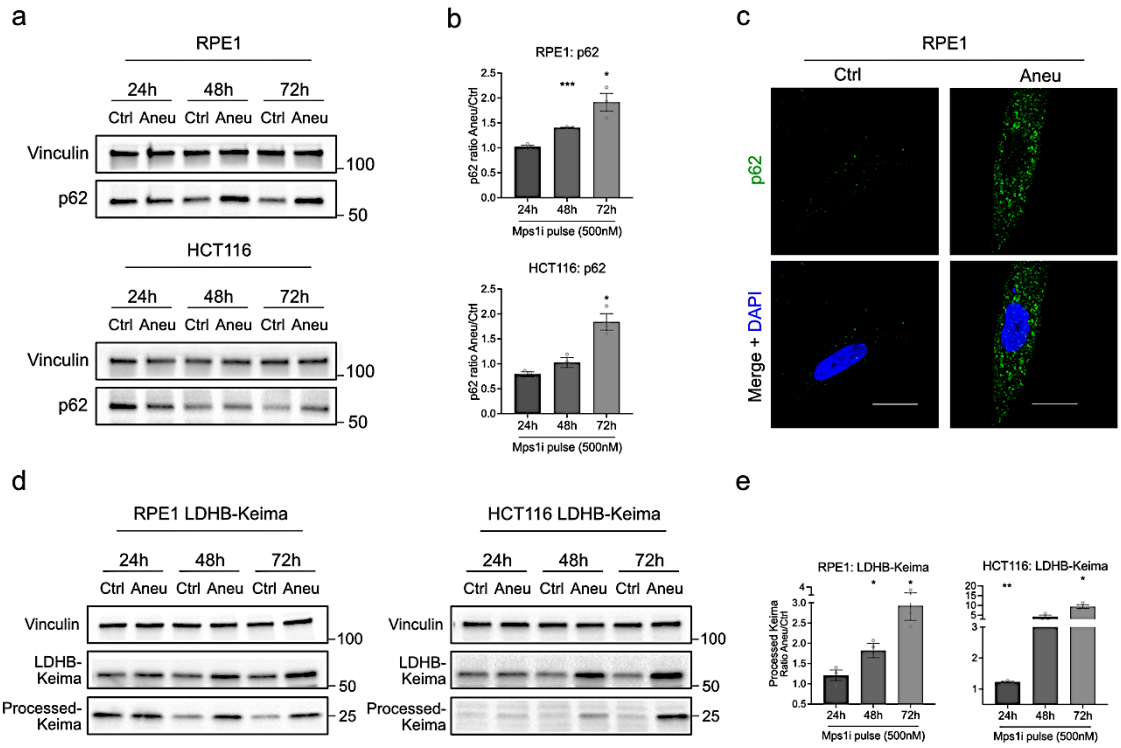

Figure 14: Bulk autophagy is increased and saturated in aneuploid cells.

(a) Representative immunoblots of p62 in the indicated cell lines, treated with Mps1 inhibitor (Aneu) or DMSO (Ctrl) and collected after either 1, 2 or 3 cell cycles (24, 48 or 72 hours). Vinculin was used as loading control. **(b)** Quantitation of p62 immunoblots obtained as in (a). Band values are normalised to the respective loading controls; values are expressed as ratios Aneu/Ctrl per each time-point. Mean ± SEM; n=3; one sample t test (Aneu at each time-point *vs* respective Ctrl=1). **(c)** Qualitative confocal images of RPE1 cells treated with Mps1 inhibitor (Aneu) or DMSO (Ctrl) and collected after about 3 cell cycles (72 hours). Immunofluorescence analysis performed with p62 antibody and DAPI (to stain DNA); scale bars, 20μm. **(d)** Representative immunoblots of the indicated LDHB-Keima cell lines, treated with Mps1 inhibitor (Aneu) or DMSO (Ctrl) and collected after either 1, 2 or 3 cell cycles (24, 48 or 72 hours). The bulk autophagic flux is determined by the increased level of processed Keima at 25KDa. Vinculin was used as loading control. **(e)** Quantitation of processed Keima immunoblots obtained as in (d). Band values are normalised to the respective loading controls; values are expressed as fold changes Aneu/Ctrl. Mean ± SEM; n=3; one sample t test (Aneu at each time-point *vs* respective Ctrl=1).

2.2 Proteomic analysis of proteins enriched in aneuploid cell autophagosomes

The next question I asked was about the nature of the cargo engulfed in the autophagosomes of aneuploid cells. To answer this, I took advantage of an experiment previously performed by our lab in collaboration with Prof. Wade Harper's lab (Harvard Medical School, Boston, USA). Autophagosomes and early autolysosomes were isolated and analysed using a SILAC approach that allows for the proteome analysis of two distinct cell populations, thanks to the incorporation of differentially labelled amino acids (light isotope aa for aneuploid sample and heavy isotope aa for the control) (Figure 15a, top). Specifically, samples were generated from RPE1 cells treated with Mps1i (aneuploid sample) or DMSO (control pseudo-diploid sample) and collected after about 3 cell cycles. The autophagic structures were firstly enriched in both samples using Bafilomycin A_1 (BafiloA_1), an antibiotic that is known to inhibit the proton pump and, therefore, the latter stages of autophagy. Through a density gradient separation protocol (Mancias et al., 2014), autophagosomes were purified and then processed for mass spectrometry (MS/MS) analysis (Figure 15a). Candidate autophagosomal proteins enriched in aneuploid samples were identified by light/heavy ratio and filtered against the relative abundance in the whole proteome, in order to remove proteins that might be not-specifically sequestered by bulk autophagy (*e.g.* mitochondrial proteins were extensively cut off). The gene ontology (GO-term) analysis performed on the list of proteins enriched in aneuploid cell autophagosomes, compared to the pseudo-diploid ones, identified some interesting functional annotation hints (Figure 15b) (in collaboration with Dr. Laura Pontano Vaites, Harvard Medical School, Boston, USA). Within the most enriched, I focused my attention on the signatures of proteins previously reported as probable selective autophagy cargo. They, in fact, represented compelling cues for further analysis of the degradative mechanisms that might be able to remodel proteostasis and, possibly, highlight specific aneuploidy-driven defects on important cellular organelles. For example, as shown in different contexts (Beese et al.,

2020), ER (Iavarone et al., 2022) and ribosomes (An & Harper, 2020) can be targeted for selective autophagy, to be cleared for multiple reasons in stress conditions.

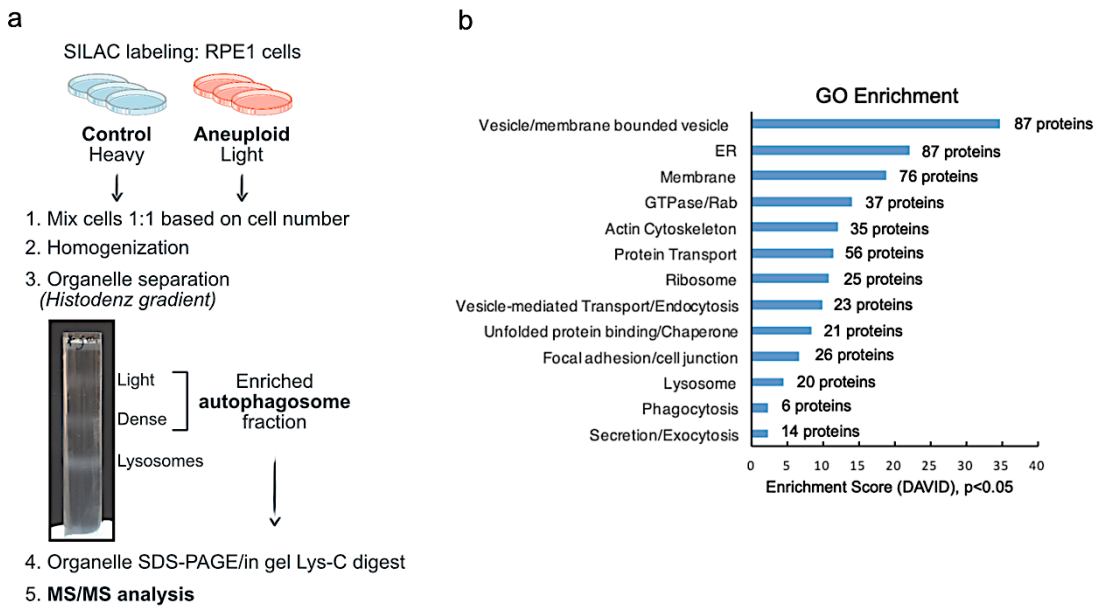

Figure 15: Proteomic analysis of proteins enriched in aneuploid cell autophagosomes.
(a) Schematic of autophagosome isolation with SILAC approach and mass spectrometry analysis in RPE1 cells treated with Mps1 inhibitor (Aneuploid) or DMSO (Ctrl) and collected after about 3 cell cycles (72 hours). **(b)** Gene ontology (GO-term) enrichment analysis on the proteins enriched in autophagosomes of aneuploid cells compared to control cells. Analysis performed using the Database for Annotation, Visualization and Integrated Discovery (DAVID) bioinformatic resource, p<0,05 (courtesy of Dr. Laura Pontano Vaites).

2.3 Analysis of selective autophagy in aneuploid cells

The previous results prompted me to test whether selective autophagic processes are effectively triggered in aneuploid cells. The first approach I chose to address this hypothesis was based on the pH-sensitive Keima reporter fused to proteins from different cell organelles. I generated stable cell lines from both HCT116 and RPE1, as I did for LDHB-Keima (see Result paragraph 2.1). Briefly, each cell line expressed either the Keima construct to monitor ER-phagy, the one to monitor ribophagy of the ribosomal small subunit or the one for ribophagy of the large subunit. In addition, I also used a reporter for mitophagy, to test if mitochondria might be involved in selective autophagy as well, even if they were not within the most enriched signatures of autophagosome content. More in detail, I used the RAMP4-Keima fusion protein construct for ER-phagy, as RAMP4 is a protein located into the endoplasmic reticulum membrane. RAMP4 is known to interact with target proteins during their translocation in the ER lumen, specifically in the course of ER stress. The two reporters I employed to monitor ribophagy were RPS3-Keima and RPL28-Keima (together referred to as Ribo-Keima). RPS3 is a ribosomal protein that is part of the 40S small subunit, forming the domain where translation initiation takes place. RPL28 is, instead, a component of the 60S large subunit of ribosomes. To track mitophagy, I took

advantage of the construct known as MT-Keima, which has been engineered to add to Keima a mitochondria-targeting sequence from COX VIII. COX VIII is the terminal enzyme of the mitochondrial respiratory chain, therefore residing in the inner membrane of this organelle. Previous works have confirmed that the presence of the Keima reporter did not impair the canonical functions and stoichiometry of the tagged proteins and organelles, establishing the reliability of the system(An & Harper, 2018; Di Lorenzo et al., 2022; Sun et al., 2017). I analysed the different selective autophagic fluxes in a time-course of aneuploid cells collected 24, 48 and 72 hours after Mps1i treatment (1, 2 or 3 cell cycles), comparing the results with the corresponding pseudo-diploid controls. Considering different time-points after chromosome mis-segregation allowed me to trace the increase in the selective autophagic fluxes in relation to the increase in aneuploidy-associated stresses. Western blot analysis of the fluxes in the respective Keima cells lines revealed that mitophagy levels in aneuploid cells (Aneu) were always comparable to those of the control samples (Ctrl); a mild increase was observed only at the latest time-point (72 hours) (Figure 16a-b). ER-phagy and ribophagy, of both 40S and 60S subunits, were particularly boosted at the same time-point (72 hours after aneuploidy induction), with an increase spotted also at 48 hours (after about 2 cell cycles). Regarding ribophagy, these results were in line with a previous work (An & Harper, 2018). Interestingly, my results showed that only the levels of ribophagy were already high (1,5- 2-fold over controls) at 24 hours, right after the induction of aneuploidy (Figure 16a-b). The trends of the three reporters were constantly maintained both in HCT116 lines and in RPE1 lines, highlighting that these are common traits of the used aneuploid systems. Another feature shared by the three selective autophagy reporters was their corresponding increase with increasing aneuploidy-associated stresses. Moreover, the results obtained for processed-LDHB-Keima and p62 accumulation (Figure 14) can suggest that at later time points the increase in bulk autophagy is high enough to also include these organelles/structures, not necessarily in a specific manner.

The early increase in the ribophagic flux, however, was worth a more in-depth analysis. A closer look to the values of the processed-Keima bands at 24 hours from the used cell lines, highlighted that, especially in HCT116 but also in RPE1, ribophagy was significantly higher, if compared to the other selective autophagies and to the bulk autophagic flux (Figure 16c). Considering the knowledge already mentioned (see Introduction paragraph 4.1.4 and ref. (An & Harper, 2020)) about the engulfment of ribosomes in autophagic structures, my results suggest that ribosomes are most likely there because of a process independent from random bulk autophagy. Bulk autophagy levels, in fact, are amplified in aneuploid cells later than the 24h time-point. As well, ribophagy in aneuploid cells cannot occur just as a bystander flux during ER degradation (*i.e.* ER-phagy), because ER does not seem to be degraded already at 24 hours after aneuploidy induction.

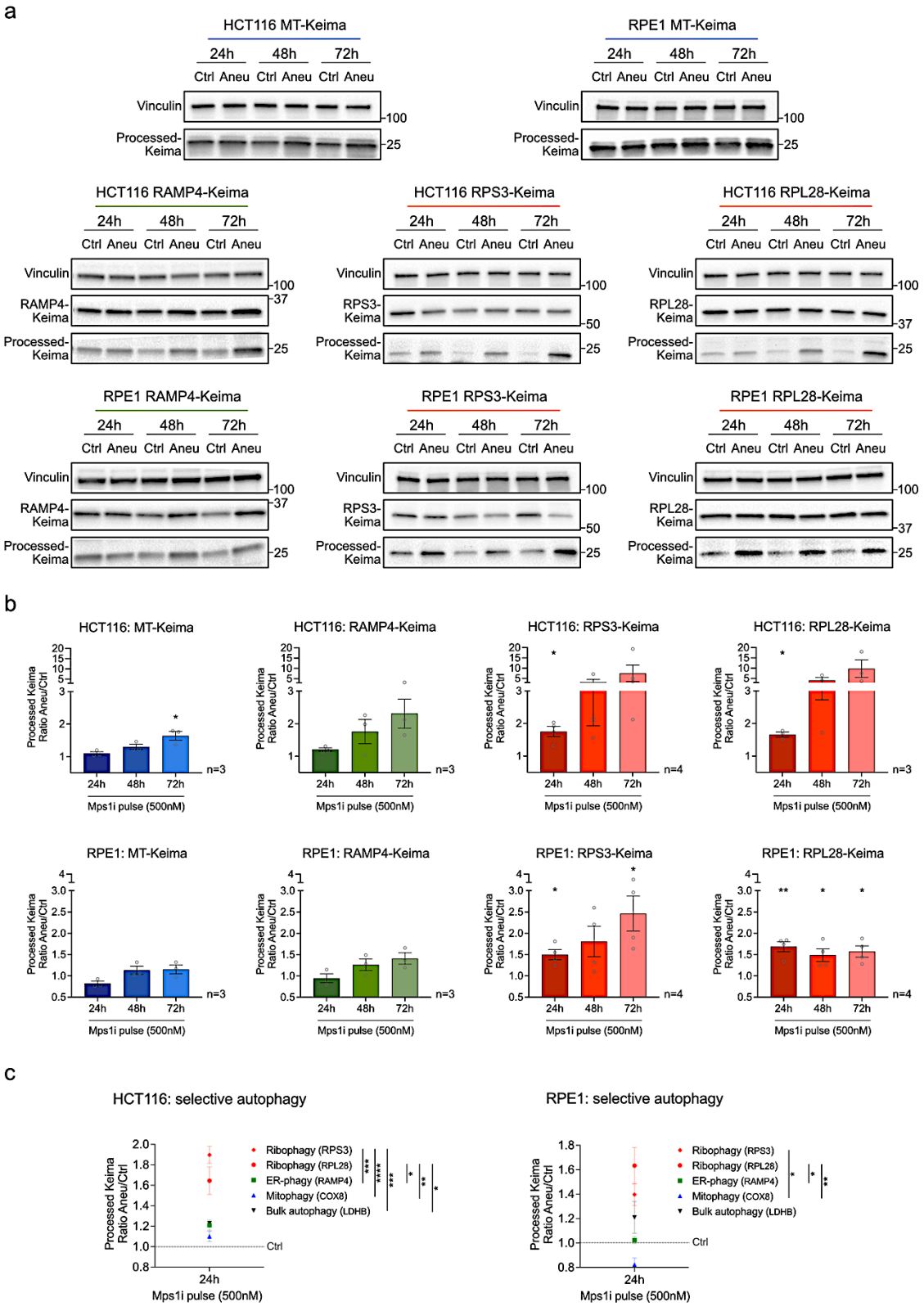

Figure 16: Selective autophagy processes in aneuploid cells.

(a) Selective autophagy monitored by western blot. Representative immunoblots of the indicated Keima cell lines, treated with Mps1 inhibitor (Aneu) or DMSO (Ctrl) and collected after either 1, 2 or 3 cell cycles (24, 48 or 72 hours). The different autophagic fluxes are determined by the increased level of the respective processed Keima at 25KDa. Vinculin was used as loading control. **(b)** Quantitation of processed Keima immunoblots obtained as in (a), from the indicated biological replicates. Band values are normalised to the respective loading controls; values are expressed as ratios Aneu/Ctrl per each time-point. Graph Y axes were scaled to have the

same range in the different conditions and facilitate their comparison. Mean ± SEM; n=3 (MT-Keima, RAMP4-Keima) or n=4 (RPS3-Keima, RPL28-Keima); one sample t test (Aneu at each time-point *vs* respective Ctrl=1). **(c)** Plot of the processed-Keima levels of the indicated samples, to highlight the different behaviour of the analysed selective autophagies and bulk autophagy right after aneuploidy induction (24 hours, about 1 cell cycle, from Mps1i/DMSO treatment). The graphed values are the same as those shown in (b) and in Figure 14(e) (Mean ± SEM); one-way ANOVA, followed by Tukey's multiple comparison test.

In conclusion, these experiments show that mitophagy is not a major selective autophagic pathway in aneuploid cells, while ER-phagy and ribophagy take place when bulk autophagy is triggered as well. It is possible that ER-phagy and ribophagy together might have a role in the general autophagic engulfment and saturation observed in aneuploid cells, few cell cycles after mis-segregation. Ribophagy, notably, seems to be the first one to be induced, right after cell aneuploidization. Further characterizations were warranted in this direction.

3. Aneuploidy leads to autophagic removal of ribosomes

Ribosomes are the central hub of protein translation and their functions in orchestrating protein homeostasis are crucial for cell survival (Pechmann et al., 2013). Therefore, maintaining healthy and properly-functioning ribosomes is a critical task for cells, especially under stress conditions. Knowing that aneuploid cells experience number of stresses, in particular at the level of the proteome (see Introduction paragraph 4.1 and refs. (Oromendia & Amon, 2014; Santaguida & Amon, 2015b; Stingele et al., 2012)), it was of foremost interest to validate the results I obtained on the selective degradation of ribosomes. Moreover, it was also important to interpret them taking into account that stressed aneuploid cells might need to re-establish functional ribosomal pools.

3.1 Aneuploidy leads to increased ribophagy

Using the Ribo-Keima cell lines previously described, I further confirmed via western blot with multiple independent biological replicates that both the small and the large subunits of ribosomes were actually degraded through the ribophagic flux, at early time points (Figure 17a-b). Western blot analysis normally gives an overview on the entire population that is examined, in this case it highlighted that the aneuploid population with random chromosome gains and losses presents, on average, the abovementioned ribophagic phenotype (Figure 17a-b).

This phenotype was also visible at the single-cell level. For this, I exploited the pH-dependent excitation spectra shift of Keima (see Introduction Figure 7 and ref. (Klionsky et al., 2021)). Keima excitation peaks at 440nm at neutral pH (such as in cytoplasm and autophagosomes) and at around 550nm at acidic pH (such as in autolysosomes and lysosomes), while emission spectra always peak at 620nm. In this way, I measured the flux of Ribo-Keima to the acidic environment of autolysosomes through live-cell imaging. Since

green-Keima signal (*i.e.* excited at 440nm in compartment with neutral pH) was technically not satisfying and widespread all-over the cell (also in nuclear fractions, where it should not be), I focused my attention only on the red-Keima signal (*i.e.* excited at 550nm, indicating the autolysosomal/lysosomal localization). With this approach, I confirmed that also at single cell level aneuploidy leads to increased ribophagy, mirrored by the accumulation of red-Keima puncta in aneuploid cell cytoplasm, compared to the pseudo-diploid counterpart (Figure 17c). The signal, however, was not equally distributed among the imaged aneuploid cells, suggesting that the ribophagic process could be accentuated in cells that experience higher level of stresses. This could be the result of the heterogeneous composition of the aneuploid population generated through Mps1 inhibition.

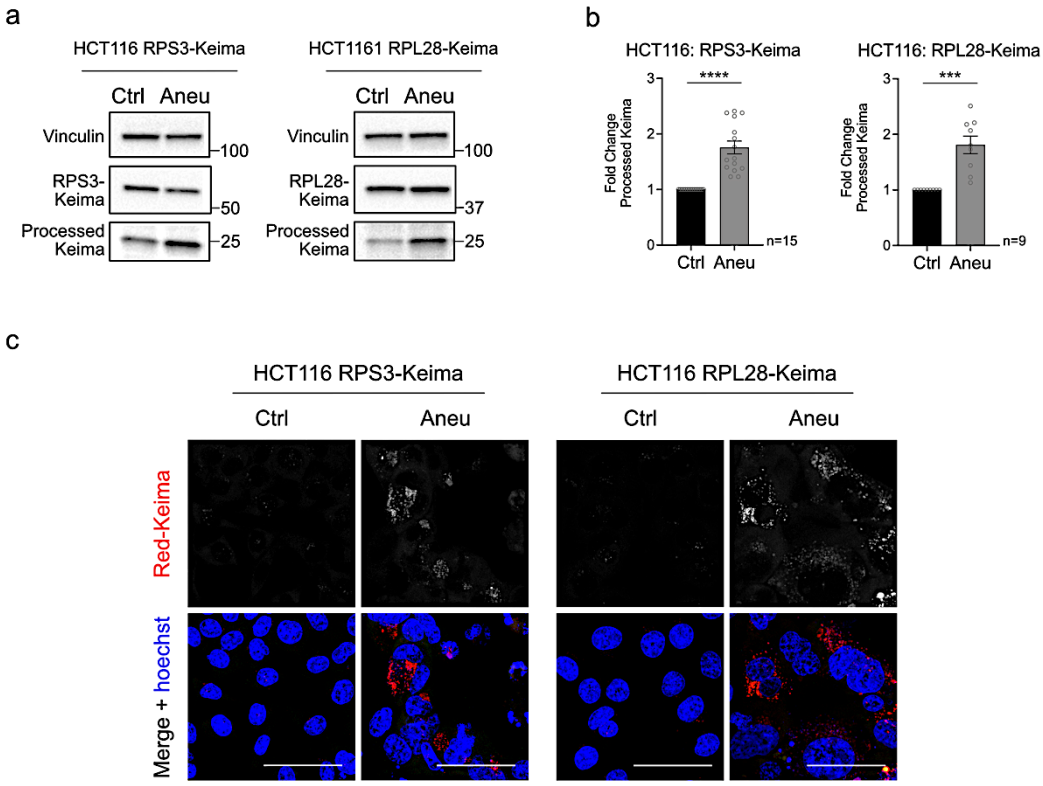

Figure 17: Aneuploidy leads to increased ribophagy.

(a) Representative immunoblots of the indicated HCT116 Ribo-Keima cell lines, treated with Mps1 inhibitor (Aneu) or DMSO (Ctrl) and collected after 24 hours. Ribophagic flux is determined by the increased level of processed Keima at 25KDa. Vinculin was used as loading control. **(b)** Quantitation of processed Keima immunoblots obtained as in (a), from the indicated biological replicates. Band values are normalised to the respective loading controls; values are expressed as fold changes Aneu/Ctrl. Mean ± SEM; n=15 (RPS3-Keima) or n=9 (RPL28-Keima); one sample t test. **(c)** Qualitative confocal live-cell images of HCT116 cells treated with Mps1 inhibitor (Aneu) or DMSO (Ctrl) and collected after 24 hours. The lysosomal degradation of ribosomes is determined by the increased amount of red-Keima puncta in cell cytoplasm; hoechst was used to stain DNA; scale bars, 50µm.

Then, I performed a more complete time-course of aneuploidy, collecting Mps1i-treated samples (and the respective DMSO-treated controls) for 72 hours every 12 hours after the treatment. This experiment was helpful to finely monitor the increase in ribophagy

concurrent with the accumulation of aneuploidy-associated stresses in the analysed populations. Indeed, the ribophagic flux seemed to perfectly correlate with the hours from Mps1i treatment (Figure 18a-b), as the previous results already suggested.

Moreover, to follow-up on the hint from the analysis at the single-cell level, I decided to titrate Mps1i concentration to generate populations of aneuploid cells with increasing degree of aneuploidy, as previously described (Santaguida et al., 2010). Interestingly, the ribophagic flux increased with increasing aneuploidy degree in the population (Figure 18c-d), confirming that the phenotype is further exacerbated when the analysed cell populations are more aneuploid.

Therefore, I concluded that the rising of aneuploidy-induced stresses triggers a selective removal of ribosomes, which in turn end up in autophagosomes and eventually in lysosomes.

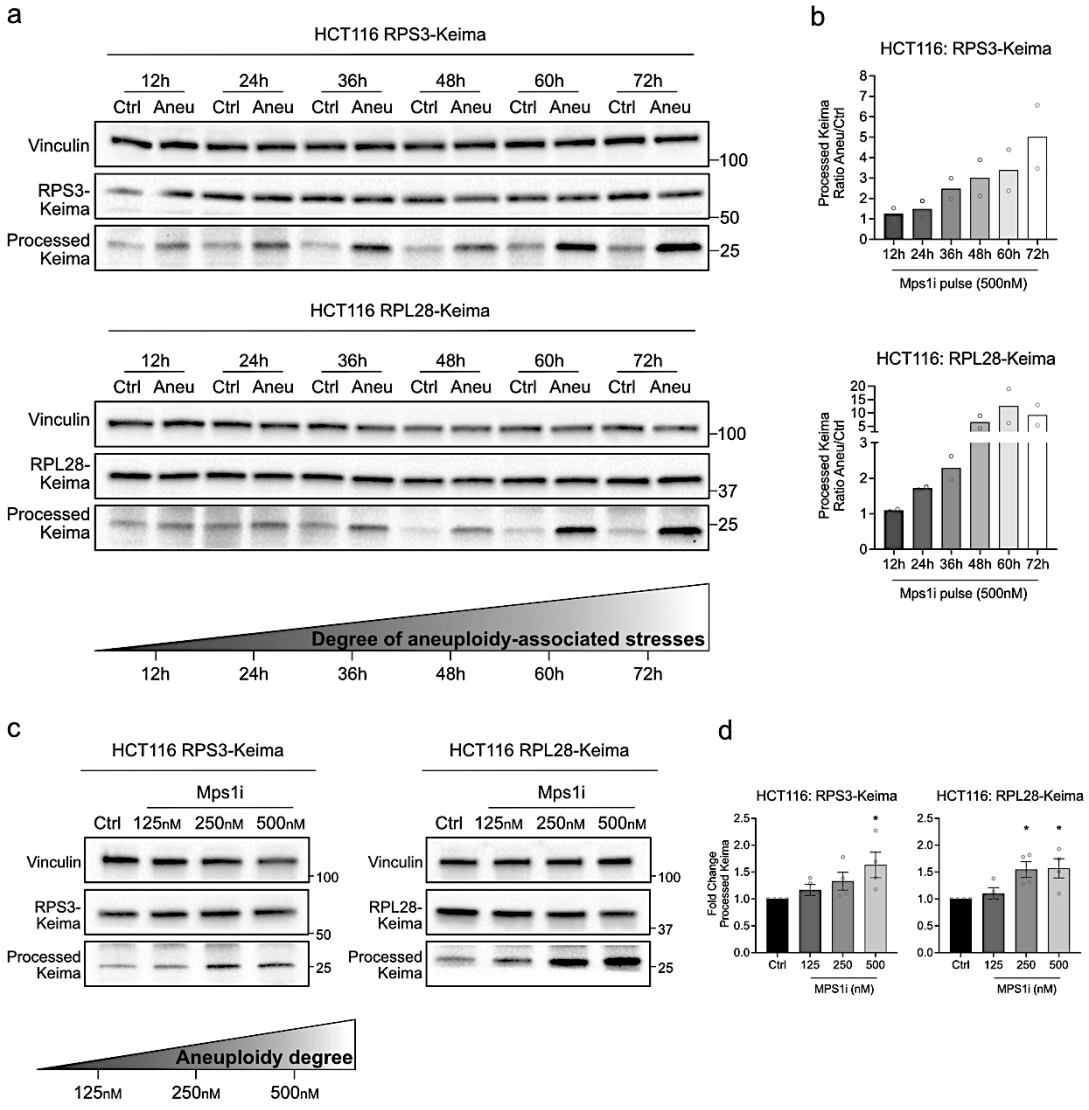

Figure 18: Aneuploid stress worsening and aneuploidy degree correlate with the onset of ribophagy.
(a) Representative immunoblots of the indicated HCT116 Ribo-Keima cell lines, treated with Mps1 inhibitor (Aneu) or DMSO (Ctrl) and collected after 12, 24, 36, 48, 60, 72 hours. Ribophagic flux is determined by the

increased level of processed Keima at 25KDa. Vinculin was used as loading control. The scheme represents the rationale of the experiment. **(b)** Quantitation of processed Keima immunoblots obtained as in (a). Band values are normalised to the respective loading controls; values are expressed as ratios Aneu/Ctrl per each time-point. Mean; n=2. **(c)** Representative immunoblots of the indicated HCT116 Ribo-Keima cell lines, treated for 24 hours with Mps1 inhibitor either 125nM, 250nM or 500nM. DMSO was used to generate the untreated control. Ribophagic flux is determined by the increased level of processed Keima at 25KDa. Vinculin was used as loading control. The scheme represents the rationale of the experiment. **(d)** Quantitation of processed Keima immunoblots obtained as in (c). Band values are normalised to the respective loading controls; values are expressed as fold changes relative to untreated control (Ctrl). Mean ± SEM; n=4; Kruskal-Wallis test, followed by Dunn's multiple comparison test.

3.2 Ribophagy occurs irrespective of the method used to generate aneuploid cells

To make sure that the ribophagic phenotype was not a specific effect of the drug that I used to generate aneuploid cells (Mps1i, namely reversine), I decided to proceed with an alternative approach. I either depleted two other SAC components, MAD2 or BUB1, with siRNA-mediated transient knock-down. I did so in both HCT116 and RPE1 RPS3-Keima cell lines. Aneuploid samples generated by individual depletion of MAD2 or BUB1 were then compared to the pseudo-diploid controls generated using non-targeting siRNAs. After checking the reduction in target components, I proceeded with the western blot analysis to detect the levels of ribophagy. In both cases and in both cell lines, the knock-down of MAD2 and BUB1 was efficient and sufficient to phenocopy the ribophagic flux already observed after the treatment with the Mps1 inhibitor (Figure 19a-b).

These data demonstrate that ribophagy occurs in aneuploid cells irrespective of the method used to induce mis-segregation. As a matter of fact, both the drug treatment to inhibit Mps1 (Mps1i) and the knock-down of MAD2 or BUB1 have the same effect on the ribophagic phenotype.

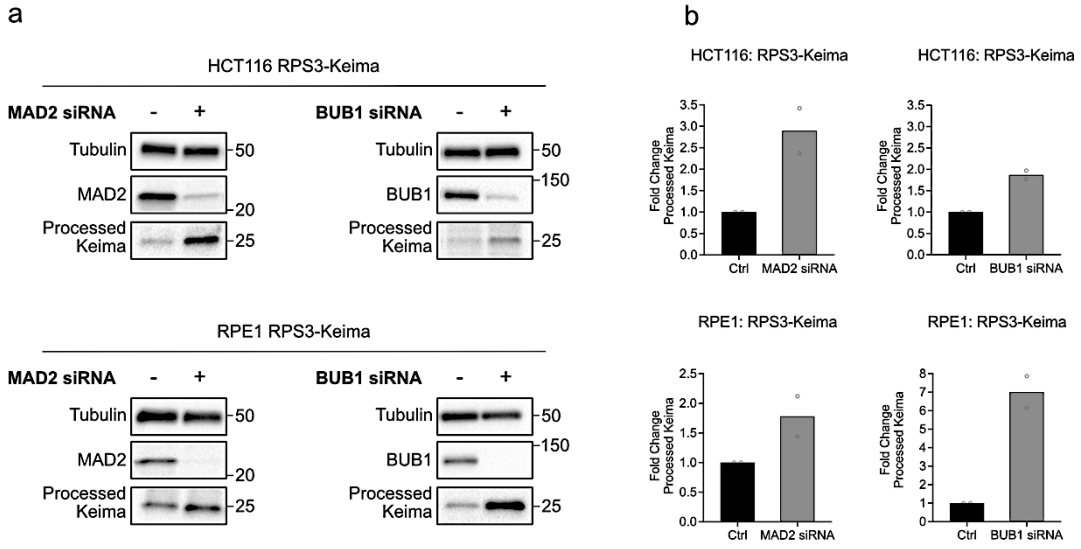

Figure 19: Ribophagy occurs irrespective of the method used to induce mis-segregation.

(a) Representative immunoblots of the indicated Ribo-Keima cell lines, in which MAD2 or BUB1 were depleted individually with siRNA-mediated transient knock-down. Samples were collected after 72 hours from transfection, a time-point that guarantees the efficient depletion of MAD2 or BUB1. Control samples were generated using non-targeting siRNAs. Ribophagic flux is determined by the increased level of processed Keima at 25KDa. Tubulin was used as loading control. **(b)** Quantitation of processed Keima immunoblots obtained as in (a). Band values are normalised to the respective loading controls; values are expressed as fold changes MAD2 siRNA/Ctrl or BUB1 siRNA/Ctrl. Mean; n=2.

3.3 Correlative light electron microscopy reveals the presence of ribosomes within autolysosomal structures

The key proof demonstrating the presence of ribosomes in autophagic structures of aneuploid cells has been provided by the correlative light electron microscopy (CLEM) technique. To directly demonstrate that ribophagy is an ongoing process in aneuploid cells, I combined the approach that exploits the reporter Keima and a high-resolution microscopy technique (EM). Keima, in fact, represented a useful and versatile tool, but indirect, since its outputs cannot demonstrate the exact presence of ribosomes in the cell autophagic structures. For this experiment I choose the RPE1 Ribo-Keima cells, since this cell type is flat and characterised by a relatively spread cytoplasmic portion. Therefore, RPE1 are more suitable for imaging techniques compared to HCT116, the morphology of which is thicker and more round-ish, with a smaller ratio cytoplasm-area/nuclear-area. For the first step of this technique, I imaged the aneuploid cells with a confocal microscope, identifying their exact position on an EM-graded grid and acquiring the nuclei (with hoechst) and the red-Keima signal (*i.e.* excited at 550nm) (Figure 20a). Those same cells were then processed for EM analysis in collaboration with Dr. Alessia Loffreda and Dr. Andrea Raimondi (Advanced Light and Electron Microscopy BioImaging Center, I.R.C.C.S. San Raffaele Hospital, Milan, Italy). This second step provided a huge resolution power to the analysis. From the correlation of the fluorescence images and the ones obtained by EM, it was possible to nicely identify the exact structures highlighted by the red-Keima signal, in this case those to the left of the nucleus (Figure 20b). A further resolution increase in those objects showed two electron-dense organelles surrounded by a single membrane (Figure 20c-d), recognised with high confidence as autolysosomal/lysosomal structures. Inside the lysosomes it was also possible to spot possibly degradative cargoes, including a large quantity of ribosomes and, in one of the two structures (right), pieces of endoplasmic reticulum membranes. Ribosomes were well recognizable thanks to the comparison with cytoplasmic membranes of intact ER, which are by definition associated with ribosomes (Figure 20e, green arrowhead).

Since the aneuploid samples for this experiment were generated to maximise the phenotype (72 hours after aneuploidy induction), it was not surprising to find also ER segments within the degradative structures. This, in fact, was in line with what was previously observed (see

Result paragraph 2.3). The high density of ribosomes inside lysosomes (left organelle and central part of the right one), however, demonstrated that ribosomes could not be encapsulated only through a bystander flux during ER-phagy. Moreover, it also helped clarify that even a random sequestration of cytoplasmic ribosomes could not, by itself, be responsible for their engulfment, since the ribosomal density in the cytoplasm was significantly lower.

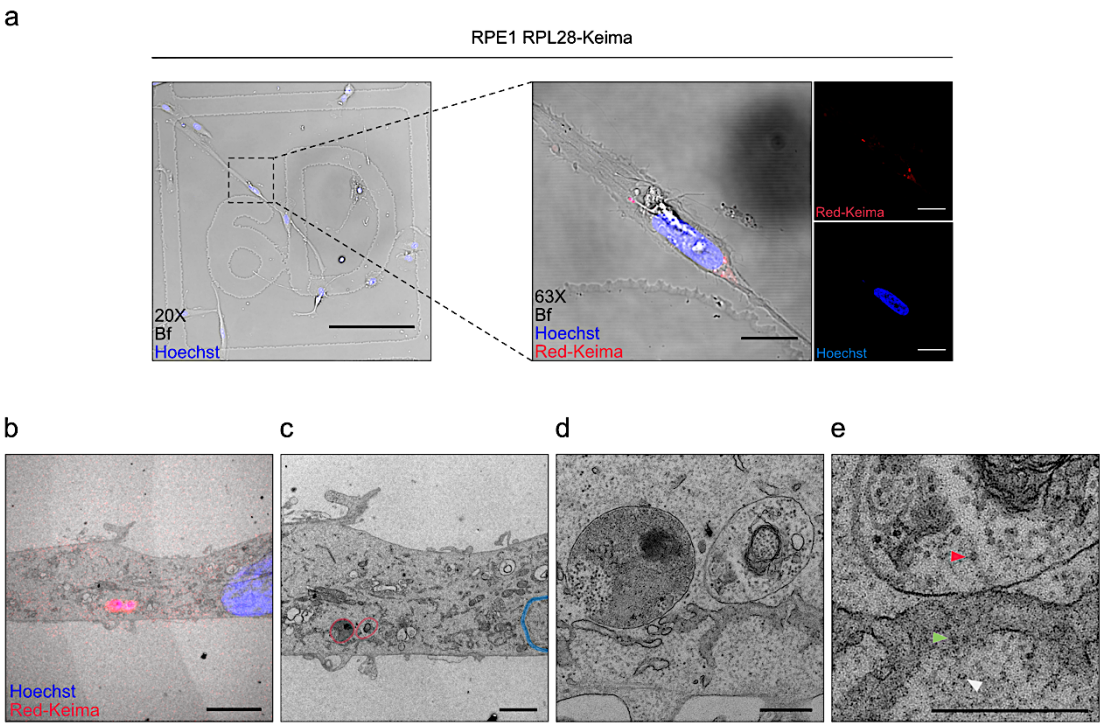

Figure 20: CLEM reveals high ribosome density within lysosomal structures.
(a) Representative confocal live-cell images of RPE1 Ribo-Keima cells treated with Mps1 inhibitor and collected after 72 hours. Hoechst was used to stain DNA; 20X image scale bar, 200μm; 63X images scale bars, 20μm. **(b)** Image of the Ribo-Keima cell in (a) (rotated of about 45°) after the alignment and merge between the images obtained with confocal microscope and electron microscope (EM). Hoechst (DNA) is in blue and red-Keima in red; scale bar, 5μm. **(c-d)** Images at higher resolution of the objects identified by red-Keima. Blue profile highlights the nucleus, while red circles the lysosomal structures; (c) scale bar, 2μm; (d) scale bar, 500nm. **(e)** Zoom on ribosomal structures. Arrowheads indicate examples of ribosomes either dispersed in the cytoplasm (white), associated with the ER (green) or engulfed in lysosomes (red); scale bar, 500nm. b-e performed by Alessia Loffreda (ALEMBIC HSR, Milan), using the samples I produced as described above.

3.4 RFP-GFP tandem construct approach confirms that aneuploid cells experience increased ribophagic flux

Next, I generated a RPE1 cell line stably expressing the fluorescent tandem construct RPS3-RFP-GFP, used as an independent reporter to monitor ribophagy. GFP and monomeric RFP (henceforth RFP) behave differently in late autophagic structures, due to their different sensitivity to the pH. In particular, GFP fluorescence is quenched in acidic conditions and it is degraded by lysosomal hydrolases. RFP fluorescence, instead, is known

to be more stable in acidic compartments (Kimura et al., 2007) (Figure 21a). I used the tandem-tagged fusion protein RPS3 (ribosomal protein of the small subunit) and RFP-GFP, to follow with this approach the localization of ribosomal proteins in the autophagic structures. I did so in aneuploid cells generated with Mps1i and analysed after about 1 or 3 cell cycles (24 or 72 hours); the results were then compared to their relative pseudo-diploid controls (treated with DMSO). The image analysis was carried out in order to obtain for each field of view of each biological replicate mean values of the ratio RFP/GFP per pixel, that was supposed to increase in conditions where the fusion protein was in autolysosomes/lysosomes (Figure 21b). The macro for the image analysis (for details, see Materials and Methods paragraph 10.2) was optimised in collaboration with Dr. Mattia Marenda (IEO imaging facility, Milan, Italy) and a threshold was applied on the ratio values to clean the results from background noise. The distribution of the ratios, normalised to the mean of the respective control samples, clearly confirmed that aneuploid cells have higher RFP/GFP ratios, compared to the pseudo-diploid ones (Figure 21c). The difference between the aneuploid sample at 24 hours and the relative pseudo-diploid control was further exacerbated in the samples at 72 hours.

These results validate the increased presence of ribosomes in lysosomal structures of aneuploid cells, which is in line with the previously observed trend of ribophagic flux.

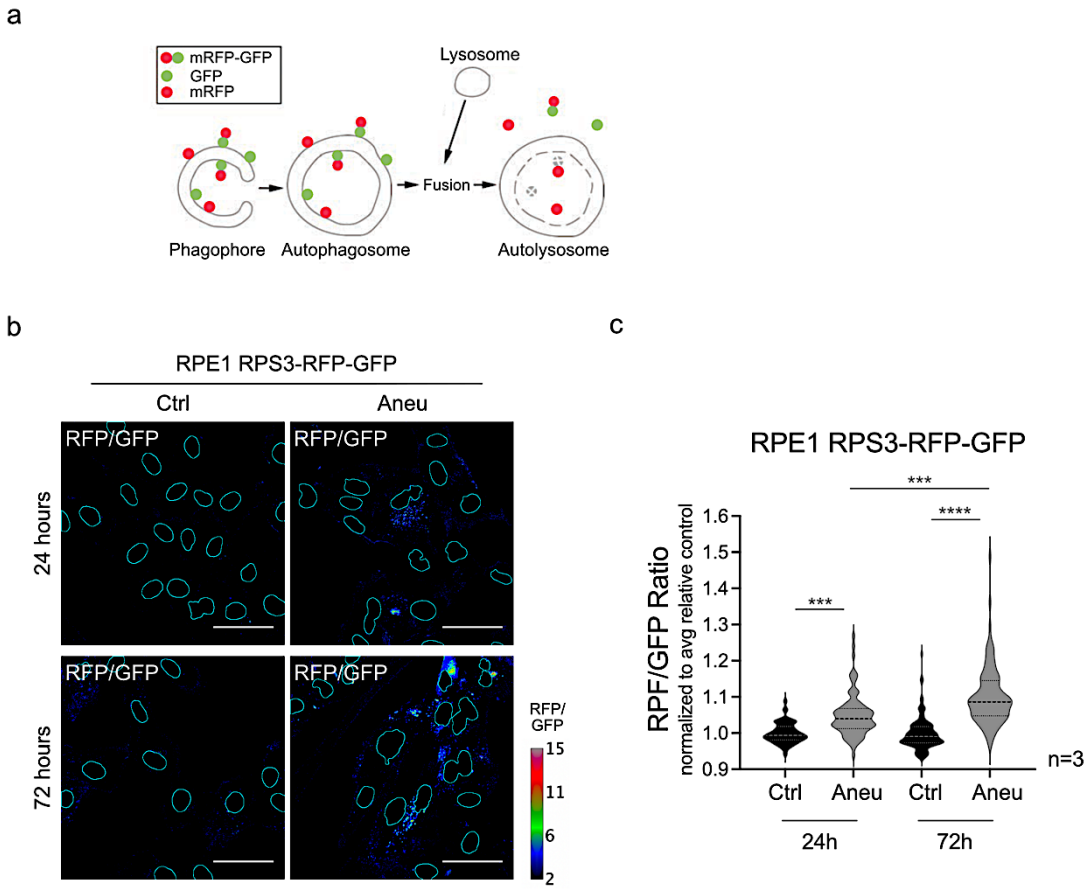

Figure 21: RPS3-RFP-GFP tandem reporter confirms ribophagy in aneuploid cells.

(a) Schematic representation of the tandem reporter RFP-GPF functioning. In early autophagic structures both GFP and RPE fluoresce, while after the fusion with lysosomes the signal from GFP is quenched and RFP can still be detected. *Adapted from (Kimura et al., 2007)*. **(b)** Representative images used for the analysis of RPE1 RPS3-RFP-GPF cells treated with Mps1 inhibitor (Aneu) or DMSO (Ctrl) and collected after either 24 or 72 hours. RFP/GFP ratio was obtained with Fiji *image calculator* function, dividing RFP channel image with GFP channel image. RFP/GFP ratios per pixel were visualised with a rainbow lookup table (calibration bar shown); applied threshold: RFP/GFP ≥ 2; cyan masks indicate primary nuclei; scale bars, 50µm. **(c)** Distribution of RFP/GFP ratios obtained with the image analysis as in (b), from three independent biological replicates. For each replicate, 30 fields of view were analysed. The mean of pixel RFP/GFP ratio for each field was plotted, after being normalised to the average mean of the respective control. Upper quartile, lower quartile and median of each violin plot are shown; n=3; Kruskal-Wallis test, followed by Dunn's multiple comparison test.

3.5 Ribophagy in aneuploid cells relies on canonical lysosomal degradation

To examine if ribophagy in aneuploid cells relies on the canonical events that succeed in the autophagic degradation pathway, I tested a panel of modulators of the established autophagy steps and then assessed their effects on the ribophagic flux. I started with mTOR inhibition using Torin1, which partially mimics starvation and is widely used to increase the autophagic flux (see Introduction paragraph 4.1.4 and ref. (Klionsky et al., 2021)). This treatment caused, as expected, a massive increase in ribophagy in control cells, that was even more exacerbated in aneuploid samples, confirming that they already display a basal ribophagic flux. The same effect emerged both from the processed-Keima western blot analysis (Figure 22a-b, top) and from the tandem reporter RFP-GFP experiment (Figure 22c-d). In addition, to block the initial steps of the autophagic pathway, I used SAR405, an inhibitor of VPS34, which is involved in phagophore and autophagosome formation (see Introduction paragraph 4.1.4 and ref. (Mizushima et al., 2010)). This condition decreased significantly the ribophagic flux in both pseudo-diploid and aneuploid cells (Figure 22a-b, centre), proving that ribosome degradation is dependent on phagophore nucleation and autophagosome formation. Finally, I treated cells with Bafilomycin A_1, an inhibitor of lysosome acidification, which blocks the last steps of autophagy (see Introduction paragraph 4.1.4 and ref. (Mizushima et al., 2010)). The decrease in processed-Keima band (Figure 22a-b, bottom) and RFP/GFP ratio (Figure 22c-d) observed upon Bafilomycin A_1 treatment further confirmed the dependency of ribophagy on lysosomal degradation.

I also demonstrated the effects of these drugs qualitatively, with live-cell imaging. Red-Keima puncta were evident in the Torin1 treated sample and homogeneously distributed in all the cells, compared to the untreated control sample (Figure 22e). On the other hand, there were no detectable puncta in the aneuploid sample treated with Bafilomycin A_1, compared to aneuploid untreated sample (Figure 22e).

Taken together, these data show that, in aneuploid cells, ribophagy of both small and large ribosomal subunits relies on lysosomal degradation taking place through canonical autophagic steps.

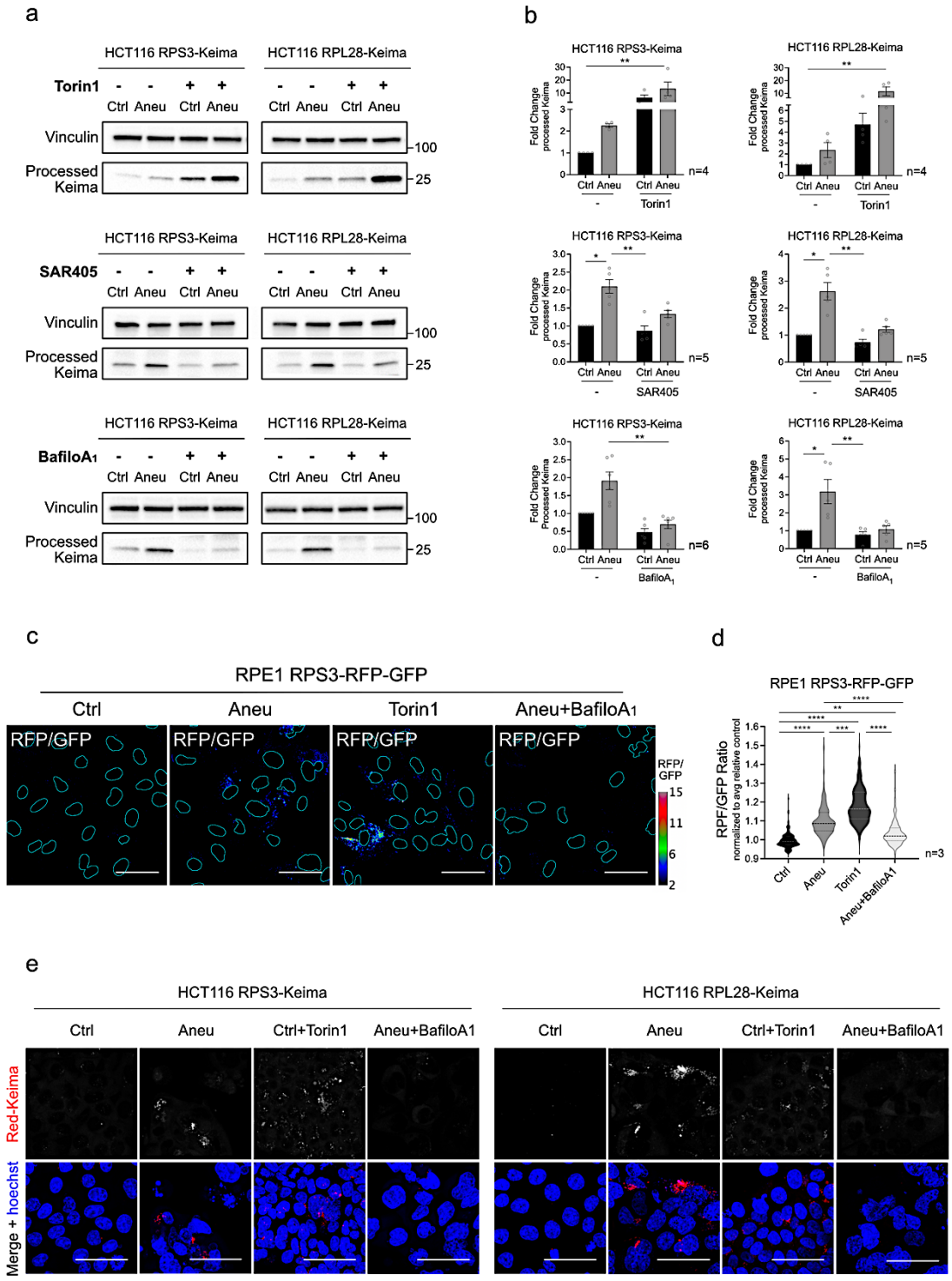

Figure 22: Ribophagy in aneuploid cells relies on canonical lysosomal degradation.

(a) Representative immunoblots of the indicated HCT116 Ribo-Keima cell lines, treated with Mps1 inhibitor (Aneu) or DMSO (Ctrl) for 24 hours. Ribophagic flux is determined by the increased level of processed Keima at 25KDa upon the indicated treatments: either Torin1 (250nM, 24h), SAR405 (1μM, 24h) or Bafilomycin A_1

(BafiloA$_1$) (100nM, 6h). Vinculin was used as loading control. **(b)** Quantitation of processed Keima immunoblots obtained as in (a), from the indicated biological replicates. Band values are normalised to the respective loading controls; values are expressed as fold changes relative to untreated controls (Ctrl). Mean ± SEM; Kruskal-Wallis test, followed by Dunn's multiple comparison test. **(c)** Representative images used for the analysis of RPE1 RPS3-RFP-GPF cells treated with Mps1 inhibitor (Aneu) or DMSO (Ctrl) and collected after 72 hours. RFP/GFP ratio, obtained as explained in Figure 21b, was determined upon either Torin1 (250nM, 24h) or Bafilomycin A$_1$ (BafiloA$_1$) (100nM, 6h) treatment. RFP/GFP ratios per pixel were visualised with a rainbow lookup table (calibration bar shown); applied threshold: RFP/GFP ≥ 2; cyan masks indicate primary nuclei; scale bars, 50µm. **(d)** Distribution of RFP/GFP ratios obtained with the image analysis as in (c), from three independent biological replicates (30 fields of view each). Data for Ctrl and Aneu samples are the same as in Figure 21c. The mean of pixel RFP/GFP ratio for each field was plotted, after being normalised to the average mean of the untreated control (Ctrl). Upper quartile, lower quartile and median of each violin plot are shown; n=3; Kruskal-Wallis test, followed by Dunn's multiple comparison test. **(e)** Qualitative confocal live-cell images of HCT116 RPS3-Keima and RPL28-Keima cells treated with Mps1 inhibitor (Aneu) or DMSO (Ctrl) for 72 hours. The lysosomal degradation of ribosomes is determined by the increased levels of red-Keima puncta upon either Torin1 (250nM, 24h) or Bafilomycin A$_1$ (BafiloA$_1$) (100nM, 6h) treatment; hoechst was used to stain DNA; scale bars, 50µm.

3.6 Lysosomal degradation of 40S is not mediated by the autophagic receptor p62

Given that the canonical steps of the autophagic pathway seemed to be involved in the lysosomal degradation of ribosomes in aneuploid cells, I then tested if also the classical receptor for the autophagic cargo, p62, mediates this selective degradation mechanism. To do this, I depleted p62 with siRNA transient knock-down (Figure 23a) and, using HCT116 Ribo-Keima cell lines, I monitored the increase in ribophagy under that condition. Unexpectedly, the two cell lines, namely the two ribosomal subunits –the small and the large– behaved differently. Whilst RPS3 (small subunit protein) degradation, on average, seemed not to be influenced by depletion of p62, RPL28 (large subunit protein) degradation was significantly decreased in that condition (Figure 23b-c), compared to the not-depleted samples.

These results suggest that the recognition of the two subunits may depend on different players. On one hand, the large subunit degradation via ribophagy seems to be mediated by the canonical autophagic receptor p62. On the other, the small subunit might require a different mechanism, even if the variability across the biological replicates (Figure 23c, left) doesn't track a consistent trend. Although these results require further investigations, they represent a promising starting point to identify the molecular actors of these selective pathways.

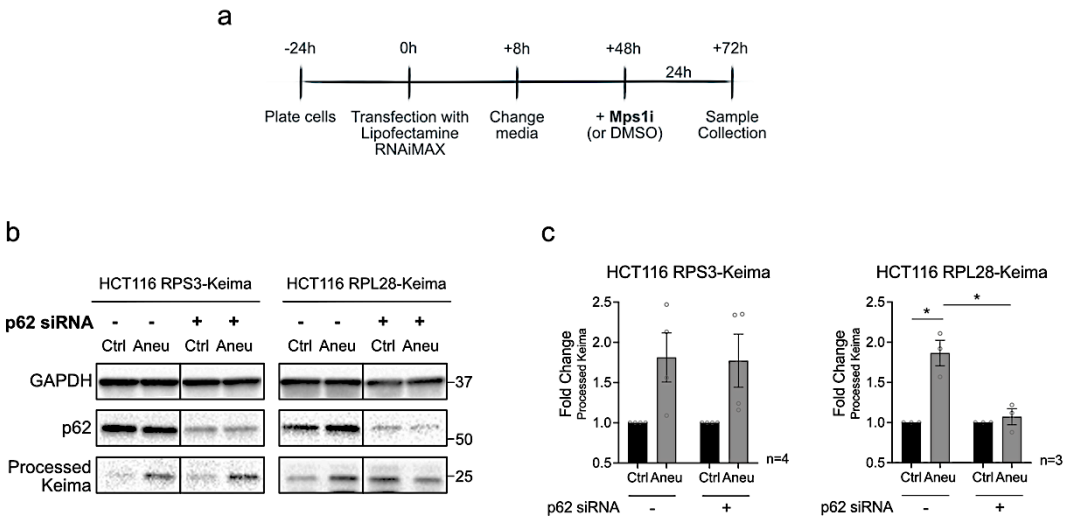

Figure 23: Lysosomal degradation of 40S is not mediated by p62 autophagic receptor.
(a) Experimental workflow for the depletion of p62 through siRNA-mediated transient knock-down. **(b)** Representative immunoblots of the indicated HCT116 Ribo-Keima cell lines, in which p62 was depleted with siRNA-mediated transient knock-down. Samples were collected after 72 hours from transfection, a time-point that guarantees the efficient depletion of p62; 24 hours before harvesting, cells were treated either with Mps1 inhibitor (Aneu) or DMSO (Ctrl) to generate aneuploid and pseudo-aneuploid samples. Controls for the transfection were generated using non-targeting siRNAs. Ribophagic flux is determined by the increased level of processed Keima at 25KDa. GAPDH was used as loading control. **(c)** Quantitation of processed Keima immunoblots obtained as in (b), from the indicated biological replicates. Band values are normalised to the respective loading controls; values are expressed as fold changes Aneu/Ctrl. Mean ± SEM; one sample t test (each Aneu *vs* respective Ctrl=1) or Student's t-test (between Aneu and Aneu-p62siRNA).

In conclusion, using different approaches to generate aneuploid cells and various techniques to monitor the degradation of ribosomes via the autophagic pathway, I have demonstrated that aneuploidy leads to ribophagy. In particular, this phenotype seems to rely on the events that characterise the canonical autophagic machinery, although it is still not clear which is the responsible autophagic receptor. Furthermore, the autophagic removal of ribosomes is exacerbated when cells experience high levels of aneuploidy-associated stresses, opening new questions about the nature of the triggering stimuli.

4. Impaired chaperone-mediated folding is involved in the autophagic removal of ribosomes

Given that aneuploid cells display various stresses, I next aimed to determine which one is most involved in the selective removal of ribosomal proteins. As already mentioned, proteotoxic stress is one of the most prominent features of aneuploidy (see Introduction paragraphs 3.2, 4.2 and ref. (Santaguida & Amon, 2015b)) and is directly involved in the overwhelming of autophagy (Santaguida et al., 2015). The accumulation of toxic aggregates

of misfolded proteins, in fact, challenges protein homeostasis and cellular fitness (see Result paragraph 1). Being chaperone-mediated folding impaired in aneuploid cells (Donnelly et al., 2014) and knowing that, together with ribosomes, chaperones are at the core of the proteome regulatory network (see Introduction paragraph 4.1.1 and ref. (Balchin et al., 2016)), I tested the implication of disrupted folding in ribosome clearance.

4.1 Hsp90 chaperone clients are impacted by impaired folding

Hsp90 is one of the most characterised heat shock protein families and coordinates the proper folding of a huge number of clients (Taipale et al., 2010). Hsp90 activity, however, has been demonstrated to be limiting in aneuploid cells (Donnelly et al., 2014). To quickly confirm that this happens also in my aneuploid system, before considering its involvement in ribophagy, I checked the protein levels of a panel of Hsp90 clients, with various cellular roles and functions. I did so in aneuploid samples generated with Msp1i treatment and compared the results with the pseudo-diploid controls and with samples treated with Geldanamycin (Geld), a selective inhibitor of Hsp90 function (Miyata, 2005). I observed a decrease in client protein levels in aneuploid cells and, interestingly, the reduction in the samples at the latest time-point (72 hours) was comparable to that obtained with the Geldanamycin treatment (Figure 24). This suggests that the impairment of Hsp90-dependent folding directly impacts its clients, most of all when aneuploid cells have time to accumulate folding stress.

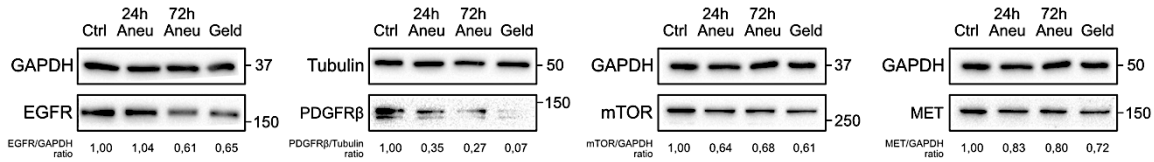

Figure 24: Hsp90 client protein levels are decreased in aneuploid cells.
Immunoblots of the indicated Hsp90 chaperone clients in RPE1 cells treated with Mps1 inhibitor (Aneu) or DMSO (Ctrl) and collected after either 24 or 72 hours. The Hsp90 inhibitor Geldanamycin (Geld) (1μM, 12h) was used as a positive control for the decreased Hsp90 client protein levels. GAPDH or Tubulin were used as loading controls. Protein level values, normalised to the respective loading control and expressed as fold changes relative to Ctrl, are shown.

4.2 Aneuploid cells in *Drosophila melanogaster* tissues are sensitive to Hsp70 depletion

I have also considered another heat shock protein family, which is strictly interconnected to Hsp90, both physically and functionally, namely Hsp70 (Balchin et al., 2016). In particular, I tested if also Hsp70 is limiting in aneuploid cells in collaboration with Prof. Marco Milán and Dr. Lara Barrio (IRB, Barcelona, Spain). In the *Drosophila melanogaster* model, in which CIN and aneuploidy are generated through the depletion of the *Bub3* SAC gene, high

levels of proteotoxic stress have been already observed (Joy et al., 2021). This was in line with the results obtained in my cellular aneuploid system (see Result paragraph 1) and, thus, we decided to follow-up on this. Interestingly, when Hsp70 was depleted through RNA interference (RNAi), aneuploid adult eyes showed a worsening of their phenotypes. Eye phenotypes can be expressed as "weak" or "strong", comparing the size and the shape (roughness) with a wild-type eye. When CIN is induced, aneuploid eyes (ey>bub3-i) already show compromised phenotypes (Figure 25a), mostly weak, due to the negative effects of aneuploidy on normal tissues. In the experiment for the evaluation of the effects of Hsp70 modulation, two Hsp70 RNAi (Hsp70Ai-42639 and Hsp70Bi-32997) resulted in more "stronger" phenotypes than the control aneuploid eye (GFP-i) (Figure 25b, top and 25c). Importantly, the over-expression of Hsp70 in aneuploid eyes significantly improved their phenotype, reducing the "strong" effects (Figure 25b, top and 25c). Conversely, in wild-type eyes, no changes in the phenotypes before and after Hsp70 depletion/over-expression were spotted (colour is not to be considered, since the used flies present a mutant background for the "white" gene) (Figure 25b, bottom). These data indicate that aneuploid eye tissue is highly sensitive to Hsp70 depletion, and the over-expression of the chaperone helps restore eye size and shape.

Another approach used in the *Drosophila* model to monitor the deleterious effects of a given phenotype is based on the quantification of apoptosis-mediated cell death in larval wing imaginal disc. After inducing aneuploidy together with a red fluorescent protein (myrTomato, MyrT, to mark the aneuploid region), an immunostaining for the cleaved effector caspase Dcp1 (homolog of human caspase-7) was performed to evaluate apoptosis. The depletion of Hsp70, with the same two RNAi of the previous experiment, caused a significant increase in the apoptotic signal in the aneuploid region (ap>myrT, bub3-i), namely an increase in the cleaved Dcp1 (cDcp1) (Figure 25d, top and 25e). This was perfectly in line with the results of the eye experiment and, actually, the over-expression of Hsp70 led to a phenotype rescue also in this context (Figure 25d, top and 25e). Hsp70 depletion and over-expression, instead, had no effect in the wild-type tissue (ap>myrT) (Figure 25d, bottom).

Together, these experiments were crucial to assess the dependency of aneuploid cells on chaperone-mediated folding, also in an *in vivo* model. The higher sensitivity of aneuploid cells to chaperone depletion indicates that they already present some issues at the folding level, which is in line with previous reports (Donnelly et al., 2014; Khan et al., 2018). Since this phenotype has been confirmed in a CIN context, it is possible to hypothesise that folding problems are common features of both stable and unstable aneuploidies, opening new interesting perspective in the field of cancer, where CIN and aneuploidy are its hallmarks (Hanahan & Weinberg, 2011; Holland & Cleveland, 2012).

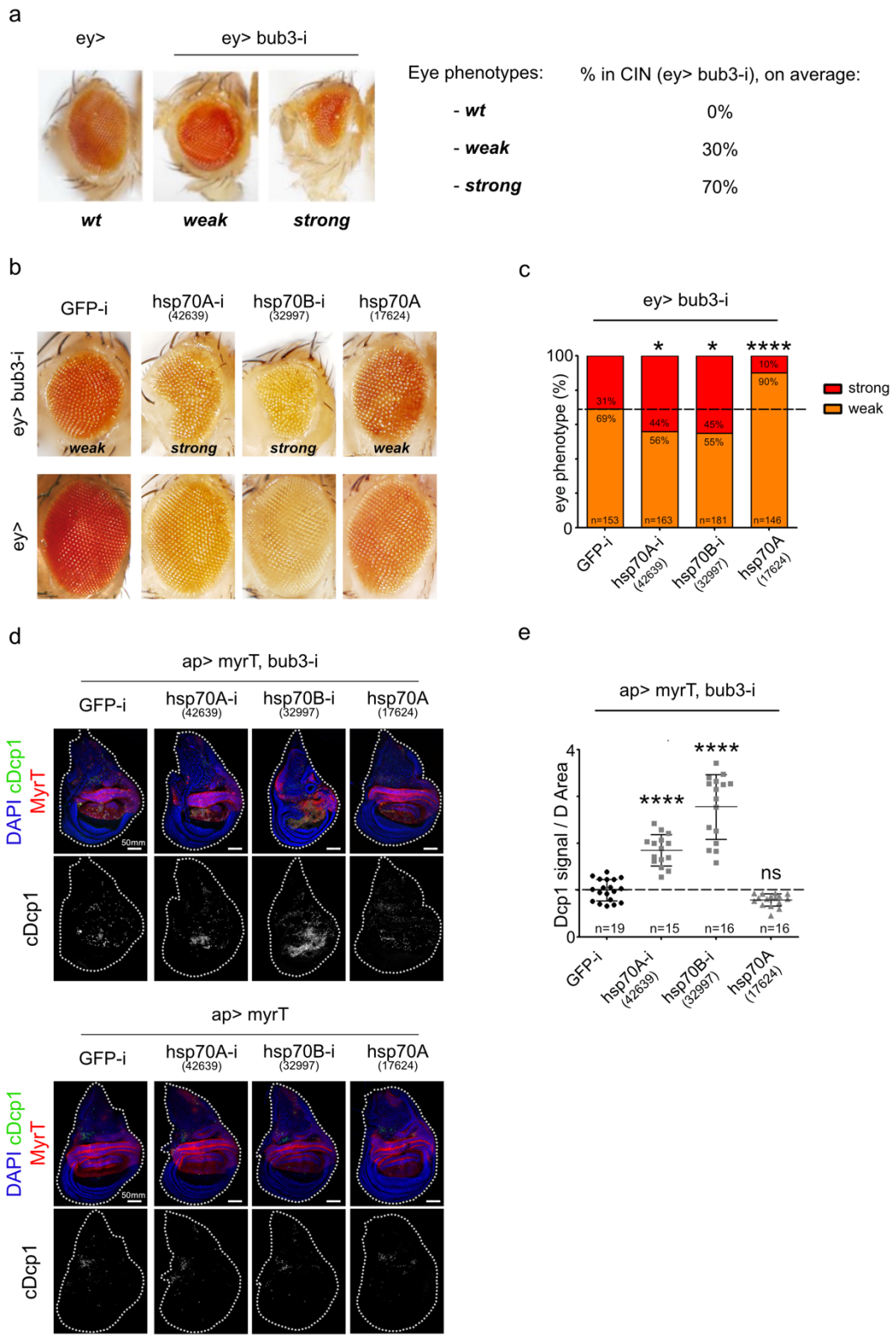

Figure 25: CIN *Drosophila* tissues are sensitive to Hsp70 depletion.

(a) Example of adult eye phenotypes after CIN induction with an eye-specific Gal4 driving bub3-RNAi (ey>bub3-i) in epithelial tissue (courtesy of Dr. Lara Barrio). Phenotypes can be divided into “weak” or “strong”, comparing the size and the shape with a wild-type eye (ey>). This approach can be used also to study the effects of Hsp70 depletion in wild-type or aneuploid adult eye, evaluating the relative differences in the number of “weak” or “strong” phenotypes, across the various conditions. **(b)** Representative adult eyes in which CIN was induced with an eye-specific Gal4 driving bub3-RNAi (ey>bub3-i) or control wild-type eyes (ey>), where the indicated

transgenes for either the depletion of Hsp70 (Hsp70A-i / Hsp70B-i) or its overexpression (Hsp70A) were expressed. **(c)** Quantification of the analysed eye phenotypes, obtained as in (b) and expressed as the percentage of each phenotype across the samples. Red indicates the "strong" phenotypes and orange the "weak" ones; number of replicates is shown on each histogram bar; Fisher's exact test. **(d)** Qualitative images of larval wing discs in which CIN was induced with an apterous-specific Gal4 driving bub3-RNAi fused with a MyrT fluorescent protein (ap>myrT, bub3-i) or control wild-type tissues (ap>myrT), where the indicated transgenes for either the depletion of Hsp70 (Hsp70A-i / Hsp70B-i) or its overexpression (Hsp70A) were expressed. Immunostaining performed with cleaved-Dcp1 (cDcp1) antibody and DAPI (to stain DNA); MyrT signal marks the aneuploid region; scale bars, 50μm. **(e)** Quantification of the area positive for cDcp1 signal, obtained as in (d) and normalised to the area of the dorsal region (D) (where ap>myrT, bub3-i is expressed) in the indicated samples. Number of replicates is shown; one-way ANOVA, followed by Dunnett's multiple comparison test (GFP-i *vs* each other sample). a-e performed by Lara Barrio (IRB, Barcelona), following the experimental design we discussed together.

4.3 Hsp90 and Hsp70 inhibition induce the autophagic removal of ribosomes

Having demonstrated with different approaches and aneuploid models that Hsp90 and Hsp70 chaperones play major roles in the proteotoxic phenotype of aneuploid cells, I proceeded with the analysis of their possible involvement on ribosome clearance. The idea was that the increased folding demand in aneuploid cells and the consequent overwhelming of Hsp90/Hsp70 folding activities would challenge the translation of new polypeptides, with also dramatic effects on the machine in charge for making proteins, *i.e.* the ribosome. To test this hypothesis, I started to inhibit the function of these two chaperone families. Firstly, I tested the effects of Geldanamycin (Geld), a selective inhibitor of Hsp90 (Miyata, 2005), using HCT116 Ribo-Keima cell lines. Geld-treated samples, interestingly, showed a significant increase in ribophagy that mimicked the levels already observed in aneuploid cells (Figure 26a-b). I have also confirmed it by treating cells with17-AAG, the clinically-active inhibitor of the same chaperone family (Miyata, 2005), to exclude that it could be a specific response to Geldanamycin treatment (Figure 26c).

Next, I used the same approach to interfere with Hsp70 as well. I treated the Ribo-Keima cells with VER-155008 (VER), which is a potent inhibitor of the Hsp70 family of chaperones (Massey et al., 2010). Also in this case, chaperone inhibition partially phenocopied the ribophagy measured in aneuploid cells, and this was true particularly for degradation of the small subunit of the ribosome (Figure 26d-e).

Importantly, the same approach on HCT116 LDHB-Keima cells did not give the same result. Indeed, bulk autophagy (*i.e.* processed Keima) was not influenced by the inhibition of Hsp90 through Geldanamycin treatment (Geld) (Figure 26f-g). This suggests that impaired chaperone activity does not trigger aspecific bulk autophagy right after aneuploidy induction, pointing out that its effect is most likely specific for ribophagy.

These data indicate that if chaperone activity, either of Hsp90 family or Hsp70 family, is inhibited in perfectly functioning pseudo-diploid cells, ribosomes are impacted as well and are degraded via the autophagic pathway. This is happening already in aneuploid cells, which are known to have an impaired chaperone-mediated folding activity.

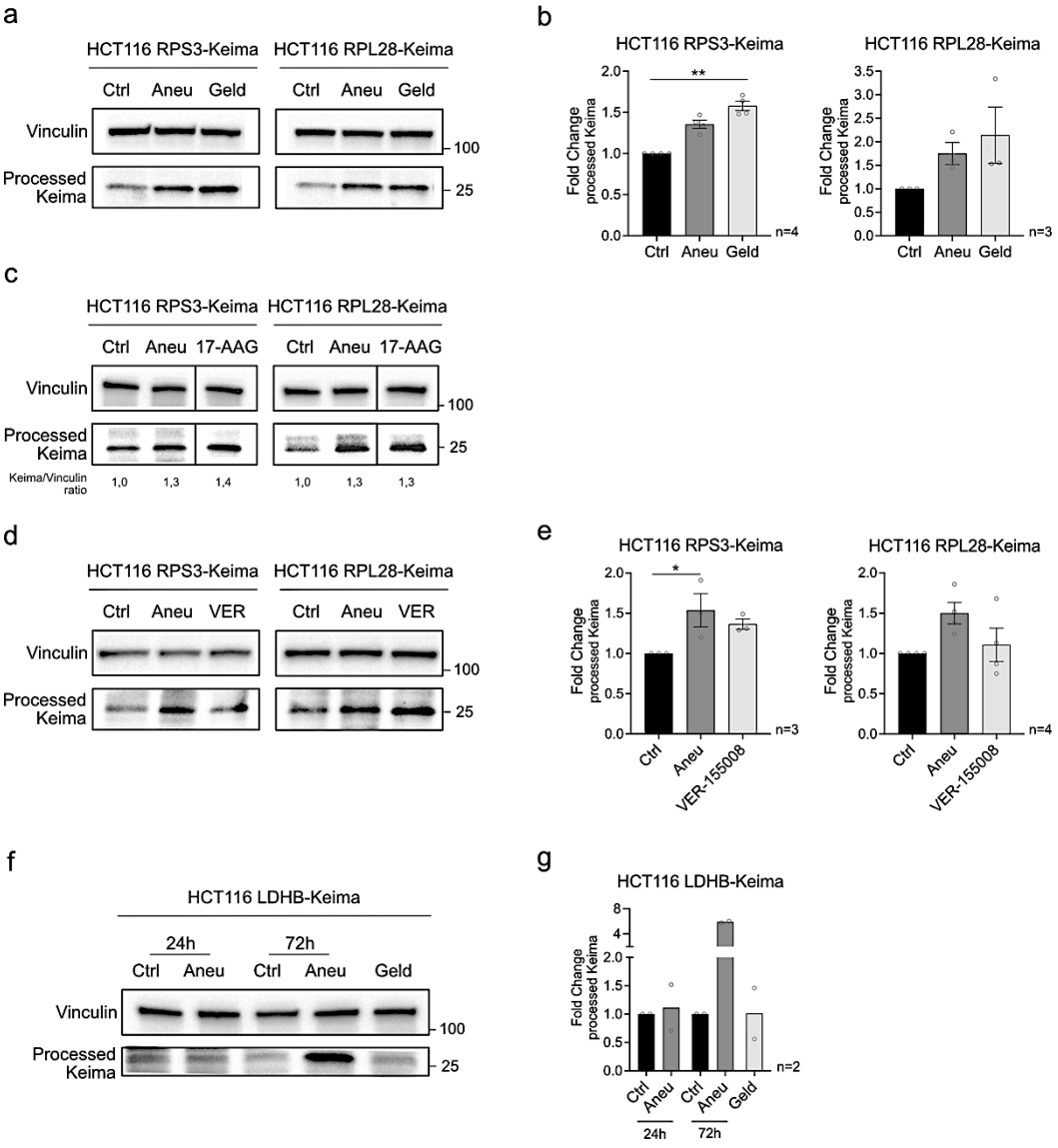

Figure 26: Hsp90 and Hsp70 inhibition induces ribophagy.

(a) Representative immunoblots of the indicated HCT116 Ribo-Keima cell lines, treated for 24 hours either with Mps1 inhibitor to generate the aneuploid samples (Aneu), DMSO for the control samples (Ctrl) or Geldanamycin (Geld, 1µM). Ribophagic flux is determined by the increased level of processed Keima at 25KDa. Vinculin was used as loading control. **(b)** Quantitation of processed Keima immunoblots obtained as in (a), from the indicated biological replicates. Band values are normalised to the respective loading controls; values are expressed as fold changes relative to Ctrl. Mean ± SEM; Kruskal-Wallis test, followed by Dunn's multiple comparison test. **(c)** Representative immunoblots of the indicated HCT116 Ribo-Keima cell lines, treated for 24 hours either with 17-AAG (1µM), Mps1 inhibitor (Aneu) or DMSO (Ctrl). Ribophagic flux is determined by the increased level of processed Keima at 25KDa. Vinculin was used as loading control. Processed Keima values, normalised to the respective loading control and expressed as fold changes relative to Ctrl, are shown. **(d)** Representative immunoblots of the indicated HCT116 Ribo-Keima cell lines, treated for 24 hours either with Mps1 inhibitor

(Aneu), DMSO (Ctrl) or VER-155008 (VER, 50μM). Ribophagic flux is determined by the increased level of processed Keima at 25KDa. Vinculin was used as loading control. **(e)** Quantitation of processed Keima immunoblots obtained as in (d), from the indicated biological replicates. Band values are normalised to the respective loading controls; values are expressed as fold changes relative to Ctrl. Mean ± SEM; Kruskal-Wallis test, followed by Dunn's multiple comparison test. **(f)** Representative immunoblot of HCT116 LDHB-Keima cells, treated for 24 hours either with Geldanamycin (Geld, 1μM), Mps1 inhibitor (Aneu) or DMSO (Ctrl). Samples collected after 72h from Mps1i/DMSO treatment were also included as positive control for the increase in bulk autophagy. Bulk autophagy flux is determined by the increased level in processed Keima at 25KDa. Vinculin was used as loading control. **(g)** Quantitation of processed Keima immunoblots obtained as in (f). Band values are normalised to the respective loading controls; values are expressed as fold changes Aneu/Ctrl or Geld/Ctrl(24h). Mean; n=2.

4.4 Restoring chaperone-mediated folding reduces ribophagy in aneuploid cells

If an impaired chaperone-mediated folding is implicated in the degradation of ribosomes, *i.e.* ribophagy, I wondered whether restoring this function would rescue this phenotype in aneuploid cells. A powerful way to modulate chaperone levels and to understand if this would have a role in the consequences of a deficient folding was to increase HSF1 activity. HSF1 is the heat shock master regulator that induces the expression of genes involved in proteostasis, first of all chaperones, including those of the Hsp90 and Hsp70 families (Zuo et al., 1995). HSF1 activity is controlled by its regulatory domain that allows the protein to be sequestered in the cytoplasm. When its function of transcription factor is required, HSF1 trimerises to translocate into the nucleus and bind DNA to induce *Hsp* genes (Hoter et al., 2019). The regulatory domain deletion, however, results in constitutive DNA binding, therefore constantly inducing the target genes (Zuo et al., 1995). Using a constitutively-active truncated HSF1 plasmid, I transiently transfected HCT116 Ribo-Keima cells (Figure 27a), in the attempt to restore the folding activity as described above. The main target chaperones were, indeed, increased. In particular, when truncated HSF1 - namely constitutively active - was expressed, Hsp70 and Hsp27 protein levels were about 2-fold and 4-fold higher than the control samples, respectively (Figure 27b-c). Hsp90 levels, however, were just slightly increased, requiring further experiments to elucidate the phenotype. Importantly, with this approach I was able to rescue the ribophagic phenotype of aneuploid cells, meaning that restoring, at least in part, their folding activity prevented the degradation of ribosomes via the autophagic pathway (Figure 27b-c).

As an alternative approach to increase the levels of Hsp90, I transiently over-expressed Hsp90 itself with a hemagglutinin (HA) tag (Figure 27a). In this condition, ribophagy substantially decreased in aneuploid cells, highlighting the involvement of this chaperone family too in the induction of the ribophagic phenotype (Figure 27d-e).

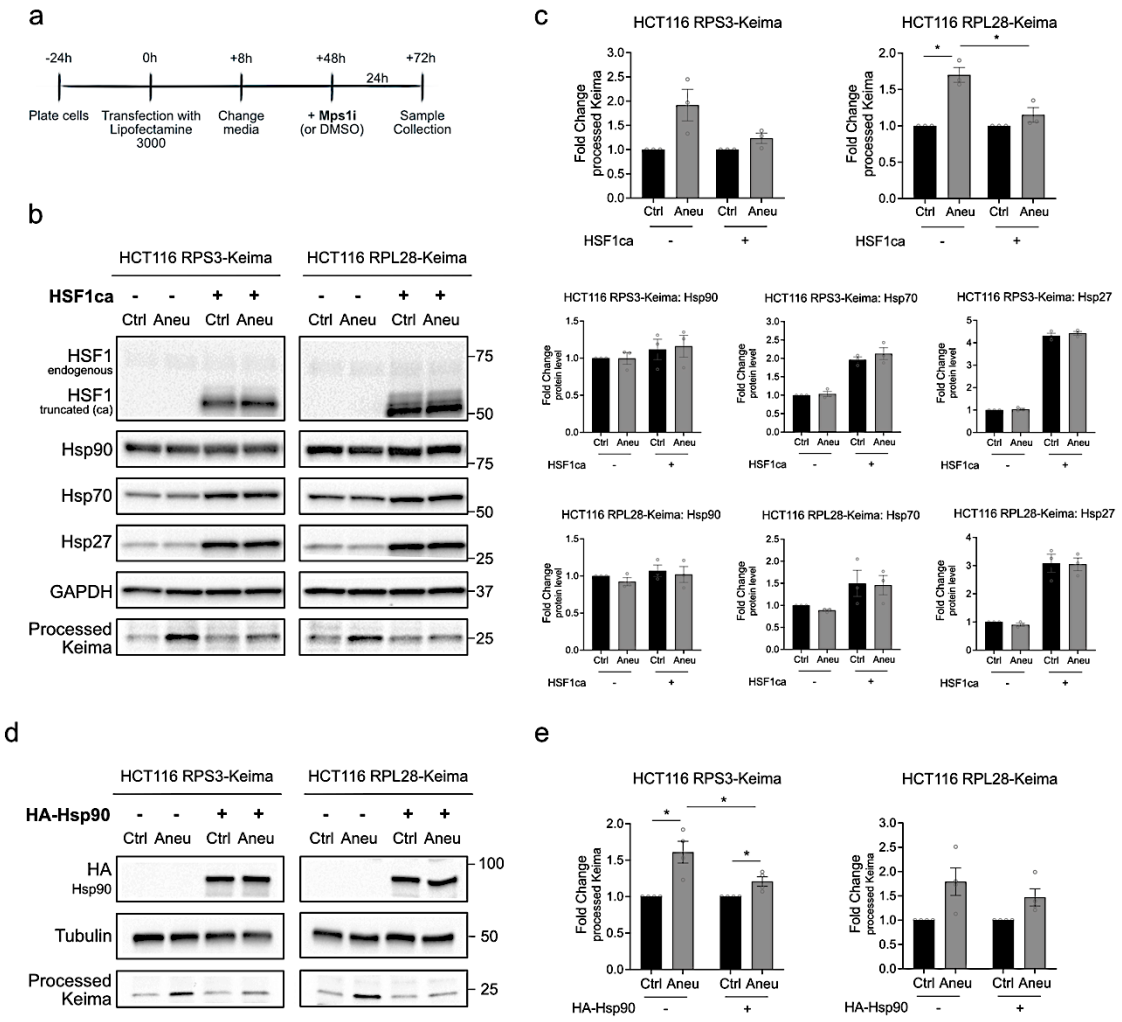

Figure 27: Chaperone induction and over-expression reduce ribophagy in aneuploid cells.

(a) Experimental workflow for the transient expression of either HSF1ca or Hsp90-HA plasmids. **(b)** Representative immunoblots of the indicated HCT116 Ribo-Keima cell lines, in which HSF1ca was expressed. Samples were collected after 72 hours from transfection, a time-point that guarantees the efficient expression of HSF1ca; 24 hours before harvesting, cells were treated either with Mps1 inhibitor (Aneu) or DMSO (Ctrl) to generate aneuploid and pseudo-aneuploid samples. Controls for the transfection were generated using the empty backbone vector. Ribophagic flux is determined by the increased level of processed Keima at 25KDa. GAPDH was used as loading control. **(c)** Quantitation of processed Keima immunoblots and indicates Hsps protein levels obtained as in (b). Band values are normalised to the respective loading controls; processed Keima values are expressed as fold changes Aneu/Ctrl, while Hsps values are expressed as fold changes relative to empty-Ctrl. Mean ± SEM; n=3; for processed Keima, one sample t test (each Aneu *vs* respective Ctrl=1) or Student's t-test (between Aneu-empty and Aneu-HSF1ca); for Hsps, Kruskal-Wallis test, followed by Dunn's multiple comparison test. **(d)** Representative immunoblots of the indicated HCT116 Ribo-Keima cell lines, in which Hsp90-HA was over-expressed. Samples were collected after 72 hours from transfection, a time-point that guarantees the efficient over-expression of Hsp90-HA; 24 hours before harvesting, cells were treated either with Mps1 inhibitor (Aneu) or DMSO (Ctrl) to generate aneuploid and pseudo-aneuploid samples. Ribophagic flux is determined by the increased level of processed Keima at 25KDa. Tubulin was used as loading control. **(e)** Quantitation of processed Keima obtained as in (d). Band values are normalised to the respective loading controls; processed Keima values are expressed as fold changes Aneu/Ctrl. Mean ± SEM; n=4; one sample t test (each Aneu *vs* respective Ctrl=1) or Student's t-test (between Aneu-empty and Aneu-Hsp90-HA).

Altogether, these experiments demonstrate that aneuploid cells suffer chaperone overwhelming, confirming the role of chaperone decreased activity in inducing proteotoxic stress. Furthermore, they show that the impaired chaperone-mediated folding in aneuploid cells is specifically involved in the autophagic removal of ribosomes, although the exact molecular mechanism and chain of events need to be elucidated.

5. Aneuploidy impacts global protein synthesis and translation efficiency

The previous results argued that chaperone overwhelming leads to the degradation of ribosomes via autophagy. The principal contact point of these two elements, chaperones and ribosomes, occur at the translation level, where they strictly interact to ensure new-protein quality control and to maintain proteome homeostasis (Pechmann et al., 2013). This raised the possibility that, if cells struggle with folding newly synthesised polypeptides, they would slow down protein production itself, to alleviate the quality control systems and avoid conspicuous waste of energy. This would be in line with previous observations, which reported a crucial role of a disrupted folding environment in pausing of protein synthesis at early elongation (B. Liu et al., 2013).

5.1 Aneuploid cells show reduced global protein synthesis rates

To investigate this hypothesis, I firstly assessed the rates of protein production in aneuploid cells, compared to the pseudo-diploid counterpart. I measured global protein synthesis employing a non-radioactive labelling method, the SunSET (Surface Sensing of Translation) assay (Goodman & Hornberger, 2013), which consists in puromycin incorporation into newly synthetised polypeptides. Puromycin is a structural analogue of the tyrosyl tRNA, which normally presents a hydrolysable ester bond between the tRNA ribose moiety and the attached amino acid molecule. Puromycin, instead, contains a non-hydrolysable amide bond and this chemical difference causes the release of truncated puromycin-bound-peptide from the ribosome (Figure 28a). Hence, this antibiotic labels new polypeptides with good fidelity and dynamic range. Protein synthesis rates, then, can be determined by detecting puromycin via immunoblot, with an anti-puromycin antibody. By employing this method and incubating cells for 30 minutes with the compound, I found out that aneuploid samples incorporated less puromycin than control cells (Figure 28b-c). This confirmed that aneuploidy negatively impacts the production of proteins. From the experimental point of view, I produced a negative control treating cells with cycloheximide (CHX), a compound that is known to inhibit translation elongation (Schmidt et al., 2009). As expected, in this condition no- or faint- puromycin smear was detected after immunoblot analysis (Figure 28b), confirming the reliability of the assay in my hands.

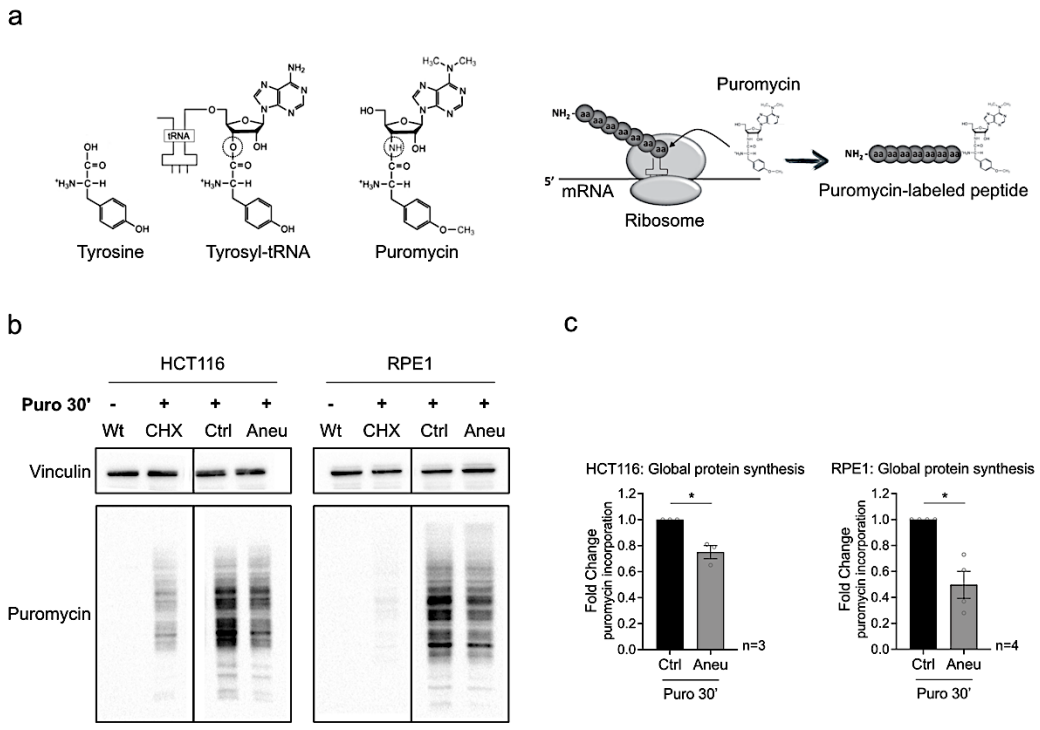

Figure 28: Aneuploid cells show reduced global protein synthesis rates.

(a) Schematic representation of puromycin structure and its mechanism of action as a strategy for the measurement of global protein synthesis. *Adapted from (Goodman & Hornberger, 2013)*. **(b)** Representative immunoblot of indicated cell lines, treated with Mps1i (Aneu) or DMSO (Ctrl) for 24 hours (HCT116) or 72 hours (RPE1) and analysed upon SUnSET assay. Global protein synthesis is determined by the level of puromycin incorporated into newly synthesised polypeptides, over 30 minutes. Treatment with cycloheximide (CHX) (10µg/mL, 6h) was used as a negative control; vinculin was used as loading control. **(c)** Quantitation of puromycin immunoblots (smear) obtained as in (b) from the indicated biological replicates. Smear values are normalised to the respective loading controls; values are expressed as fold changes Aneu/Ctrl. Mean ± SEM; one sample t test.

5.2 Protein synthesis reduction correlates with aneuploid stress onset and aneuploidy degree

To further characterise this phenotype in relation to aneuploidy, I performed the SunSET assay in a time-course of aneuploid samples and control samples (generated with Mps1i/DMSO 24, 48 or 72 hours). With this approach I wanted to check if the reduction in protein synthesis correlated with accumulation of aneuploidy-associated stresses. Indeed, aneuploid cells at late time-points (48 hours and 72 hours), which had time to develop more severe stresses, showed a significant decrease in protein synthesis rates, compared to the respective controls (Figure 29a-b).

Knowing that one of the prominent characteristics of aneuploid cells is the folding stress, I have also treated pseudo-diploid samples with the chaperone inhibitor Geldanamycin (Geld) and I looked at the global protein synthesis rates with the SunSET assay, once again.

When folding homeostasis was challenged, indeed, also pseudo-diploid cells exhibited less puromycin incorporation, which was even lower of that observed in the aneuploid sample (Figure 29c-d). Aneuploid cell incorporation levels could not be expected to decrease as much as those of Geld-treated samples, simply because the former continue cycling in culture, even if at lower rates, and still present a residual folding capacity, even if decreased compared to the untreated pseudo-diploid counterpart. The correlation between proteotoxic stress and protein synthesis attenuation is in line with previous studies (B. Liu et al., 2013).

Given that immunoblot is the SunSET most reliable analysis method, results coming from this assay are representative of the entire population that has been analysed. In the case of a heterogeneous population, as the one I considered in my experiments on aneuploidy, the risk was a “buffering” of the phenotype coming from the aneuploid cells. The next experiment I conducted to better correlate translation slowdown and aneuploidy was based on the titration of the Mps1 inhibitor that, as already mentioned, generates more aneuploid cells in the treated population as its concentration increases (Santaguida et al., 2010). The consequence of higher Mps1i concentration was, indeed, a decrease in protein synthesis (Figure 29e-f), indicating that a population with more aneuploid cells shows, on average, more limitations in the rate of new protein synthesis.

Interestingly, with these approaches I noticed that the trends of protein synthesis anticorrelated with the previously-observed ribophagic phenotype, upon increasing or decreasing the aneuploidy degree of the analysed populations. Hence, it is plausible that aneuploid cells reduce translation rate to match their impaired folding capacity, with implications for the slowed-down ribosomes.

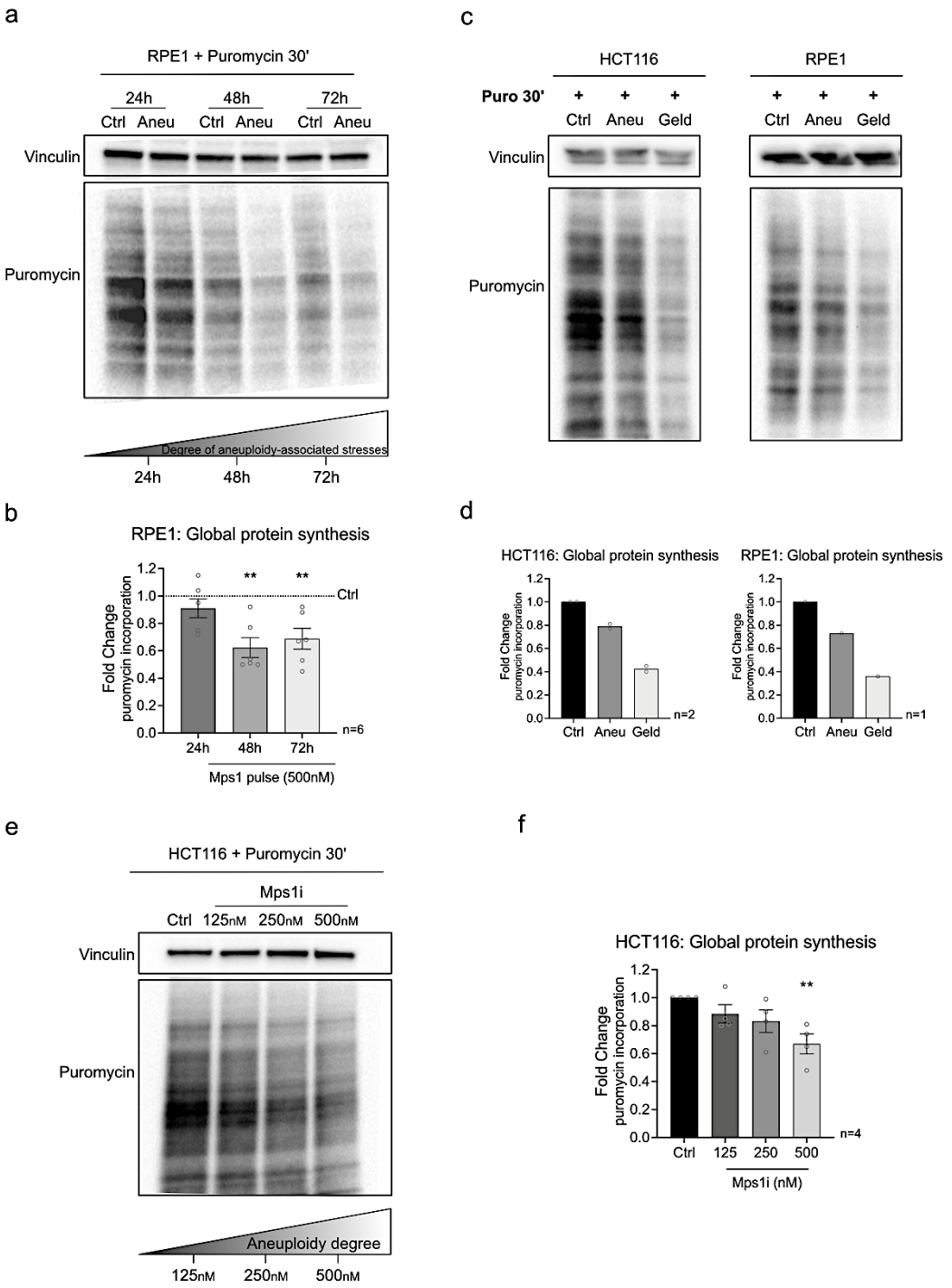

Figure 29: Protein synthesis reduction correlates with aneuploid onset and aneuploidy degree.

(a) Representative immunoblot of RPE1 cells, treated with Mps1 inhibitor (Aneu) or DMSO (Ctrl) and collected after 24, 48, 72 hours. Global protein synthesis is determined by the level of puromycin incorporation over 30 minutes. Vinculin was used as loading control. The scheme represents the rationale of the experiment. **(b)** Quantitation of puromycin immunoblots (smear) obtained as in (b). Smear values are normalised to the respective loading controls; values are expressed as fold changes Aneu/Ctrl. Mean ± SEM; n=6; one sample t test (Aneu at each time-point *vs* respective Ctrl=1). **(c)** Representative immunoblot of indicated cell lines, treated with either Geldanamycin (Geld, 500nM, 24h), Mps1i (Aneu) or DMSO (Ctrl) for 24 hours (HCT116) or 72 hours (RPE1) and analysed upon SUnSET assay. Global protein synthesis is determined by the level of puromycin incorporation over 30 minutes. Vinculin was used as loading control. **(d)** Quantitation of puromycin immunoblots obtained as in (c) from the indicated biological replicates. Smear values are normalised to the respective loading

controls; values are expressed as fold changes relative to Ctrl. Mean. (HCT116) and n=1 (RPE1). **(e)** Representative immunoblot of HCT116 cells, treated for 24 hours with Mps1 inhibitor either 125nM, 250nM or 500nM. DMSO was used to generate the untreated control. Global protein synthesis is determined by the level of puromycin incorporation over 30 minutes. Vinculin was used as loading control. The scheme represents the rationale of the experiment. **(f)** Quantitation of puromycin immunoblots (smear) obtained as in (e). Smear values are normalised to the respective loading controls; values are expressed as fold changes relative to untreated control (Ctrl). Mean ± SEM; n=4; Kruskal-Wallis test, followed by Dunn's multiple comparison test.

5.3 Aneuploidy impacts translation efficiency

I also took advantage of an independent and complementary translation assay, based on the analysis of polysome profiling. This technique allows for the evaluation of mRNA engagement with the translational machinery, by studying the sedimentation of cell lysate components in a sucrose gradient. Single ribosome subunits (either 40S or 60S), monosomes (80S) and poorly translated mRNAs accumulate near the top of the gradient, while actively translated mRNAs (associated in polysomes) sediment to the bottom (Figure 30a). In collaboration with Dr. Gabriella Viero lab (Institute of Biophysics, CNR Unit, Trento, Italy) the profiles of aneuploid and pseudo-diploid RPE1 cells were analysed (Figure 30b, top). The validation of the technique was given by the co-sedimentation profiles via immunoblot on the fractions obtained from the sucrose gradient. From them, it was clear that a ribosomal protein from the large subunit (RPL26) was mostly present in the 4th and 5th fractions (corresponding to the 60S and 80S, respectively), while a small subunit protein (RPS6) was enriched in the 3rd and 5th fractions (40S and 80S), as expected (Figure 30b, bottom). Then, from the polysome profiles obtained with aneuploid and control cell lysates, the fraction of ribosomes engaged in polysomes (FRP) was calculated. This function depends on two different factors, the area underlying the curve of polysomes and the area under the 80S peak and it is calculated as the ratio of the former and the sum of the same plus the latter (Figure 30a). The obtained results argued that aneuploid cells have a lower FRP, namely a significantly reduced efficiency in recruiting ribosomes in polysomes, compared to the euploid counterpart (Figure 30c). Then, to understand which factor was primarily responsible for this phenotype, the relative distribution of component absorbances was compared. The analysis indicated that aneuploid cells do not exhibit significant problems in the production of the ribosomal subunits, or in the assembly of the 80S, but have issues at the level of polysomes (Figure 30d). Typically, an increase in the 80S and a decrease in the polysome fraction suggest translation inhibition, while an increase in polysomes and FRP values occurs during upregulation of translation.

Together with the puromycin incorporation data, these results confirm that aneuploidy *per se* causes translation deficiency and, in particular, polysome profiling reveals a defective loading of ribosomes on polysomes. This observation could be in line with early elongation pausing caused by proteotoxic stress, which has been shown to induce ribosomal pausing and -with high probability- obstruction of the following ribosome trail (B. Liu et al., 2013).

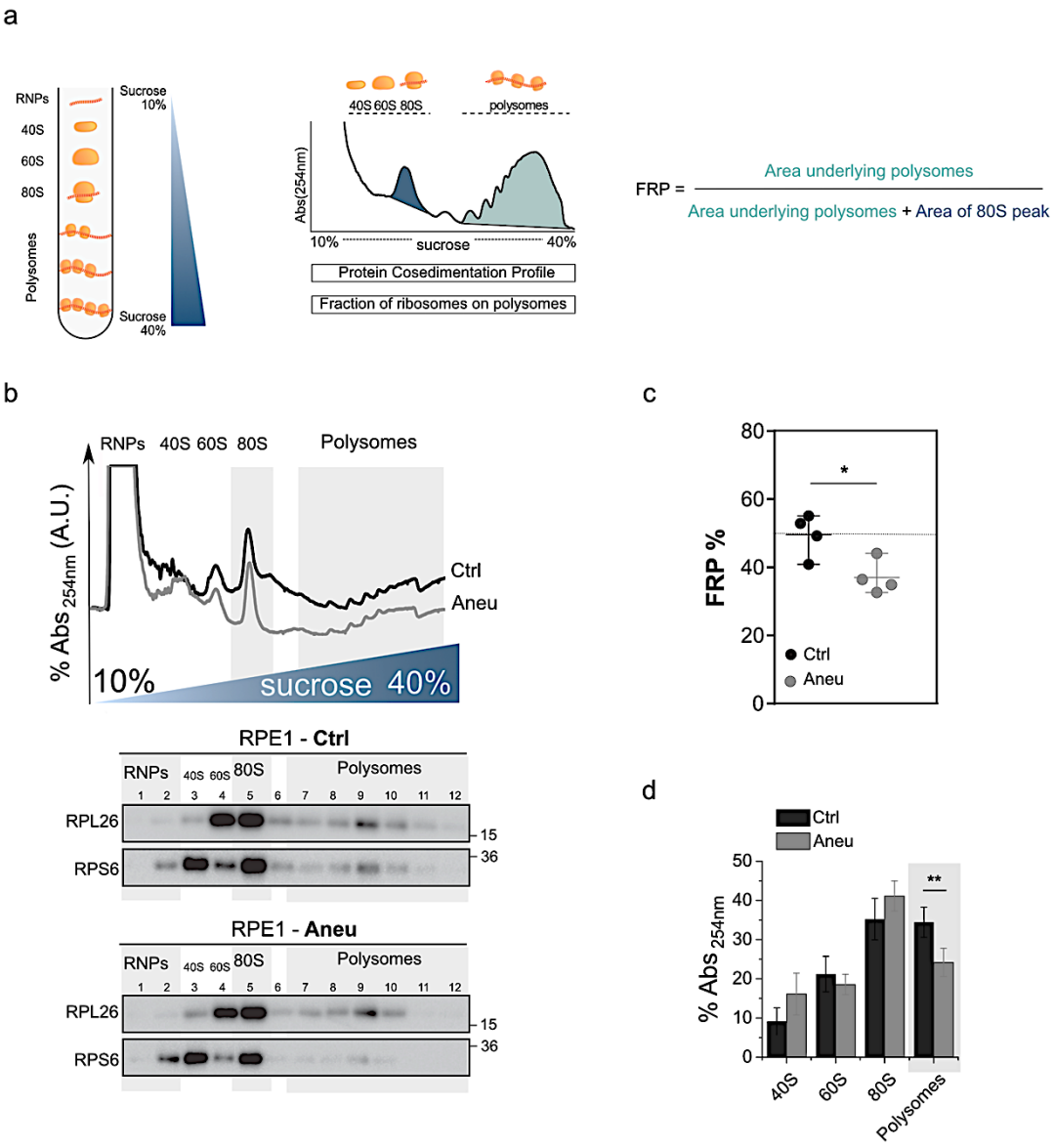

Figure 30: Polysome profiling indicates that aneuploidy impacts translation efficiency.

(a) Schematic representation of the polysome profiling technique: mRNA engagement with the translational machinery is determined by polysome sedimentation in 10-40% sucrose gradient (left). Schematic description of the function to calculate the fraction of ribosomes in polysomes (FRP) as $Area_{(polysomes)}$ / ($Area_{(polysomes)}$+$Area_{(80S)}$). *Adapted from (Bernabò et al., 2017)* (right). **(b)** Representative sucrose gradient absorbance profiles (top) obtained from the cytoplasmic lysates of RPE1 treated either with Mps1i (Aneu) or DMSO (Ctrl) and analysed after 72 hours. Representative immunoblot for the co-sedimentation profiles of two ribosomal subunit markers (RPL26 and RPS6) (bottom). **(c)** Comparison between the fraction of ribosomes in polysomes (FRP) in aneuploid and control samples. FRP values were calculated from the profiles obtained as in (b), with the function described in (a). Mean ± SD; n=4; t test. **(d)** Quantitation of the relative absorbance distribution of each component in aneuploid and control samples obtained as in (b). Mean ± SD; n=4; t test (Aneu *vs* Ctrl). b-d performed by Gabriella Viero (CNR, Trento), using the samples I produced as described above.

5.4 Global protein synthesis reduction is in agreement with UPR activation and stress granules accumulation in aneuploid cells

The reduction in protein synthesis rates is also a widely recognised consequence of stress response activation, first of all the unfolded protein response (UPR). The phosphorylation of eIF2α by stress kinases, in fact, prevents the formation of the translation initiation complex and reduces global protein synthesis (see Introduction paragraph 4.1.2 and ref. (Walter & Ron, 2011)). Since aneuploid cells showed a slight activation of UPR (see Result paragraph 1.2), their impaired translation rates might be partially due to this phenotype. UPR-mediated eIF2α phosphorylation is known to block translation initiation, rather than blocking elongating polysomes.

One way to check if also translation initiation might be negatively affected was investigating the formation of stress granules (SG) (Kedersha et al., 2002). As a matter of fact, SG are considered as cytoplasmic "storages" that temporarily protect stalled mRNAs with RNA-binding proteins, as well as factors of the pre-initiation complex (Decker & Parker, 2012; Panas et al., 2016). I have addressed this question by immunostaining aneuploid cells and the pseudo-diploid counterpart for the mRNA-binding protein G3BP1, a known marker of SG (Figure 31a). Aneuploid samples were generated at the time-point that previously showed lower translation rates (72 hours), to increase the possibility of spotting these structures. Interestingly, the percentage of cells presenting stress granules was higher in aneuploid cells, compared to that of pseudo-diploid ones, although the phenotype was not homogeneously distributed in all the imaged cells (Figure 31a and 31b, first two samples). As positive controls, I have treated both pseudo-diploid and aneuploid samples with sodium arsenite ($NaAsO_2$), which is a strong inducer of phospho-eIF2α and, therefore, stress granules assembly (B. Liu et al., 2013). When cells were incubated for 30 minutes with the compound, almost all of them, both aneuploid and pseudo-diploid, presented lots of stress granules (Figure 31a and 31b, last two samples). With a 10-minute treatment, instead, the percentage of pseudo diploid cells was comparable to that of the untreated ones, while the aneuploid cells with stress granules were much more, further exacerbating the difference already spotted in the untreated samples (Figure 31a and 31b, samples in the middle). This result supports the idea that aneuploid cells already suffer from translational stress under basal conditions and are, therefore, more sensitive to $NaAsO_2$ treatment. To complete the analysis of the stress granules, in collaboration with Chiara Soriani (IEO imaging facility, Milan, Italy) who implemented the macro script for Fiji (for details, see Materials and Methods paragraph 10.1), the number of SG per cell and the mean area of SG in each sample were also considered, but, unfortunately, no appreciable changes were observed (Figure 31c-d).

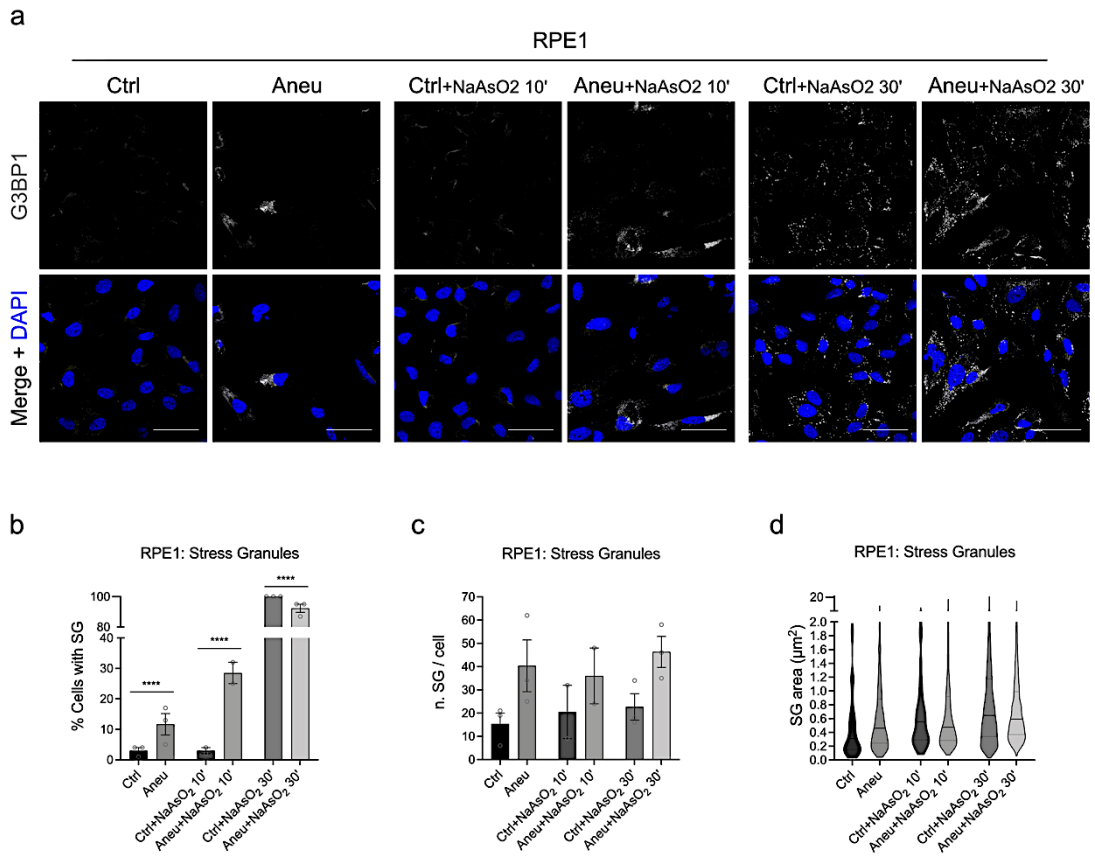

Figure 31: Stress granules accumulation in aneuploid cells.

(a) Representative confocal images of RPE1 cells treated with Mps1 inhibitor (Aneu) or DMSO (Ctrl) and collected after about 3 cell cycles (72 hours). $NaAsO_2$ (500µM, 10 or 30 minutes, as indicated) was used to produce positive controls. Immunofluorescence analysis performed with G3BP1 antibody and DAPI (to stain DNA); scale bars, 50µm. **(b)** Percentage of cells with stress granules (SG) from immunofluorescence as in (a). Data are from three biological replicates (Ctrl/Aneu and Ctr/Aneul+$NaAsO_2$30') or from two biological replicates (Ctr/Aneul+$NaAsO_2$10') and >100 cells were analysed per each replicate. Mean ± SEM; Fisher's exact test. **(c)** Quantitation of number of stress granules (SG) per cell from immunofluorescence as in (a). Data are from three biological replicates (Ctrl/Aneu and Ctr/Aneul+$NaAsO_2$30') or from two biological replicates (Ctr/Aneul+$NaAsO_2$10') and >100 cells were analysed per each replicate. Mean ± SEM; Kruskal-Wallis test, followed by Dunn's multiple comparison test. **(d)** Distribution of stress granules (SG) area (μm^2) from immunofluorescence as in (a). Data are from three biological replicates (Ctrl/Aneu and Ctr/Aneul+$NaAsO_2$30') or from two biological replicates (Ctr/Aneul+$NaAsO_2$10'). Upper quartile, lower quartile and median of each violin plot are shown.

The results presented here clearly demonstrate that aneuploidy impacts global protein synthesis and impairs translation efficiency. This seems to happen, at least partially, at the translation initiation level, as indicated by SG assembly and phospho-eIF2α-mediated UPR activation. On the other hand, aneuploid cell chaperone overwhelming and previous studies (B. Liu et al., 2013) suggest that translation might be slowed down during early elongation stages, to alleviate the folding stress.

6. The E3-ligase ZNF598 mediates the autophagic removal of ribosomes in aneuploid cells

As ribosomes have been described to carry out also a central role in tuning translation since they are able to sense a deficient folding environment (B. Liu et al., 2013), I wondered if this function might have negative consequences for ribosomes themselves in chronic stress conditions. Early elongation pausing orchestrated by ribosomes in response to folding stress results, most likely, in a pileup of ribosomes in the first region of the transcript. This condition would cause a decrease in inter-ribosome distance in that region, increasing the probability of collision events (Collart & Weiss, 2019). If this situation is transient, translation can resume, once the stress has been alleviated. Whilst, when the collision lasts for a sufficiently long time, downstream events of ribosome-associated quality control (RQC) are triggered (Zhao et al., 2019). Typically, ribosomes involved in slowdown or collisions are dissociated from the transcript and recycled (Joazeiro, 2019). The recognition of collided ribosomes and translation slowdown is guaranteed by the E3-ligase ZNF598, which normally ubiquitylates the collided ribosomes to initiate RQC. The most characterised ubiquitylation events on ribosomal subunits have regulatory functions (RRubs) (Garshott et al., 2020; Higgins et al., 2015), while only recently a role of specific RRubs in driving 40S proteasomal degradation has been identified (Garshott et al., 2021). Hence, I reasoned that since aneuploidy leads to a persistent folding stress and to a persistent translation slowdown, it might be worth addressing a possible role of the E3-ligase ZNF598 in the ribophagic phenotype I observed in aneuploid cells.

A first indication of ZNF598 activity in aneuploid cells has been given by the co-sedimentation profile of the E3-ligase in the fractions obtained from a polysome profiling analysis on HCT116 cells. From a preliminary analysis (n=1), in fact, ZNF598 seemed to be slightly enriched in the 3rd fraction of the aneuploid sample (corresponding to the 40S small subunit fraction), compared to the pseudo-diploid control (Figure 32a-b). However, the difficulties in replicating the experiment and the fact that the immunoblot was not technically satisfactory prompted me to use a different approach.

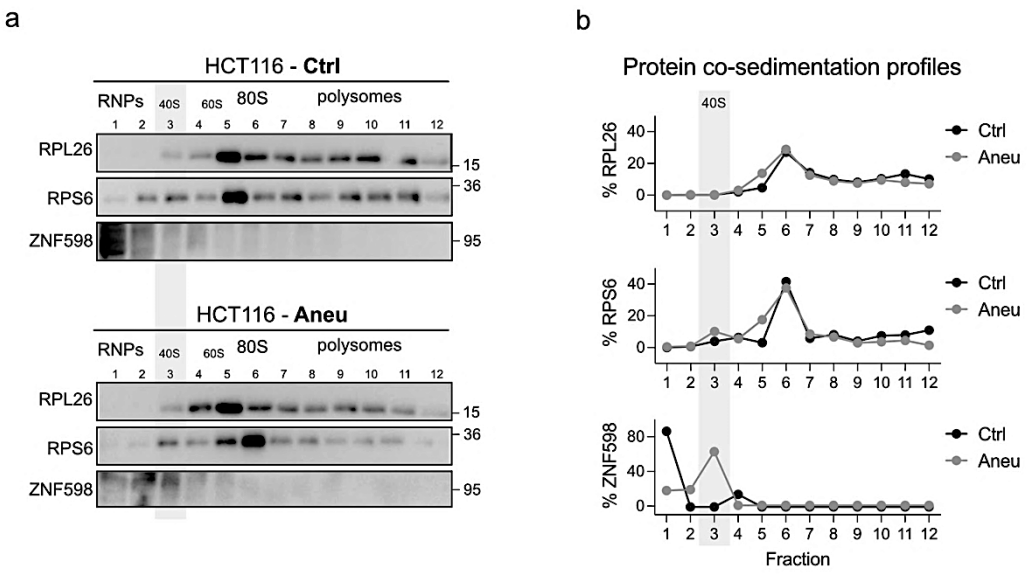

Figure 32: ZNF598 seems to shift in the 40S fraction in aneuploid cells.

(a) Immunoblots for the co-sedimentation profiles of two ribosomal subunit markers (RPL26 for the large subunit and RPS6 for the small one) and the E3-ligase ZNF598, obtained from polysome profile analysis of HCT116 cells treated either with Mps1i (Aneu) or DMSO (Ctrl) for 24 hours. **(b)** Quantitation of the co-sedimentation profiles in (a). The fraction corresponding to the 40S small subunit (fraction number 3) was highlighted.

6.1 ZNF598 depletion leads to a decreased ribophagic flux in aneuploid cells

To directly test the potential role of ZNF598 in the degradation of ribosomes, besides its canonical task of RQC inducer, I depleted it through a siRNA-mediated transient knock-down (Figure 33a) in HCT116 Ribo-Keima cells and then monitored the ribophagic flux in that condition. Importantly, the amount of processed Keima in the aneuploid samples was significantly reduced upon ZNF598 knock-down (Figure 33b-c), indicating that the E3-ligase is actually a mediator of this process. The rescue was particularly evident in the RPS3-Keima cell lines, highlighting once again that the small and the large subunit degradation might rely on different mechanisms. Moreover, ZNF598 ubiquitylation is specific for the small subunit, as it occurs on the surface between collided ribosomes, as previously shown (Juszkiewicz et al., 2018). Since the reduction in ribophagy in ZNF598 knock-down conditions was consistent across distinct biological replicates (Figure 33c) and it was also clear at single cell level (Figure 33d), I concluded that there is a dependency of the ribophagic flux on the E3-ligase ZNF598.

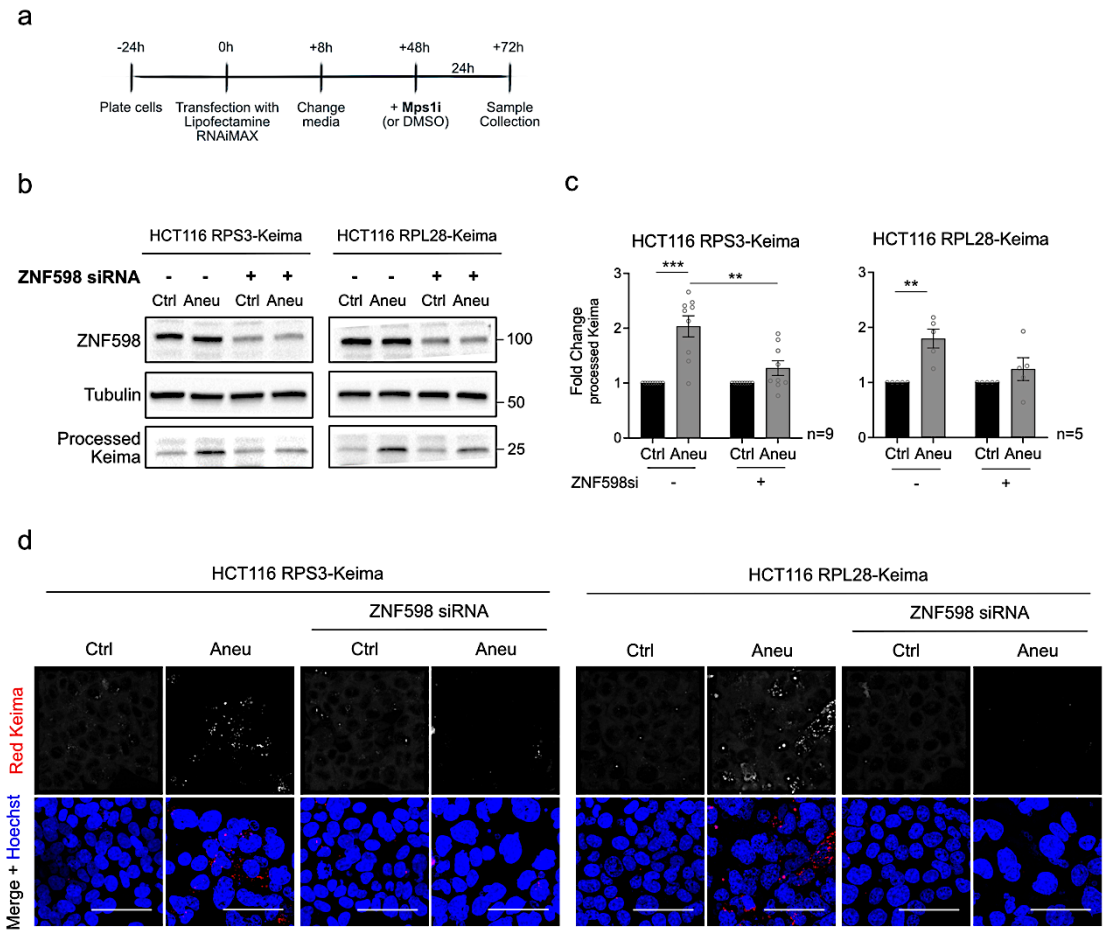

Figure 33: ZNF598 depletion leads to a decreased ribophagic flux in aneuploid cells.

(a) Experimental workflow for the depletion of ZNF598 through siRNA-mediated transient knock-down. **(b)** Representative immunoblots of the indicated HCT116 Ribo-Keima cell lines, in which ZNF598 was depleted with siRNA-mediated transient knock-down. Samples were collected after 72 hours from transfection, a time-point that guarantees the efficient depletion of ZNF598; 24 hours before harvesting, cells were treated either with Mps1 inhibitor (Aneu) or DMSO (Ctrl) to generate aneuploid and pseudo-aneuploid samples. Controls for the transfection were generated using non-targeting siRNAs. Ribophagic flux is determined by the increased level of processed Keima at 25KDa. Tubulin was used as loading control. **(c)** Quantitation of processed Keima immunoblots obtained as in (b), from the indicated biological replicates. Band values are normalised to the respective loading controls; values are expressed as fold changes Aneu/Ctrl. Mean ± SEM; one sample t test (each Aneu *vs* respective Ctrl=1) or Student's t-test (between Aneu and Aneu-ZNF598siRNA). **(d)** Qualitative confocal live-cell images of HCT116 RPS3-Keima and RPL28-Keima cells treated with Mps1 inhibitor (Aneu) or DMSO (Ctrl) for 24 hours. The lysosomal degradation of ribosomes and its rescue is determined by the increased/decreased levels of red-Keima puncta upon ZNF598 transient knock-down; hoechst was used to stain DNA; scale bars, 50μm.

To exclude that ZNF598 directly triggers ribophagy, and to verify that it is rather a mediator of the process, I over-expressed it in HCT116 Ribo-Keima cells (Figure 34a). The over-expression neither increased ribophagy in pseudo-diploid cells, nor changed the proportions of the ribophagic flux between aneuploid and control cells (Figure 34b-c). This assay indicated that, as expected, ZNF598 is not the first trigger of the mechanism, otherwise the levels of ribophagy would have increased upon its over-expression.

Therefore, ZNF598 is probably a mediator of the degradation of ribosomes via the autophagic pathway, which has been already triggered by folding stress, as previously demonstrated (see Results paragraph 4).

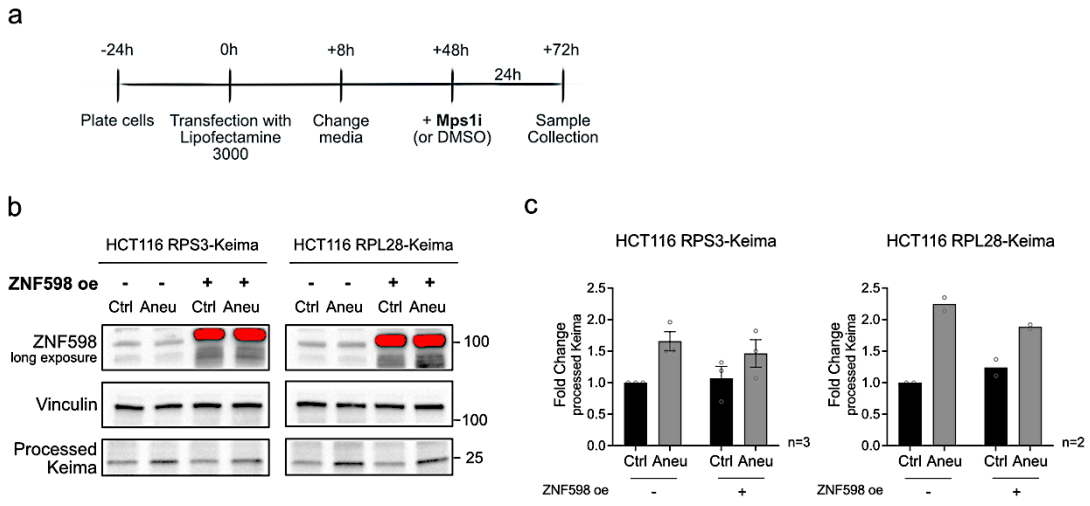

Figure 34: ZNF598 over-expression does not increase the ribophagic flux.
(a) Experimental workflow for the transient over-expression of ZNF598. **(b)** Representative immunoblots of the indicated HCT116 Ribo-Keima cell lines, in which ZNF598 was over-expressed. Samples were collected after 72 hours from transfection, a time-point that guarantees the efficient over-expression of ZNF598; 24 hours before harvesting, cells were treated either with Mps1 inhibitor (Aneu) or DMSO (Ctrl) to generate aneuploid and pseudo-aneuploid samples. Ribophagic flux is determined by the increased level of processed Keima at 25KDa. Vinculin was used as loading control. **(c)** Quantitation of processed Keima immunoblots obtained as in (b), from the indicated biological replicates. Band values are normalised to the respective loading controls; processed Keima values are expressed as fold changes respective to the not-transfected Ctrl. Mean ± SEM (where it applies); Kruskal-Wallis test, followed by Dunn's multiple comparison test (where it applies).

6.2 ZNF598 mediates ribophagy in a specific time-frame

Since the ribophagic phenotype was even increased in aneuploid populations that had enough time to accumulate more stresses (*i.e.* 48h and 72h after chromosome mis-segregation) (see Results paragraphs 3.1 and 3.4), I wanted to check if also ZNF598 role was more evident at longer time-points. I did so through the analysis of the ribophagic flux in an aneuploidy time-course (samples at 24, 48, 72 hours from Mps1i treatment) in conditions where ZNF598 was either depleted or not. To be sure that ZNF598 was equally depleted in all the samples, I collected all of them 84 hours after transfection and added the Mps1 inhibitor (or DMSO) at different time-points before harvesting, to generate the different aneuploid (and pseudo-diploid) samples (Figure 35a). Surprisingly, while the rescue was confirmed for the samples at 24 hours, this was not the case at later time-points (Figure 35b-d). Considering that my previous results (see Results paragraph 2) showed, at those later time-points, an increase in bulk autophagy, as well as other types of autophagy (*i.e.* ER-phagy and, to a smaller extent, mitophagy) I reasoned that ribophagy in aneuploid cells might be selective just at the beginning. In other words, ribosomes could be already

degraded at 24 hours post aneuploidy induction in a selective manner, a process allegedly mediated by ZNF598, because the aneuploidy-induced stresses are still manageable by the cell. When those stresses increase, *i.e.* later in the time-course, ribosomes could become just one of the autophagic cargoes targeted by the increased bulk autophagy.

To corroborate this hypothesis, I treated cells with Torin1, a known inducer of bulk autophagy, after having depleted ZNF598. In this way, I wanted to test whether by increasing the aspecific degradative cargoes (in which ribosomes are included in a non-selective manner), the non-selective ribophagy would be rescued or not by ZNF598 depletion. Importantly, the ribophagic flux induced by the treatment was not decreased upon ZNF598, meaning that this E3-ligase does not mediate non-selective ribophagy.

This finding supports the idea that massive ribophagic flux, either induced by a drug (Torin1) or by the increasing aneuploidy-associated stresses (in aneuploid cells at later time-points), is not selective and not mediated by the E3-ligase ZNF598.

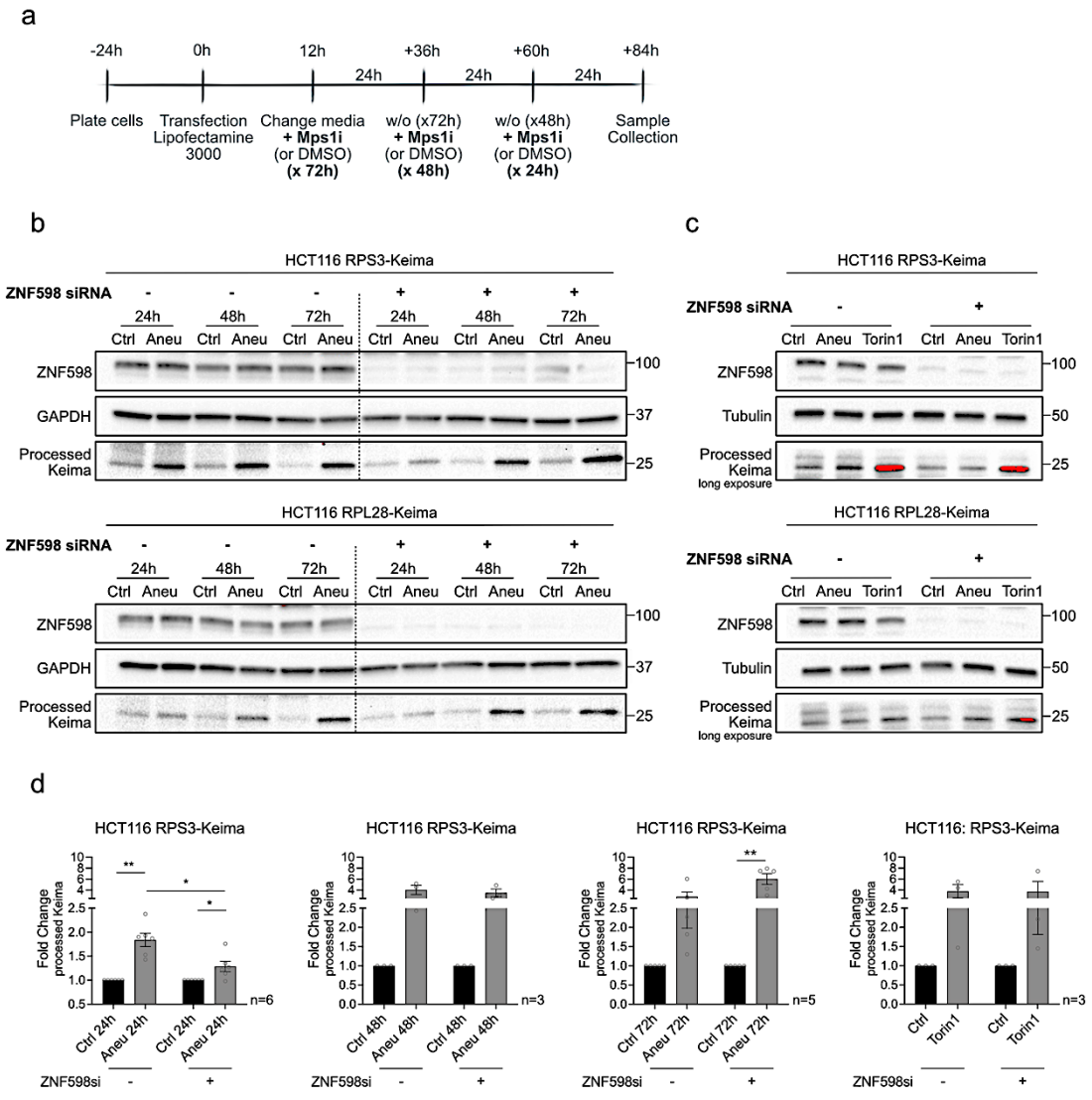

Figure 35: ZNF598 depletion does not rescue ribophagy at later time-points.

(a) Experimental workflow for ZNF598 transient knock-down and aneuploidy time-course. **(b)** Representative immunoblots of the indicated HCT116 Ribo-Keima cell lines, in which ZNF598 was transiently depleted. Samples were collected after 84 hours from transfection; 72, 48 or 24 hours before harvesting, cells were treated either with Mps1 inhibitor (Aneu) or DMSO (Ctrl) to generate aneuploid and pseudo-aneuploid samples at different time-points. Controls for the transfection were generated using non-targeting siRNAs. Ribophagic flux is determined by the increased level of processed Keima at 25KDa. GAPDH was used as loading control. **(c)** Representative immunoblot of HCT116 RPS3-Keima cell lines, in which ZNF598 was transiently depleted. Samples were collected after 72 hours from transfection; 24 hours before harvesting, cells were treated either with Torin1 (250nM) Mps1 inhibitor (Aneu) or DMSO (Ctrl). Controls for the transfection were generated using non-targeting siRNAs. Ribophagic flux is determined by the increased level of processed Keima at 25KDa. Tubulin was used as loading control. **(d)** Quantitation of processed Keima immunoblots (HCT116 RPS3-Keima) obtained as in (b) and (c), from the indicated biological replicates. Band values are normalised to the respective loading controls; processed Keima values are expressed as fold changes Aneu/Ctrl or Torin1/Ctrl. Graph Y axes were scaled to have the same range in the different conditions and facilitate their comparison. Mean ± SEM; one sample t test (each Aneu *vs* respective Ctrl=1) or Student's t-test (between Aneu and Aneu-ZNF598siRNA).

Together, these data point out that ribophagy is early activated in aneuploid cells, as ribosomes can sense in advance the onset of specific stresses, including the impaired folding activity and consequent proteotoxic stress. Since these problems cannot be resolved, as they are intrinsic characteristics of aneuploidy, cells might try, at the beginning, to cope with them by activating specific quality controllers, such as ZNF598, to get rid of translationally deficient ribosomes. When the degree of proteotoxicity and other aneuploidy-associated stress reach severe levels, instead, cells experience the saturation of the autophagic pathway, because of the random engulfment of degradative load, and the selectivity of ribophagy cannot be detected anymore.

A further cue in this direction is given by the same assay performed in the Results paragraph 4.4, in which folding is enhanced by the expression of a constitutively active HSF1 (HSF1ca). When the same experiment was conducted in aneuploid cells at later time-points (72 hours post aneuploidization), the rescue obtained at 24 hours was not detected (Figure 36a-b). This strongly suggests that when folding stress is still addressable and fixable, right after the induction of aneuploidy, cells sense it and activate the downstream mechanisms to control its consequences. Whilst, with the worsening of the stresses related to aneuploidy, cells become too overwhelmed, even in conditions where folding activity is enhanced.

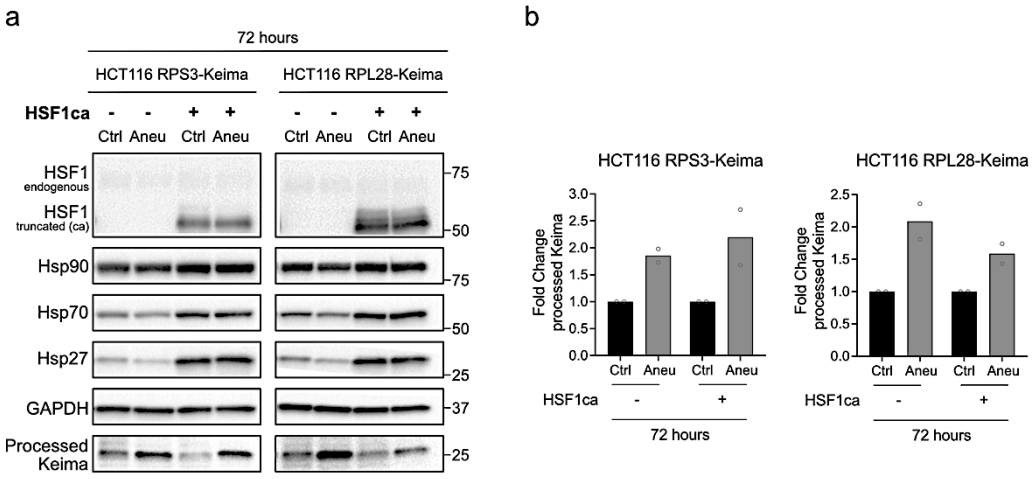

Figure 36: Folding induction is not sufficient to rescue ribophagy at later time-points.
(a) Representative immunoblots of the indicated HCT116 Ribo-Keima cell lines, in which HSF1ca was expressed. Samples were collected after 84 hours from transfection; 72 hours before harvesting, cells were treated either with Mps1 inhibitor (Aneu) or DMSO (Ctrl) to generate aneuploid and pseudo-aneuploid samples. Controls for the transfection were generated using the empty backbone vector. Ribophagic flux is determined by the increased level of processed Keima at 25KDa. GAPDH was used as loading control. **(c)** Quantitation of processed Keima immunoblots obtained as in (a). Band values are normalised to the respective loading controls; processed Keima values are expressed as fold changes Aneu/Ctrl. Mean; n=2.

7. Highly aneuploid cancers tend to downregulate ribosome signature and to correlate with ZNF598 expression

My data indicate that ribophagy is a quality control mechanism activated in aneuploid cells to cope with the onset of folding stress. Given that the vast majority of cancers harbour aneuploid karyotypes (see Introduction paragraph 3), it will be of foremost interest to check if this control mechanisms is activated in transformed contexts. Cancer cells, in fact, must have developed or enhanced protective mechanisms against the negative consequences of aneuploidy, to ensure optimal survival and sustain aggressive proliferation.

7.1 Highly aneuploid cancer cell lines decrease ribosome signatures

To start investigating this idea from a comprehensive point of view, I took advantage of the Broad Institute DepMap (the Cancer Dependency Map portal), a database of cancer cell lines containing genomic data from the CCLE project (Cancer Cell Line Enciclopedia). The portal has been recently integrated with the aneuploidy profiles of over a thousand cancer cell lines, expressed as aneuploidy scores (Cohen-Sharir et al., 2021). In collaboration with Dr. Uri Ben-David and Yonatan Eliezer (Tel Aviv University, Tel Aviv, Israel), cancer cell lines were divided into a “high aneuploidy” group, defined as the top-quartile of the number of arm-level events (either chromosome gains or losses), and a “low aneuploidy” group,

with the bottom-quartile of the number of arm-level events. These two cell line groups were used to identify possible differences in the expression of specific signatures of interests. Since it is not possible to obtain signatures of ribophagy or selective autophagy, as they are not identified by specific pathways, I firstly interrogated the association between the aneuploidy degree (belonging to one of the two groups of cell lines) and ribosomal signatures. Interestingly, the analysis of the relative signature scores (ssGSEA) highlighted that highly aneuploid cancer cell lines tend to negatively correlate with both ribosome biogenesis and ribosome assembly signatures. The functional signature for ribosomes was decreased as well in highly aneuploid cancers (Figure 37a). This information is compelling considering the important roles of ribosomes in cell metabolism, indicating that also transformed cells with highly aneuploid karyotypes can experience, to some extent, ribosomal stress.

Along the same direction, the association between ER signatures and the aneuploidy degree was evaluated. In this case, protein folding signatures seemed not impacted by aneuploidy, while a strong positive correlation was found between aneuploidy and UPR regulation signature (Figure 37b). Although these data might seem contradictory, they give an interesting hint to evaluate the role of the UPR stress response in helping aneuploid cancer cells to manage and partially resolve folding stress.

Lastly, the comparison of mitochondrial signatures between the two groups, high- and low-aneuploidy, did not show any major difference, suggesting that aneuploidy has no effect on mitochondria-related processes and genes (Figure 37c). This was in line with my previous results indicating that mitochondria are not subjected to enhanced degradation.

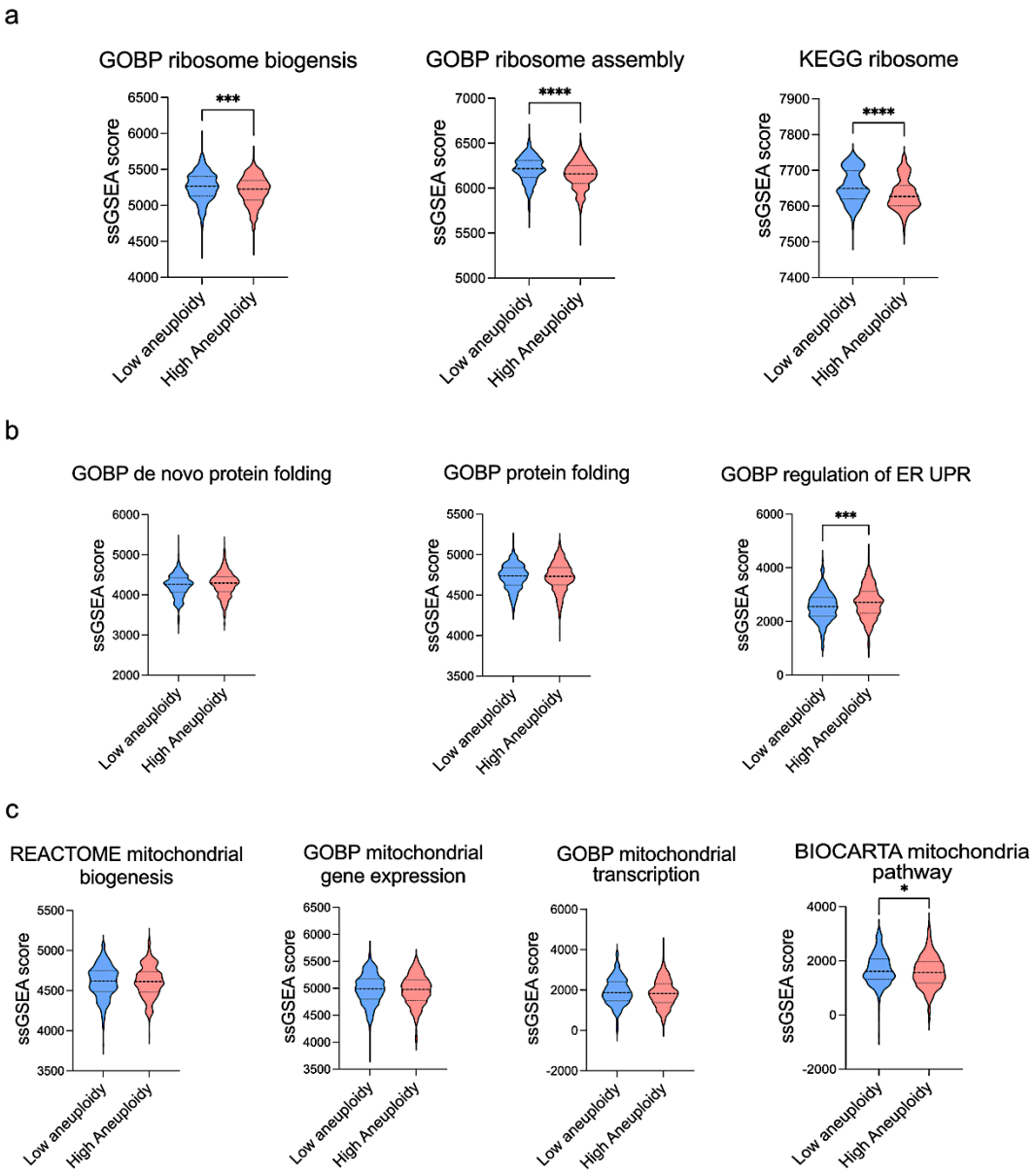

Figure 37: High aneuploidy score is associated with decreased ribosomal and increased UPR regulation signatures.

(a) Association between ssGSEA score for the gene ontology biological processes signatures GOBP ribosome biogenesis, GOBP ribosome assembly, the functional KEGG ribosome signature and aneuploidy score in bottom (low aneuploidy) *vs* top quartiles (high aneuploidy) of human cancer cell lines from the CCLE. Upper quartile, lower quartile and median of each violin plot are shown; t test. **(b)** Association between ssGSEA score for GOBP de-novo protein folding, GOBP protein folding and GOBP regulation of ER unfolded protein response and the aneuploidy score in bottom (low aneuploidy) *vs* top quartiles (high aneuploidy) of human cancer cell lines from the CCLE. Upper quartile, lower quartile and median of each violin plot are shown; t test. **(c)** Association between ssGSEA score for GOBP mitochondrial expression, GOBP mitochondrial transcription, the signatures REACTOME mitochondrial biogenesis and BIOCARTA mitochondria pathway and the aneuploidy score in bottom (low aneuploidy) *vs* top quartiles (high aneuploidy) of human cancer cell lines from the CCLE. Upper quartile, lower quartile and median of each violin plot are shown; t test. a-c performed by Yonatan Eliezer (Tel Aviv University) as discussed together.

7.2 Highly aneuploid cancers and ZNF598 expression positively correlate with each other

I also looked into possible correlations between the aneuploid state of cancer cells and the molecular player ZNF598, which I demonstrated to be involved in ribophagy. In particular, the analysis was performed from TCGA (The Cancer Genome Atlas) data, which contains the information of about 11000 patient primary cancer samples. The pancancer analysis correlating the aneuploidy score of the tumours with ZNF598 expression showed a positive trend (Figure 38a). Further, analysing the respective correlation coefficient between the aneuploidy score and ZNF598 expression of each cancer type independently highlighted the different behaviours among the sample types, with some of them showing compelling positive correlations (Figure 38b).

Moreover, we also looked at the gene signatures whose expression correlates with ZNF598 expression. Using DepMap, among the positive correlations, we found signatures of cell cycle, ubiquitylation and cellular response to stress (highlighted in Figure 38c). Interestingly, among the signatures that anti-correlate with ZNF598 there were those of ribosome biogenesis, cytoplasmic translation, translation elongation and translation initiation (highlighted in Figure 38d). These observations are in line with the data from the *in vitro* experiments, giving a starting point for further characterizations using cancer models.

Taken together, these data suggest that highly aneuploid cancers tend to over-express ZNF598, although the high heterogeneity between the different tumor types should be taken in consideration. Accordingly, highly aneuploid cancers also tend to downregulate ribosome-related pathway, compared to pseudo-diploid tumours. Moreover, the analysis of the individual correlation coefficients between the aneuploidy score and ZNF598 expression of each cancer type, highlights that only positive correlations are significant, pointing at the importance of further investigations in this direction.

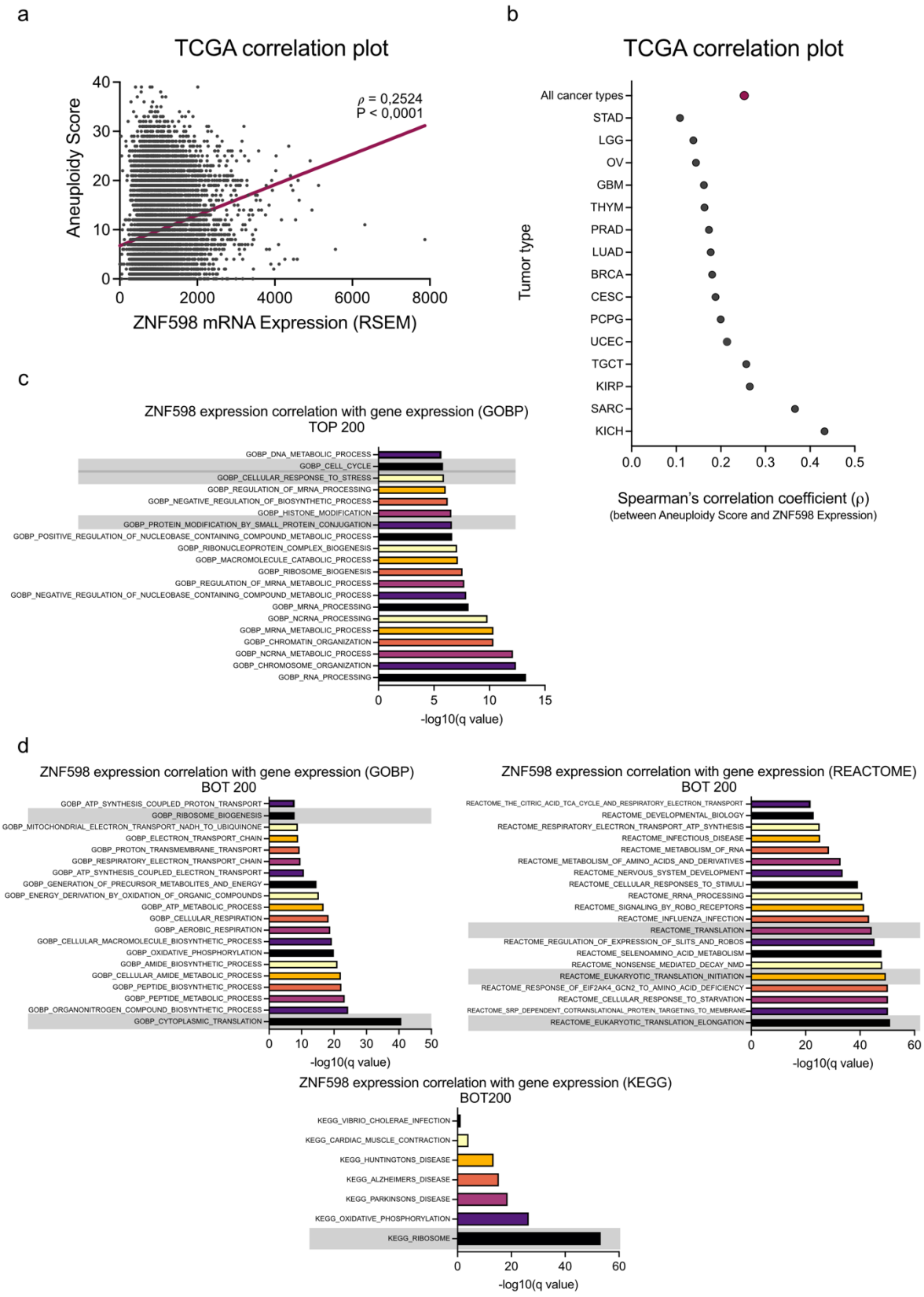

Figure 38: Highly aneuploid cancers tend to positively correlate with ZNF598 expression and ZNF598 expression anti-correlates with translation and ribosomal signatures.

(a) Pancancer correlation plot between the aneuploid score and ZNF598 expression (RSEM) from TCGA primary tumour samples. The trend line for Spearman's correlation is in purple; ρ=0,2524, P<0.0001. **(b)** Dot-plot with individual cancer types and the respective Spearman's correlation coefficient between aneuploidy score and ZNF598 expression (RSEM) from TCGA dataset (where ρ=0 indicates no correlation, ρ=1 perfect positive correlation and ρ=-1 perfect negative correlation), for tumour types with a significant correlation (P<0,05)

(black dots). Pancancer Spearman's correlation coefficient was reported (purple dot). **(c)** Correlation plot between ZNF598 expression and the indicated signatures among the most positively correlated genes (TOP 200), from DepMap database. X axis represents $-\log_{10}$(q-value). Grey bars highlight the signatures of interest. **(d)** Correlation plot between ZNF598 expression and the indicated signatures among the most negatively correlated genes (BOT 200), from DepMap database. X axis represents $-\log_{10}$(q-value). Grey bars highlight the signatures of interest. a, c, d performed by Yonatan Eliezer (Tel Aviv University) as discussed together.

Discussion

Chromosome mis-segregation and the consequent aneuploid state cause a plethora of cellular stresses that have been described in multiple studies (Gordon et al., 2012; Levine & Holland, 2018; Santaguida & Amon, 2015b; Siegel & Amon, 2012; Torres et al., 2008). One of the most prominent features of aneuploidy is proteotoxic stress, which is characterised by the aggregation of aberrant proteins in the cytoplasm (Choe et al., 2016; Chunduri & Storchová, 2019; Oromendia & Amon, 2014; Santaguida & Amon, 2015b). Proteotoxicity is thought to be a consequence of gene copy number changes and it is triggered at various levels in aneuploid cells, impacting negatively cell physiology (Oromendia et al., 2012; Stingele et al., 2012; Tang & Amon, 2013; Torres et al., 2007). Furthermore, aneuploid cells are particularly sensitive to conditions where protein folding is saturated, because of their already-compromised folding machinery (Donnelly et al., 2014; Tang et al., 2011). The continual aggregation of not-properly folded proteins leads to the overwhelming of the quality control mechanisms in aneuploid cells, first of all the autophagic pathway (Santaguida et al., 2015; Santaguida & Amon, 2015a) that is typically in charge for the degradation of extra, misfolded or defective proteins and complexes (Ding & Yin, 2008; Kirkin et al., 2009).

Although many progresses have been made in characterizing the consequences of aneuploidy, a deep understanding of the mechanisms that counteract proteotoxic stress is still missing. In an attempt to fill this gap, I have carried out this project by applying multiple experimental methodologies and ultimately demonstrating that, in aneuploid cells, a deficient protein folding is strictly connected to the lysosome-mediated degradation of ribosomes.

For my studies, I induced aneuploidy in pseudo-diploid cell lines, RPE1 and HCT116, by interfering with the components of the spindle assembly checkpoint, in particular Mps1 (Santaguida et al., 2010). The obtained aneuploid system is a heterogeneous population of aneuploid cells with random chromosome gains and losses (Figure 11). The analysis of a heterogeneous population is useful to disentangle common features of aneuploid cells, despite their karyotypes. By using this approach, in fact, it is possible to identify mechanisms used by aneuploid cells to cope with shared stresses and, possibly, exploit this knowledge to characterise how aneuploid cancer cells successfully overcome these problems.

1. A model to summarise the events that leads to the lysosome-mediated degradation of ribosomes in aneuploid cells

Previous evidence showed the overwhelming of the autophagic pathway in aneuploid cells, as a consequence of the mounting proteotoxicity((Santaguida et al., 2015; Santaguida & Amon, 2015a) and Figure 14), and this prompted me to dissect in details the mechanisms

involved. By studying the nature of the cargo engulfed in autophagosomes, it became clear the presence of organelles known to be subjected to selective autophagy under stress conditions (Figures 15, 16). Since, among them, ribosomes already undergo degradation at early time-points after the induction of aneuploidy, I focused my attention on them. Indeed, I observed an increased ribophagic flux in my aneuploid system, compared to pseudo-diploid control (Figures 17, 19, 20, 21) and I followed-up investigating the causes and the molecular bases underlying this phenotype. My data indicate that accumulation of misfolded and unfolded proteins (Figure 12) in aneuploid cells is caused and exacerbated, at least in part, by impaired activity of chaperones, in particular by the Hsp90 and Hsp70 families (Figures 24, 25, 26, 27). The onset of proteotoxic stress, in turn, leads to an attenuation of translation to cope with folding deficiency (Figures 28, 29, 30). Most likely, this increases the probability of ribosome stalling and consequent collision. Translational deficiency and paused-ribosomes do not go unnoticed: aneuploid cells recruit a quality control mediator, the E3-ligase ZNF598 (Figures 33, 34), which is in charge for the ubiquitylation of defective ribosomes, typically driving the onset of ribosome-associated quality control. This specific targeting drives ribosomal subunits for selective autophagic degradation through the lysosomes (summarised in Figure 39a).

The described chain of events, however, seems to take place when cells can manage the initial trigger of this response, *i.e.* the folding deficiency that causes the proteotoxic stress. Aneuploid cells that have been cultured for 2, 3 or more days after the induction of chromosome mis-segregation, indeed, have time to accumulate higher levels of the stresses associated with aneuploidy (Santaguida et al., 2017). This condition exacerbates the overwhelming of the autophagic pathway, which becomes saturated because the lysosomes cannot keep up with the increased degradative load (Figures 14, 16; 48h and 72h time-points). The growing autophagic flux is also reflected at the level of ribophagy (Figures 16, 18, 20, 21). Importantly, under these circumstances, ribosome engulfment in autophagic structures increases, but, on the other hand, the selectivity of the process is lost. Indeed, the dependency of ribophagy on ZNF598 activity is not detectable anymore (Figure 35). This is further confirmed by the fact that even if aneuploid cells at these stages are enhanced to fold proteins, the ribophagic flux is not rescued (Figure 36). LDHB, ER and, to a lower extent, mitochondria undergoing autophagy at later time-points (48, 72 hours after aneuploidy induction) represent an additional proof of the random sequestration of cytoplasmic material during the increase in bulk autophagy (Figures 14, 16). Together, these data support the idea that aneuploid cells with increasing stresses are not able to discriminate in a selective manner the cargo to be degraded, and ribosomes themselves end up in lysosomes as a result of bystander flux (Figure 39b).

The worsening of genomic instability triggered by even a single chromosome mis-segregation event is known to cause the evolution of severe karyotype abnormalities in the

analysed population (Garribba et al., 2023; Santaguida et al., 2017). Moreover, aneuploid cells harbouring complex karyotypes ultimately cease to divide and undergo senescence (Santaguida et al., 2017), as the ability to proliferate negatively correlates with the increase in karyotype aberrations. In a population of aneuploid cells, generated by inducing chromosome segregation errors as in my system, around 30-40% of cells arrest within 3 days of culture (corresponding to the “72 hours” time-point in my experimental set-up) (Santaguida et al., 2017), due to the unbearable increase in stresses, which scales up with the degree of aneuploidy. Hence, it is highly probable that cells at this time-point cannot manage the folding and proteotoxic stresses as well, leading to the increase in bulk autophagy that randomly sequesters non-selective cargo.

Thus, this work has identified two main processes that cause the lysosome-mediated degradation of ribosomes. One is selective and it is orchestrated by defined molecular mechanisms, and one is not-selective and driven by acute proteotoxic stress response.

2. Towards the identification of the role(s) played by ribophagy

This study proposes an active role of ribophagy in sensing and handling the consequences of proteotoxic stress in aneuploid cells. The accumulation and aggregation of misfolded/unfolded proteins, even if mild, represent a tremendous stress for the cell. In turn, multiple responses can be activated with the aim of buffering its toxic consequences. In this project, I also considered the activation of canonical stress responses, first of all the Unfolded Protein Response (UPR) (Walter & Ron, 2011). The increased phosphorylation of the translation initiation factor eIF2α in aneuploid cells, which is known to decrease protein synthesis and enhance folding capacity, indicates that this pathway is triggered (Figure 13). The activation of this response in aneuploid cells is also demonstrated by their higher sensitivity to the inhibition of PERK, one of the principal mediators of UPR (Figure 13c). eIF2α phosphorylation is also a key event of a broader stress response, the integrated stress response (ISR). Hence, given the constant production of extra proteins and their possible aggregation in aneuploid cells, I speculate that they exploit multiple mechanisms to address proteotoxicity, probably depending on the degree of stress they face. The activation of ribophagy, as well as its link to the ribosome-associated quality control, is an exciting and novel direction for the field of aneuploidy.

2.1 Ribophagy as a protective mechanism against proteotoxic stress

In a population of cells analysed within the first cell cycle after chromosome mis-segregation, the degree of aneuploidy (namely the extent of chromosomal aberrations) is not yet dramatic. Then, the degree of karyotype aberrations in the aneuploid population is worsened in the following cell cycles, as a consequence of the genomic instability of cells

already harbouring aneuploid karyotypes (Garribba et al., 2023; Santaguida et al., 2017). However, as previously demonstrated (Oromendia et al., 2012; Oromendia & Amon, 2014; Stingele et al., 2012; Tang & Amon, 2013; Torres et al., 2007), even a single chromosome gain can have a profound impact on proteome homeostasis. The increased protein translation demand, due to the extra genetic material, leads to an overload of the folding machinery (Donnelly et al., 2014), a condition that is promptly sensed by cells. One possible solution would be to mitigate the emerging stress by giving the cell time to fold the nascent polypeptide chains, through attenuation of global protein synthesis achieved by elongation pausing of ribosomes (B. Liu et al., 2013; Zhao et al., 2019). This response can be risky because of the higher probability of widespread ribosome stalling and collisions (Collart & Weiss, 2019). My results are in line with this hypothesis as they demonstrate that aneuploid cells suffer chaperone overwhelming (Figures 24, 25) and downregulate global protein synthesis at various levels (Figures 28, 29, 30, 31). The ribosome-associated quality control (RQC) pathway is typically triggered by the recognition of collisions by the E3-ligase ZNF598 (Garzia et al., 2017; Joazeiro, 2019; Juszkiewicz et al., 2018; Sundaramoorthy et al., 2017), which ubiquitylates the interface between the collided ribosomes. ZNF598 acts, with good reliability, downstream of the protein synthesis impairment, as the depletion of this E3-ligase does not rescue the lower puromycin incorporation in aneuploid cells (data not shown). The fact that ZNF598 is a mediator of the lysosomal degradation of ribosomes (Figures 32, 33, 34) strongly suggests a slightly different role of this E3-ligase. In canonical RQC, ribosome subunit fate is not clear, but they are most likely recycled (Joazeiro, 2019). Mounting evidence, however, indicates that regulatory ubiquitylations of ribosomes can regulate their activity or degradation, depending on the stress conditions and contexts (Garshott et al., 2020, 2021; Higgins et al., 2015; C. Meyer et al., 2020). Therefore, I speculate that the “chronic” nature of folding stress, right after chromosome mis-segregation, not only triggers the RQC, but also leads to the degradation of the translationally-deficient ribosomes. Decrease in protein synthesis in aneuploid cells is the result of the increasing proteotoxic stress, but it might be also kept low through degradation of persistently stalled ribosomes. This represents a protective mechanism that operates to limit the toxic effects of folding stress, by limiting uncontrolled synthesis of extra proteins that cannot be properly folded. To corroborate this conclusion, it would be interesting to test whether the viability of aneuploid cells in which this mechanism is shut down is lower than cells able to activate it, with the same aneuploidy degree. A means for the process inactivation could be silencing of the downstream mediator ZNF598, before performing the viability assay.

Ribosome stalling and collision alone are not sufficient to justify the ultimate lysosomal degradation of the ribosomes themselves. As a matter of fact, treating pseudo-diploid cells with anisomycin, an antibiotic that stalls ribosomes by blocking their peptidyl transferase

activity (Matsuo et al., 2017), no ribophagic flux increase was observed (preliminary data, not shown). In the absence of other triggering stimuli, indeed, stalled ribosomes are targeted by canonical RQC and recycled, as stalling *per se* does not cause ribophagy. Conversely, my study identified an aneuploidy-specific trigger for this phenotype, namely the mounting proteotoxic stress that aneuploid cells experience.

My data highlighted a different behavior of the small and large ribosomal subunits, regarding several processes. In particular, the canonical autophagic receptor p62 seems to mediate the large subunit (60S) degradation via lysosomes, but I was not able to outline a conclusive trend for the 40S (Figure 23). Further, while ZNF598 clearly mediates the small subunit degradation, its role in the large subunit removal was less pronounced (Figures 32, 33). It is possible that the small subunit of the ribosome is the direct target of ZNF598 ubiquitylation, which is not surprising considering the role of this E3-ligase in RQC and its known molecular targets (*i.e.* 40S proteins). My idea is that 40S degradation might be followed by 60S removal to balance the ratio between small and large subunits. Therefore, large subunit degradation might depend on a different pathway, indirectly driven by ZNF598, but mediated by the canonical autophagic receptor p62. Whether another receptor recognises the ubiquitylated small subunit remains to be determined. It would be interesting to validate this hypothesis by performing an immunoprecipitation of specific ribosomal proteins, from either the small or the large subunit, and check the different ubiquitylation patterns in presence/absence of ZNF598.

Recent works from the Bennett and Tuschl labs pointed out the roles of specific E3-ligase/de-ubiquitylating enzyme complexes in regulating ribosomal degradation or recycling, following the activation of quality control pathways (Garshott et al., 2020, 2021; Higgins et al., 2015; C. Meyer et al., 2020). Further investigation on this aspect would be interesting, to assess if regulatory ubiquitylations on ribosomes are reversible in the aneuploid system. Another possible scenario, in this respect, could involve the overwhelming of de-ubiquitylating enzymes, due to the continuous triggering of ribosome slowdown and consequent ribosome ubiquitylation.

Since misfolded proteins are continuously generated in aneuploid cells, leading to toxicity and translational defects, I also asked the question of whether aneuploid cells are able to maintain ribophagy under a stable depletion of ZNF598 E3-ligase. I performed the stable knock-out through CRISPR/Cas9 and preliminary results (data not shown) indicate that, differently from the transient depletion of ZNF598 that abolishes this process, ribophagic flux is maintained. This is strongly in accordance with the hypothesis that ribophagy is crucial for aneuploid cell survival, since they seem to activate a secondary pathway, independent from ZNF598, to preserve it. It is of foremost interest to follow-up on this, by identifying the other mechanism(s) and enzyme(s) involved.

2.2 Loss of autophagy selectivity in over-stressed cells

Aneuploid cells cultured for 2 or more days after the induction of random aneuploidies develop increasing karyotype abnormalities (Garribba et al., 2023; Santaguida et al., 2017). Changing the levels of many genes simultaneously affects cell physiology in nearly every aspect (Santaguida & Amon, 2015b). Protein abundance and stoichiometry are largely impacted and aneuploid cells answer to this stress by hyper-activating autophagy (Stingele et al., 2012; Tang et al., 2011). The additional autophagosomal content accumulates in the lysosomal compartment and, eventually, lysosome degradative capacity is surpassed. This points out that the higher the aneuploidy degree, the closer autophagy works to saturation (Joy et al., 2021; Santaguida et al., 2015; Santaguida & Amon, 2015a). Consistent with this, my data showed an increase in p62 levels (used as a proxy for autophagosome accumulation) and of the processed LDHB-Keima (used as a proxy for the bulk autophagic flux) in samples collected 2 and 3 cell cycles after aneuploidy induction (Figure 14). These results further confirm that the accumulation of excessive cargo in autolysosomes does not happen immediately after chromosome mis-segregation, but it requires the development of severe karyotype aberrations and toxic stresses. The stressed condition of aneuploid cells at these time points is reflected also at the level of protein synthesis slowdown and downstream responses. However, similarly to the bulk autophagy triggered by starvation or Torin1 treatment, the proteotoxic stress-driven bulk autophagy is not selective (Figure 35), since it randomly sequesters cytoplasmic portions in an attempt to get rid of toxic aggregates. As a result, also the specific degradation of the translationally-defective ribosomal subunits is lost in the midst of the other cargoes engulfed in the autophagic structures (including randomly-sequestered ribosomes). Indeed, the rescue of ribophagy is more difficult to obtain as the bulk autophagy increases (Figure 35). It is probable that ZNF598 knock down in over-stressed aneuploid cells can just rescue the degradation of the ribosomes involved in the previously described response, which represent only a fraction of those engulfed in lysosomes at that stage. Since this fraction is meant to become smaller as the total bulk autophagy increases, I was not able, so far, to distinguish between randomly- and selectively- engulfed ribosomes in aneuploid cells at later time points.

In line with this, aneuploid cells cultured for 2-3 days showed not only an increase in ribosome engulfment in lysosomes, but also of other organelles, such as ER (Figures 16, 20) and, to a lower extent, mitochondria (Figure 16). Importantly, the degradation of these two other components was not observed immediately after the induction of chromosome mis-segregation, indicating that aneuploidy does not impair their functions, at least at the beginning. It might be interesting to investigate whether there are already-known autophagic receptors involved in the recognition of ER portions in aneuploid cells. This would address the possibility that a selective degradation is triggered also for ER, besides the random engulfment of the organelle during bulk autophagy increase.

2.3 Ribophagy in different aneuploid contexts

Aneuploidy generated by chromosome mis-segregation leads to ribophagy, irrespective of the method used to trigger faulty mitoses. As a matter of fact, the inhibition of several SAC components (Mps1, MAD2 or BUB1) with several approaches (chemical inhibition or RNAi-driven depletion) caused the same ribophagic phenotype (Figures 17, 18, 19). If selective ribophagy is triggered by the acute effects of chromosome mis-segregation, is it detectable in aneuploidy-adapted cells as well? Preliminary data on aneuploid RPE1 clones, which present defined and stable aneuploid karyotypes, suggests that this is not the case (data not shown). It is possible that adaptation to aneuploidy, which lets these cells grow and proliferate without being affected by the genomic instability that normally characterise aneuploid cells, is also exerted through an alleviated proteotoxic stress. If this were to be confirmed, it would be interesting to also check whether or not the ribophagic phenotype occurs in healthy cells of naturally aneuploid tissues, such as liver, which presents high rates of aneuploidization and polyploidization (Duncan, 2013).

Further, a recent study highlighted that cells from trisomy 21 syndrome (Down syndrome, DS) show impaired protein synthesis, which is driven by ISR-mediated eIF2α phosphorylation (Zhu et al., 2019). This work is particularly interesting for human health, as it points out a defective protein homeostasis in DS patient cells. It is currently not known if the ribophagy-mediated protein quality control is active in this context, and it would be relevant to check it in the future.

As already mentioned in this thesis, another context that is highly characterised by aneuploid cells is cancer (Beroukhim et al., 2010; Campbell et al., 2020). Tumorigenesis is often associated with the evolution of cell karyotypes, seeking for optimal combinations useful in managing challenging and stressful conditions (Hanahan & Weinberg, 2011; Holland & Cleveland, 2012; Knouse et al., 2014). In this context, whether aneuploid cancer cells take advantage of the extra-protein quality control to cope with proteotoxic stress remains to be determined (detailed in the next paragraph).

3. Relevance for cancer biology

The fact that aneuploidy is a widely recognised hallmark of cancer (Hanahan & Weinberg, 2011; Holland & Cleveland, 2012) gives the opportunity to think of possible common features or common mechanisms to target therapeutically. On the other hand, given the vast variety of cancer types and cancer evolution trajectories, it is not trivial to identify a unique characteristic suitable for this purpose. Translation quality control network has the potential of helping the adaptation of aneuploid cancer cells to challenging conditions. This, in turn, would offer new opportunities for drug discovery with the aim of manipulating

translation. Based on these considerations, my initial effort to address this point was to check the expression levels of the E3-ligase ZNF598, which I linked to the ribophagic quality control, as a function of the aneuploidy score of primary cancer samples from TCGA. The results of this pancancer query suggest that ZNF598 tends to be over-expressed in highly aneuploid cancers, with some relevant differences across different cancer types (Figure 38).

It is possible that cancer types that upregulate ZNF598 invest in this player to better control protein homeostasis. Ribophagy-mediated quality control might prevent the toxicity of extra proteins by keeping them under control. Aneuploid cancer cells, indeed, exhibit proteotoxic stress to some extent, which has been the target of multiple therapeutic approaches (Guang et al., 2019). Blocking also this response that buffer proteotoxic stress might represent an attractive tool to sensitise cancer cells to the negative consequences of proteotoxicity. In particular, since ribophagy seems to be employed as a protective mechanism against this stress, its attenuation would exacerbate the proteotoxicity, reaching the dangerous levels observed at later time points in my aneuploid system. This strategy, in turn, would cause significant damages to cancer cell proteostasis, possibly leading to cell death.

Since the universality of this hypothesis sounds improbable given the heterogeneity of cancer diseases, another plausible scenario is that some cancer cells might downregulate ZNF598. This may happen if those cancer cells have found ways to attenuate the ZNF598-mediated ribosome quality control, with the goal of favouring a massive protein synthesis rate over quality control. This mechanism has been already observed in a physiological system: mammalian reticulocytes. Indeed, this immature cell type is naturally devoid of ZNF598 but, on the other hand, it massively translates globin mRNAs. The high translation rates of reticulocytes cause their polysomes to present stochastic ribosome collisions, due to the reduced inter-ribosomal distance. Reticulocytes tolerate this by eliminating ZNF598-mediated quality control. Hence, this cell type seems to sacrifice quality control in favour of a massive translation rate (Juszkiewicz et al., 2018; Juszkiewicz, Speldewinde, et al., 2020). The uncontrolled proliferation and accelerated metabolism of cancer cells would benefit from the downregulation of this quality control. Therefore, in this condition, it would be interesting to re-activate the control pathway to reduce the proliferative potential of these cancer types.

In this respect, it would be interesting to validate the hypothesis that, in a malignant context, highly aneuploid cells are less sensitive to proteotoxic and translational stress, as a function of the up- or down- regulation of the quality control mediated by ribosome degradation. Identifying the processes by which highly aneuploid cancer cells overcome proteotoxicity would provide important insights into cancer biology. Moreover, it might be helpful in

defining novel therapeutic interventions aimed at targeting aneuploidy-caused proteome imbalances, by manipulating translation.

In summary, this project shed light on a previously uncharacterised chain of events activated by aneuploid cells in response to the onset of proteotoxic stress. The presented data suggest a model wherein the increasing folding demand, right after chromosome mis-segregation, challenges the Hsp90 and Hsp70 chaperone families and triggers translation attenuation. Ribosomes that are continuously slowed down eventually collide and are recognised by the E3-ligase ZNF598 which, in this specific condition, tags them for degradation. Their clearance is carried out by the autophagic pathway, in particular by their selective degradation mediated by lysosomes (Figure 39a). Another well-known outcome of aneuploidy is genomic instability, which triggers the evolution of abnormal karyotypes. Populations of cells with higher aneuploidy degree also present an exacerbation of the associated stresses, first of all the proteotoxic one. To get rid of the increasing accumulation of toxic aggregates and extra proteins, cells at these stages boost bulk autophagy, leading to the random engulfment of cargo in the autophagic structures. Ribosome degradation is more intense in this condition, but the initial selectivity is lost, due to the uncontrolled increase in bulk autophagy (Figure 39b). Whether and how these regulatory mechanisms are exploited by aneuploid cancer cells to overcome proteotoxicity and favour their uncontrolled proliferation represent an exciting direction for future studies.

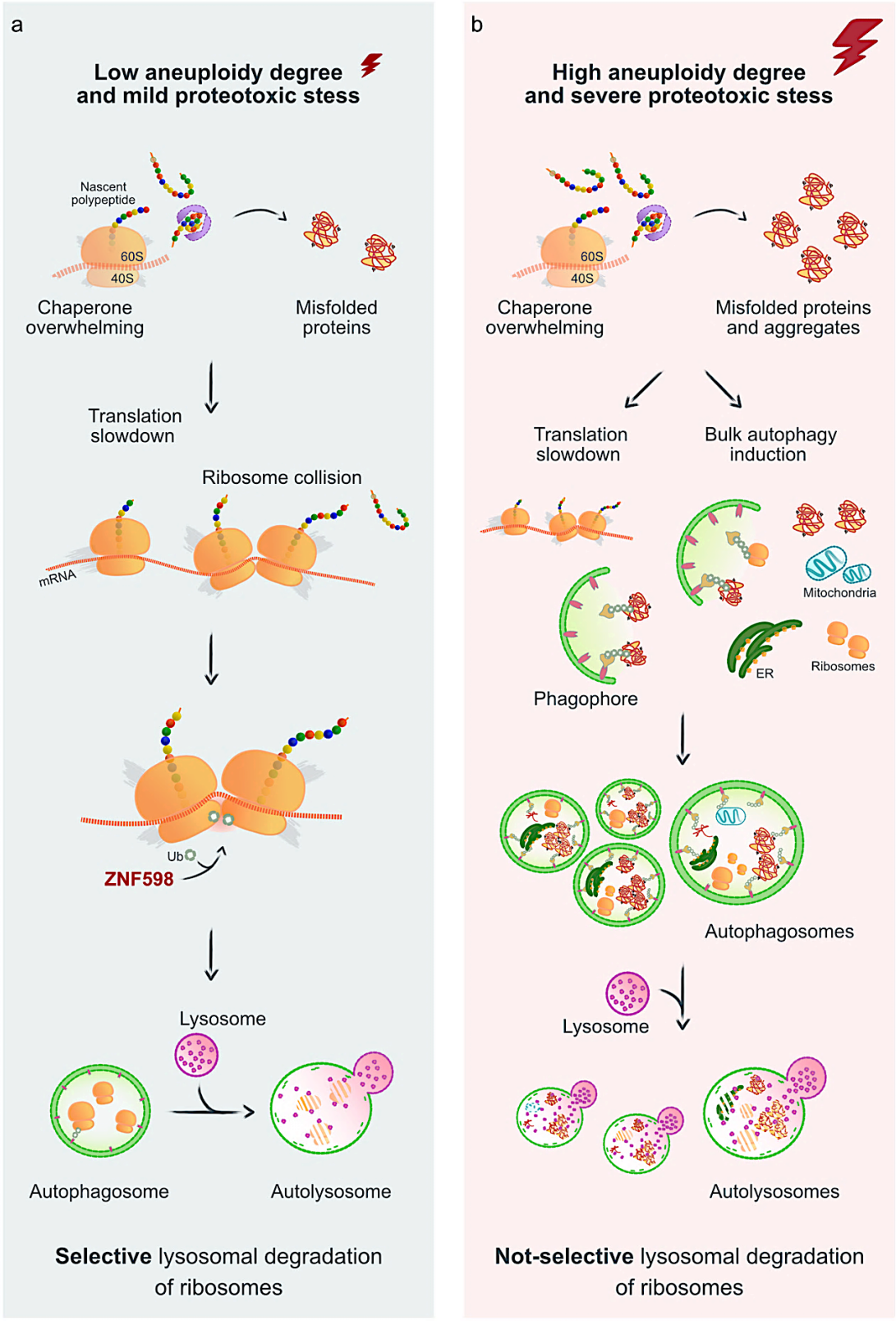

Figure 39: Working model explaining how aneuploid cells respond to altered protein homeostasis. **(a)** Right after the induction of aneuploidy, cells display chaperone impaired activity and misfolded protein accumulation (proteotoxic stress onset). As the proteotoxic stress is still manageable, cells tend to slow down translation to cope with folding deficiency and this leads to ribosome collision. ZNF598 E3-ligase recognises this aberrant structure and tags translationally-deficient ribosomes for degradation via lysosomes. **(b)** After 2-3 days from aneuploidy induction, the evolution of more karyotype aberrations in the aneuploid population leads to increased proteotoxic stress and uncontrolled bulk autophagy. This causes the random engulfment of cytosolic components in the autophagic structures, including ribosomes.

Bibliography

Acquaviva, C., & Pines, J. (2006). The anaphase-promoting complex/cyclosome: APC/C. *Journal of Cell Science*, *119*(12), 2401–2404. https://doi.org/10.1242/jcs.02937

Alberts, B., Johson, A., Lewis, J., Morgan, D., Raff, M., Roberts, K., & Walter, P. (2015). *Molecular Biology of the Cell (6th ed.)* (6th Editio). Garland Science, Taylor and Francis Group.

An, H., & Harper, J. W. (2018). Systematic analysis of ribophagy in human cells reveals bystander flux during selective autophagy. *Nature Cell Biology*, *20*(2), 135–143. https://doi.org/10.1038/s41556-017-0007-x

An, H., & Harper, J. W. (2020). Ribosome Abundance Control Via the Ubiquitin–Proteasome System and Autophagy. *Journal of Molecular Biology*, *432*(1), 170–184. https://doi.org/10.1016/j.jmb.2019.06.001

An, H., Ordureau, A., Körner, M., Paulo, J. A., & Harper, J. W. (2020). Systematic quantitative analysis of ribosome inventory during nutrient stress. *Nature*, *583*(7815), 303–309. https://doi.org/10.1038/s41586-020-2446-y

Bakhoum, S. F., Genovese, G., & Compton, D. A. (2009). Deviant Kinetochore Microtubule Dynamics Underlie Chromosomal Instability. *Current Biology*, *19*(22), 1937–1942. https://doi.org/10.1016/j.cub.2009.09.055

Bakhoum, S. F., Ngo, B., Laughney, A. M., Cavallo, J. A., Murphy, C. J., Ly, P., Shah, P., Sriram, R. K., Watkins, T. B. K., Taunk, N. K., Duran, M., Pauli, C., Shaw, C., Chadalavada, K., Rajasekhar, V. K., Genovese, G., Venkatesan, S., Birkbak, N. J., McGranahan, N., … Cantley, L. C. (2018). Chromosomal instability drives metastasis through a cytosolic DNA response. *Nature*, *553*(7689), 467–472. https://doi.org/10.1038/nature25432

Balchin, D., Hayer-Hartl, M., & Hartl, F. U. (2016). In vivo aspects of protein folding and quality control. *Science*, *353*(6294). https://doi.org/10.1126/science.aac4354

Barber, T. D., McManus, K., Yuen, K. W. Y., Reis, M., Parmigiani, G., Shen, D., Barrett, I., Nouhi, Y., Spencer, F., Markowitz, S., Velculescu, V. E., Kinzler, K. W., Vogelstein, B., Lengauer, C., & Hieter, P. (2008). Chromatid cohesion defects may underlie chromosome instability in human colorectal cancers. *Proceedings of the National Academy of Sciences of the United States of America*, *105*(9), 3443–3448. https://doi.org/10.1073/pnas.0712384105

Basto, R., Brunk, K., Vinadogrova, T., Peel, N., Franz, A., Khodjakov, A., & Raff, J. W. (2008). Centrosome Amplification Can Initiate Tumorigenesis in Flies. *Cell*, *133*(6), 1032–1042. https://doi.org/10.1016/j.cell.2008.05.039

Baumgartner, M. E., Dinan, M. P., Langton, P. F., Kucinski, I., & Piddini, E. (2021). Proteotoxic stress is a driver of the loser status and cell competition. *Nature Cell Biology*, *23*(2), 136–146. https://doi.org/10.1038/s41556-020-00627-0

Beese, C. J., Brynjólfsdóttir, S. H., & Frankel, L. B. (2020). Selective Autophagy of the Protein Homeostasis Machinery: Ribophagy, Proteaphagy and ER-Phagy. *Frontiers in Cell and Developmental Biology*, *7*(January), 1–12. https://doi.org/10.3389/fcell.2019.00373

Ben-David, U., & Amon, A. (2020). Context is everything: aneuploidy in cancer. *Nature Reviews Genetics*, *21*(1), 44–62. https://doi.org/10.1038/s41576-019-0171-x

Bernabò, P., Tebaldi, T., Groen, E. J. N., Lane, F. M., Perenthaler, E., Mattedi, F., Newbery, H. J., Zhou, H., Zuccotti, P., Potrich, V., Shorrock, H. K., Muntoni, F., Quattrone, A., Gillingwater, T. H., & Viero, G. (2017). In Vivo Translatome Profiling in Spinal Muscular Atrophy Reveals a Role for SMN Protein in Ribosome Biology. *Cell Reports*, *21*(4), 953–965. https://doi.org/10.1016/j.celrep.2017.10.010

Beroukhim, R., Mermel, C. H., Porter, D., Wei, G., Raychaudhuri, S., Donovan, J., Barretina, J., Boehm, J. S., Dobson, J., Urashima, M., McHenry, K. T., Pinchback, R. M., Ligon, A. H., Cho, Y. J., Haery, L., Greulich, H., Reich, M., Winckler, W., Lawrence, M. S., … Meyerson, M. (2010). The landscape of somatic copy-number alteration across human cancers. *Nature*, *463*(7283), 899–905. https://doi.org/10.1038/nature08822

Brancolini, C., & Iuliano, L. (2020). Proteotoxic stress and cell death in cancer cells. *Cancers*, *12*(9), 1–22. https://doi.org/10.3390/cancers12092385

Brandman, O., & Hegde, R. S. (2016). Ribosome-associated protein quality control. *Nature Structural and Molecular Biology*, *23*(1), 7–15. https://doi.org/10.1038/nsmb.3147

Brennan, C. M., Vaites, L. P., Wells, J. N., Santaguida, S., Paulo, J. A., Storchova, Z., Harper, J. W., Marsh, J. A., & Amon, A. (2019). Protein aggregation mediates stoichiometry of protein complexes in aneuploid cells. *Genes and Development*, *33*, 1031–1047. https://doi.org/10.1101/gad.327494.119

Campbell, P. J., Getz, G., Korbel, J. O., Stuart, J. M., Jennings, J. L., Stein, L. D., Perry, M. D., Nahal-Bose, H. K., Ouellette, B. F. F., Li, C. H., Rheinbay, E., Nielsen, G. P., Sgroi, D. C., Wu, C. L., Faquin, W. C., Deshpande, V., Boutros, P. C., Lazar, A. J., Hoadley, K. A., … Zhang, J. (2020). Pan-cancer analysis of whole genomes. *Nature*, *578*(7793), 82–93. https://doi.org/10.1038/s41586-020-1969-6

Chandrasekaran, V., Juszkiewicz, S., Choi, J., Puglisi, J. D., Brown, A., Shao, S., Ramakrishnan, V., & Hegde, R. S. (2019). Mechanism of ribosome stalling during translation of a poly(A) tail. *Nature Structural and Molecular Biology*, *26*(12), 1132–1140. https://doi.org/10.1038/s41594-019-0331-x

Chen, M. Z., Moily, N. S., Bridgford, J. L., Wood, R. J., Radwan, M., Smith, T. A., Song, Z., Tang, B. Z., Tilley, L., Xu, X., Reid, G. E., Pouladi, M. A., Hong, Y., & Hatters, D. M. (2017). A thiol probe for measuring unfolded protein load and proteostasis in cells. *Nature Communications*, *8*(1), 1–10. https://doi.org/10.1038/s41467-017-00203-5

Choe, Y. J., Park, S. H., Hassemer, T., Körner, R., Vincenz-Donnelly, L., Hayer-Hartl, M., & Hartl, F. U. (2016). Failure of RQC machinery causes protein aggregation and proteotoxic stress. *Nature*, *531*(7593), 191–195. https://doi.org/10.1038/nature16973

Chunduri, N. K., Barthel, K., & Storchova, Z. (2022). Consequences of Chromosome Loss: Why Do Cells Need Each Chromosome Twice? *Cells*, *11*(9), 1–18. https://doi.org/10.3390/cells11091530

Chunduri, N. K., Menges, P., Zhang, X., Wieland, A., Gotsmann, V. L., Mardin, B. R., Buccitelli, C., Korbel, J. O., Willmund, F., Kschischo, M., Raeschle, M., & Storchova, Z. (2021). Systems approaches identify the consequences of monosomy in somatic human cells. *Nature Communications*, *12*(1). https://doi.org/10.1038/s41467-021-25288-x

Chunduri, N. K., & Storchová, Z. (2019). The diverse consequences of aneuploidy. *Nature Cell Biology*, *21*(1), 54–62. https://doi.org/10.1038/s41556-018-0243-8

Cimini, D., Howell, B., Maddox, P., Khodjakov, A., Degrassi, F., & Salmon, E. D. (2001). Merotelic kinetochore orientation is a major mechanism of aneuploidy in mitotic mammalian tissue cells. *Journal of Cell Biology*, *152*(3), 517–527. https://doi.org/10.1083/jcb.153.3.517

Clemente-Ruiz, M., Murillo-Maldonado, J. M., Benhra, N., Barrio, L., Pérez, L., Quiroga, G., Nebreda, A. R., & Milán, M. (2016). Gene Dosage Imbalance Contributes to Chromosomal Instability-Induced Tumorigenesis. *Developmental Cell*, *36*(3), 290–302. https://doi.org/10.1016/j.devcel.2016.01.008

Cohen-Sharir, Y., McFarland, J. M., Abdusamad, M., Marquis, C., Bernhard, S. V., Kazachkova, M., Tang, H., Ippolito, M. R., Laue, K., Zerbib, J., Malaby, H. L. H., Jones, A., Stautmeister, L. M., Bockaj, I., Wardenaar, R., Lyons, N., Nagaraja, A., Bass, A. J., Spierings, D. C. J., … Ben-David, U. (2021). Aneuploidy renders cancer cells vulnerable to mitotic checkpoint inhibition. *Nature*, *590*(7846), 486–491. https://doi.org/10.1038/s41586-020-03114-6

Collart, M. A., & Weiss, B. (2019). Ribosome pausing, a dangerous necessity for co-translational events. *Nucleic Acids Research*, *48*(3), 1043–1055. https://doi.org/10.1093/NAR/GKZ763

Crasta, K., Ganem, N. J., Dagher, R., Lantermann, A. B., Ivanova, E. V., Pan, Y., Nezi, L., Protopopov, A., Chowdhury, D., & Pellman, D. (2012). DNA breaks and chromosome pulverization from errors in mitosis. *Nature*, *482*(7383), 53–58. https://doi.org/10.1038/nature10802

D'Orazio, K. N., Wu, C. C.-C., Sinha, N., Loll-Krippleber, R., Brown, G. W., & Green, R. (2019). The endonuclease Cue2 cleaves mRNAs at stalled ribosomes during No Go Decay. *ELife*, *8*, 1–27. https://doi.org/10.7554/elife.49117

De Leonibus, C., Cinque, L., & Settembre, C. (2019). Emerging lysosomal pathways for quality control at the endoplasmic reticulum. *FEBS Letters*, *593*(17), 2319–2329. https://doi.org/10.1002/1873-3468.13571

Decker, C. J., & Parker, R. (2012). P-bodies and stress granules: Possible roles in the control of translation and mRNA degradation. *Cold Spring Harbor Perspectives in Biology*, *4*(9). https://doi.org/10.1101/cshperspect.a012286

Dephoure, N., Hwang, S., O'Sullivan, C., Dodgson, S. E., Gygi, S. P., Amon, A., & Torres, E. M. (2014). Quantitative proteomic analysis reveals posttranslational responses to aneuploidy in yeast. *ELife*, *3*(July2014), 1–27. https://doi.org/10.7554/eLife.03023

Di Lorenzo, G., Iavarone, F., Maddaluno, M., Plata-Gómez, A. B., Aureli, S., Meza, C. P. Q., Cinque, L., Palma, A., Reggio, A., Cirillo, C., Sacco, F., Stolz, A., Napolitano, G., Marin, O., Pinna, L. A., Ruzzene, M., Limongelli, V., Efeyan, A., Grumati, P., & Settembre, C. (2022). Phosphorylation of FAM134C by CK2 controls starvation-induced ER-phagy. *Science Advances*, *8*(35), 1–18. https://doi.org/10.1126/sciadv.abo1215

Ding, W. X., & Yin, X. M. (2008). Sorting, recognition and activation of the misfolded protein degradation pathways through macroautophagy and the proteasome. *Autophagy*, *4*(2), 141–150. https://doi.org/10.4161/auto.5190

Dodgson, S. E., Santaguida, S., Kim, S., Sheltzer, J., & Amon, A. (2016). The pleiotropic deubiquitinase ubp3 confers aneuploidy tolerance. *Genes and Development*, *30*(20), 2259–2271. https://doi.org/10.1101/gad.287474.116

Donnelly, N., Passerini, V., Dürrbaum, M., Stingele, S., & Storchová, Z. (2014). HSF 1 deficiency and impaired HSP 90-dependent protein folding are hallmarks of aneuploid human cells . *The EMBO Journal*, *33*(20), 2374–2387. https://doi.org/10.15252/embj.201488648

Duncan, A. W. (2013). Aneuploidy, polyploidy and ploidy reversal in the liver. *Seminars in Cell and Developmental Biology*, *24*(4), 347–356. https://doi.org/10.1016/j.semcdb.2013.01.003

Garribba, L., De Feudis, G., Martis, V., Galli, M., Dumont, M., Eliezer, Y., Wardenaar, R., Rosaria Ippolito, M., Iyer, D. R., Tijhuis, A. E., Spierings, D. C., Schubert, M., Taglietti, S., Soriani, C., Gemble, S., Basto, R., Rhind, N., Foijer, F., Ben-David, U., … Santaguida, S. (2023). Short-term molecular consequences of chromosome mis-segregation for genome stability. *Nature Communications*, *14*(1353). https://doi.org/10.1038/s41467-023-37095-7

Garribba, L., & Santaguida, S. (2022). The Dynamic Instability of the Aneuploid Genome. *Frontiers in Cell and Developmental Biology*, *10*(February), 1–7. https://doi.org/10.3389/fcell.2022.838928

Garribba, L., Wu, W., Özer, Ö., Bhowmick, R., Hickson, I. D., & Liu, Y. (2018). Inducing and Detecting Mitotic DNA Synthesis at Difficult-to-Replicate Loci. *Methods in Enzymology*, *601*, 45–58. https://doi.org/10.1016/bs.mie.2017.11.025

Garshott, D. M., An, H., Sundaramoorthy, E., Leonard, M., Vicary, A., Harper, J. W., & Bennett, E. J. (2021). iRQC, a surveillance pathway for 40S ribosomal quality control during mRNA translation initiation. *Cell Reports*, *36*(9), 109642. https://doi.org/10.1016/j.celrep.2021.109642

Garshott, D. M., Sundaramoorthy, E., Leonard, M., & Bennett, E. J. (2020). Distinct regulatory ribosomal ubiquitylation events are reversible and hierarchically organized. *ELife*, *9*, 1–22. https://doi.org/10.7554/eLife.54023

Garzia, A., Jafarnejad, S. M., Meyer, C., Chapat, C., Gogakos, T., Morozov, P., Amiri, M., Shapiro, M., Molina, H., Tuschl, T., & Sonenberg, N. (2017). The E3 ubiquitin ligase and RNA-binding protein ZNF598 orchestrates ribosome quality control of premature polyadenylated mRNAs. *Nature Communications*, *8*(May). https://doi.org/10.1038/ncomms16056

Geigl, J. B., Obenauf, A. C., Schwarzbraun, T., & Speicher, M. R. (2008). Defining "chromosomal instability." *Trends in Genetics*, *24*(2), 64–69. https://doi.org/10.1016/j.tig.2007.11.006

Goldberg, A. L. (2003). Protein degradation and protection against misfolded or damaged proteins. *Nature*, *426*(6968), 895–899. https://doi.org/10.1038/nature02263

Goodman, C. A., & Hornberger, T. A. (2013). Measuring protein synthesis with SUnSET: A valid alternative to traditional techniques? *Exercise and Sport Sciences Reviews*, *41*(2), 107–115. https://doi.org/10.1097/JES.0b013e3182798a95

Gordon, D. J., Resio, B., & Pellman, D. (2012). Causes and consequences of aneuploidy in cancer. *Nature Reviews Genetics*, *13*(3), 189–203. https://doi.org/10.1038/nrg3123

Guang, M. H. Z., Kavanagh, E. L., Dunne, L. P., Dowling, P., Zhang, L., Lindsay, S., Bazou, D., Goh, C. Y., Hanley, C., Bianchi, G., Anderson, K. C., O'Gorman, P., & McCann, A. (2019). Targeting proteotoxic stress in cancer: A review of the role that protein quality control pathways play in oncogenesis. *Cancers*, *11*(1). https://doi.org/10.3390/cancers11010066

Hagting, A., Den Elzen, N., Vodermaier, H. C., Waizenegger, I. C., Peters, J.-M., & Pines, J. (2002). Human securin proteolysis is controlled by the spindle checkpoint and reveals when the APC/C switches from activation by Cdc20 to Cdh1. *The Journal of Cell Biology*, *157*(7), 1125–1137. https://doi.org/10.1083/jcb.200111001

Hanahan, D., & Weinberg, R. A. (2011). Hallmarks of cancer: The next generation. *Cell*, *144*(5), 646–674. https://doi.org/10.1016/j.cell.2011.02.013

Harper, J. W., & Bennett, E. J. (2016). Proteome complexity and the forces that drive proteome imbalance. *Nature*, *537*(7620), 328–338. https://doi.org/10.1038/nature19947

Hatch, E. M., & Hetzer, M. W. (2015). Linking Micronuclei to Chromosome Fragmentation. *Cell*, *161*(7), 1502–1504. https://doi.org/10.1016/j.cell.2015.06.005

Hidalgo San Jose, L., Sunshine, M. J., Dillingham, C. H., Chua, B. A., Kruta, M., Hong, Y., Hatters, D. M., & Signer, R. A. J. (2020). Modest Declines in Proteome Quality Impair Hematopoietic Stem Cell Self-Renewal. *Cell Reports*, *30*(1), 69-80.e6. https://doi.org/10.1016/j.celrep.2019.12.003

Higgins, R., Gendron, J. M., Rising, L., Mak, R., Webb, K., Kaiser, S. E., Zuzow, N., Riviere, P., Yang, B., Fenech, E., Tang, X., Lindsay, S. A., Christianson, J. C., Hampton, R. Y., Wasserman, S. A., & Bennett, E. J. (2015). The Unfolded Protein Response Triggers Site-Specific Regulatory Ubiquitylation of 40S Ribosomal Proteins. *Molecular Cell*, *59*(1), 35–49. https://doi.org/10.1016/j.molcel.2015.04.026

Holland, A. J., & Cleveland, D. W. (2012). Losing balance: The origin and impact of aneuploidy in cancer. *EMBO Reports*, *13*(6), 501–514. https://doi.org/10.1038/embor.2012.55

Hoter, A., Rizk, S., & Naim, H. Y. (2019). The multiple roles and therapeutic potential of molecular chaperones in prostate cancer. *Cancers*, *11*(8), 1–36. https://doi.org/10.3390/cancers11081194

Hwang, S., Cavaliere, P., Li, R., Zhu, L. J., Dephoure, N., & Torres, E. M. (2021). Consequences of aneuploidy in human fibroblasts with trisomy 21. *Proceedings of the National Academy of Sciences of the United States of America*, *118*(6). https://doi.org/10.1073/pnas.2014723118

Iavarone, F., Di Lorenzo, G., & Settembre, C. (2022). Regulatory events controlling ER-phagy. *Current Opinion in Cell Biology*, *76*, 102084. https://doi.org/10.1016/j.ceb.2022.102084

Ippolito, M. R., Martis, V., Martin, S., Tijhuis, A. E., Hong, C., Wardenaar, R., Dumont, M., Zerbib, J., Spierings, D. C. J., Fachinetti, D., Ben-David, U., Foijer, F., & Santaguida, S. (2021). Gene copy-number changes and chromosomal instability induced by aneuploidy confer resistance to chemotherapy. *Developmental Cell*, *56*(17), 2440-2454.e6. https://doi.org/10.1016/j.devcel.2021.07.006

Izawa, D., & Pines, J. (2015). The mitotic checkpoint complex binds a second CDC20 to inhibit active APC/C. *Nature*, *517*(7536), 631–634. https://doi.org/10.1038/nature13911

Janssen, A., Van Der Burg, M., Szuhai, K., Kops, G. J. P. L., & Medema, R. H. (2011). Chromosome segregation errors as a cause of DNA damage and structural chromosome aberrations. *Science*, *333*(6051), 1895–1898. https://doi.org/10.1126/science.1210214

Ji, Z., Chuen, J., Kiparaki, M., & Baker, N. (2021). Cell competition removes segmental aneuploid cells from drosophila imaginal disc-derived tissues based on ribosomal protein gene dose. *ELife*, *10*, 1–33. https://doi.org/10.7554/ELIFE.61172

Jiang, H.-Y., Wek, S. A., McGrath, B. C., Lu, D., Hai, T., Harding, H. P., Wang, X., Ron, D., Cavener, D. R., & Wek, R. C. (2004). Activating Transcription Factor 3 Is Integral to the Eukaryotic Initiation Factor 2 Kinase Stress Response. *Molecular and Cellular Biology*, *24*(3), 1365–1377. https://doi.org/10.1128/mcb.24.3.1365-1377.2004

Joazeiro, C. A. P. (2019). Mechanisms and functions of ribosome-associated protein quality control. *Nature Reviews Molecular Cell Biology*, *20*(6), 368–383. https://doi.org/10.1038/s41580-019-0118-2

Johnson, V. L., Scott, M. I. F., Holt, S. V., Hussein, D., & Taylor, S. S. (2004). Bub1 is required for kinetochore localization of BubR1, Cenp-E, Cenp-F and Mad2, and chromosome congression. *Journal of Cell Science*, *117*(8), 1577–1589. https://doi.org/10.1242/jcs.01006

Joy, J., Barrio, L., Santos-Tapia, C., Romão, D., Giakoumakis, N. N., Clemente-Ruiz, M., & Milán, M. (2021). Proteostasis failure and mitochondrial dysfunction leads to aneuploidy-induced senescence. *Developmental Cell*, *56*(14), 2043-2058.e7. https://doi.org/10.1016/j.devcel.2021.06.009

Juszkiewicz, S., Chandrasekaran, V., Lin, Z., Kraatz, S., Ramakrishnan, V., & Hegde, R. S. (2018). ZNF598 Is a Quality Control Sensor of Collided Ribosomes. *Molecular Cell*, *72*(3), 469-481.e7. https://doi.org/10.1016/j.molcel.2018.08.037

Juszkiewicz, S., & Hegde, R. S. (2017). Initiation of Quality Control during Poly(A) Translation Requires Site-Specific Ribosome Ubiquitination. *Molecular Cell*, *65*(4), 743-750.e4. https://doi.org/10.1016/j.molcel.2016.11.039

Juszkiewicz, S., & Hegde, R. S. (2018). Quality Control of Orphaned Proteins. *Molecular Cell*, *71*(3), 443–457. https://doi.org/10.1016/j.molcel.2018.07.001

Juszkiewicz, S., Slodkowicz, G., Lin, Z., Freire-Pritchett, P., Peak-Chew, S. Y., & Hegde, R. S. (2020). Ribosome collisions trigger cis-acting feedback inhibition of translation initiation. *ELife*, *9*, 1–29. https://doi.org/10.7554/eLife.60038

Juszkiewicz, S., Speldewinde, S. H., Wan, L., Svejstrup, J. Q., & Hegde, R. S. (2020). The ASC-1 Complex Disassembles Collided Ribosomes. *Molecular Cell*, *79*(4), 603-614.e8. https://doi.org/10.1016/j.molcel.2020.06.006

Kedersha, N., Chen, S., Gilks, N., Li, W., Miller, I. J., Stahl, J., & Anderson, P. (2002). Evidence That Ternary Complex (eIF2-GTP-tRNAi Met)– Deficient Preinitiation Complexes Are Core Constituents of Mammalian Stress Granules. *Molecular Biology of the Cell*, *13*, 195–210. https://doi.org/10.1091/mbc.01

Khan, M., Shaukat, Z., Saint, R., & Gregory, S. L. (2018). Chromosomal instability causes sensitivity to protein folding stress and ATP depletion. *Biology Open*, *7*(10). https://doi.org/10.1242/bio.038000

Kimura, S., Noda, T., & Yoshimori, T. (2007). Dissection of the autophagosome maturation process by a novel reporter protein, tandem fluorescent-tagged LC3. *Autophagy*, *3*(5), 452–460. https://doi.org/10.4161/auto.4451

Kirkin, V., McEwan, D. G., Novak, I., & Dikic, I. (2009). A Role for Ubiquitin in Selective Autophagy. *Molecular Cell*, *34*(3), 259–269. https://doi.org/10.1016/j.molcel.2009.04.026

Klionsky, D. J., Abdel-Aziz, A. K., Abdelfatah, S., Abdellatif, M., Abdoli, A., Abel, S., Abeliovich, H., Abildgaard, M. H., Abudu, Y. P., Acevedo-Arozena, A., Adamopoulos, I. E., Adeli, K., Adolph, T. E., Adornetto, A., Aflaki, E., Agam, G., Agarwal, A., Aggarwal, B. B., Agnello, M., … Tong, C. K. (2021). Guidelines for the use and interpretation of assays for monitoring autophagy (4th edition)1. *Autophagy*, *17*(1), 1–382. https://doi.org/10.1080/15548627.2020.1797280

Knouse, K. A., Wu, J., Whittaker, C. A., & Amon, A. (2014). Single cell sequencing reveals low levels of aneuploidy across mammalian tissues. *Proceedings of the National Academy of Sciences of the United States of America*, *111*(37), 13409–13414. https://doi.org/10.1073/pnas.1415287111

Kraft, C., Deplazes, A., Sohrmann, M., & Peter, M. (2008). Mature ribosomes are selectively degraded upon starvation by an autophagy pathway requiring the Ubp3p/Bre5p ubiquitin protease. *Nature Cell Biology*, *10*(5), 602–610. https://doi.org/10.1038/ncb1723

Lara-Gonzalez, P., Westhorpe, F. G., & Taylor, S. S. (2012). The spindle assembly checkpoint. *Current Biology*, *22*(22), R966–R980. https://doi.org/10.1016/j.cub.2012.10.006

Larrimore, K. E., Barattin-Voynova, N. S., Reid, D. W., & Ng, D. T. W. (2020). Aneuploidy-induced proteotoxic stress can be effectively tolerated without dosage compensation, genetic mutations, or stress responses. *BMC Biology*, *18*(1), 1–19. https://doi.org/10.1186/s12915-020-00852-x

Lauria, F., Bernabò, P., Tebaldi, T., Groen, E. J. N., Perenthaler, E., Maniscalco, F., Rossi, A., Donzel, D., Clamer, M., Marchioretto, M., Omersa, N., Orri, J., Dalla Serra, M., Anderluh, G., Quattrone, A., Inga, A., Gillingwater, T. H., & Viero, G. (2020). SMN-primed ribosomes modulate the translation of transcripts related to spinal muscular atrophy. *Nature Cell Biology*, *22*(10), 1239–1251. https://doi.org/10.1038/s41556-020-00577-7

Le Guerroué, F., Eck, F., Jung, J., Starzetz, T., Mittelbronn, M., Kaulich, M., & Behrends, C. (2017). Autophagosomal Content Profiling Reveals an LC3C-Dependent Piecemeal Mitophagy Pathway. *Molecular Cell*, *68*(4), 786-796.e6. https://doi.org/10.1016/j.molcel.2017.10.029

Lee, Y.-K., & Lee, J.-A. (2016). Role of the mammalian ATG8/LC3 family in autophagy: differential and compensatory roles in the spatiotemporal regulation of autophagy. *BMB Reports*, *49*(8), 424–430. https://doi.org/10.5483/bmbrep.2016.49.8.081

Levine, M. S., & Holland, A. J. (2018). The impact of mitotic errors on cell proliferation and tumorigenesis. *Genes and Development*, *32*(9–10), 620–638. https://doi.org/10.1101/gad.314351.118

Li, M., Fang, X., Baker, D. J., Guo, L., Gao, X., Wei, Z., Han, S., Van Deursen, J. M., & Zhang, P. (2010). The ATM-p53 pathway suppresses aneuploidy-induced tumorigenesis. *Proceedings of the National Academy of Sciences of the United States of America*, *107*(32), 14188–14193. https://doi.org/10.1073/pnas.1005960107

Lin, X., Li, S., Zhao, Y., Ma, X., Zhang, K., He, X., & Wang, Z. (2013). Interaction domains of p62: A bridge between p62 and selective autophagy. *DNA and Cell Biology*, *32*(5), 220–227. https://doi.org/10.1089/dna.2012.1915

Liu, B., Han, Y., & Qian, S. B. (2013). Cotranslational Response to Proteotoxic Stress by Elongation Pausing of Ribosomes. *Molecular Cell*, *49*(3), 453–463. https://doi.org/10.1016/j.molcel.2012.12.001

Liu, W. J., Ye, L., Huang, W. F., Guo, L. J., Xu, Z. G., Wu, H. L., Yang, C., & Liu, H. F. (2016). P62 Links the Autophagy Pathway and the Ubiqutin-Proteasome System Upon Ubiquitinated Protein Degradation. *Cellular and Molecular Biology Letters*, *21*(1), 1–14. https://doi.org/10.1186/s11658-016-0031-z

London, N., & Biggins, S. (2014). Signalling dynamics in the spindle checkpoint response. *Nature Reviews Molecular Cell Biology*,

15(11), 735–747. https://doi.org/10.1038/nrm3888

Lukow, D. A., Sausville, E. L., Suri, P., Chunduri, N. K., Wieland, A., Leu, J., Smith, J. C., Girish, V., Kumar, A. A., Kendall, J., Wang, Z., Storchova, Z., & Sheltzer, J. M. (2021). Chromosomal instability accelerates the evolution of resistance to anti-cancer therapies. *Developmental Cell*, *56*(17), 2427-2439.e4. https://doi.org/10.1016/j.devcel.2021.07.009

Ly, P., Brunner, S. F., Shoshani, O., Kim, D. H., Lan, W., Pyntikova, T., Flanagan, A. M., Behjati, S., Page, D. C., Campbell, P. J., & Cleveland, D. W. (2019). Chromosome segregation errors generate a diverse spectrum of simple and complex genomic rearrangements. *Nature Genetics*, *51*(4), 705–715. https://doi.org/10.1038/s41588-019-0360-8

Lykke-Andersen, J., & Bennett, E. J. (2014). Protecting the proteome: Eukaryotic cotranslational quality control pathways. *Journal of Cell Biology*, *204*(4), 467–476. https://doi.org/10.1083/jcb.201311103

Lyumkis, D., Dos Passosb, D. O., Tahara, E. B., Webb, K., Bennett, E. J., Vinterbo, S., Potter, C. S., Carragher, B., & Joazeiro, C. A. P. (2014). Structural basis for translational surveillance by the large ribosomal subunit-associated protein quality control complex. *Proceedings of the National Academy of Sciences of the United States of America*, *111*(45), 15981–15986. https://doi.org/10.1073/pnas.1413882111

Maciejowski, J., Li, Y., Bosco, N., Campbell, P. J., & De Lange, T. (2015). Chromothripsis and Kataegis Induced by Telomere Crisis. *Cell*, *163*(7), 1641–1654. https://doi.org/10.1016/j.cell.2015.11.054

MacKenzie, K. J., Carroll, P., Martin, C. A., Murina, O., Fluteau, A., Simpson, D. J., Olova, N., Sutcliffe, H., Rainger, J. K., Leitch, A., Osborn, R. T., Wheeler, A. P., Nowotny, M., Gilbert, N., Chandra, T., Reijns, M. A. M., & Jackson, A. P. (2017). CGAS surveillance of micronuclei links genome instability to innate immunity. *Nature*, *548*(7668), 461–465. https://doi.org/10.1038/nature23449

Maiato, H., & Logarinho, E. (2014). Mitotic spindle multipolarity without centrosome amplification. *Nature Cell Biology*, *16*(5), 386–394. https://doi.org/10.1038/ncb2958

Mancias, J. D., Wang, X., Gygi, S. P., Harper, J. W., & Kimmelman, A. C. (2014). Quantitative proteomics identifies NCOA4 as the cargo receptor mediating ferritinophagy. *Nature*, *508*(7498), 105–109. https://doi.org/10.1038/nature13148

Mapelli, M., Massimiliano, L., Santaguida, S., & Musacchio, A. (2007). The Mad2 Conformational Dimer: Structure and Implications for the Spindle Assembly Checkpoint. *Cell*, *131*(4), 730–743. https://doi.org/10.1016/j.cell.2007.08.049

Marciniak, S. J., Yun, C. Y., Oyadomari, S., Novoa, I., Zhang, Y., Jungreis, R., Nagata, K., Harding, H. P., & Ron, D. (2004). CHOP induces death by promoting protein synthesis and oxidation in the stressed endoplasmic reticulum. *Genes and Development*, *18*(24), 3066–3077. https://doi.org/10.1101/gad.1250704

Marino, S. M., & Gladyshev, V. N. (2010). Cysteine Function Governs Its Conservation and Degeneration and Restricts Its Utilization on Protein Surfaces. *Journal of Molecular Biology*, *404*(5), 902–916. https://doi.org/10.1016/j.jmb.2010.09.027

Martin, S., & Santaguida, S. (2020). Understanding Complexity of Cancer Genomes: Lessons from Errors. *Developmental Cell*, *53*(5), 500–502. https://doi.org/10.1016/j.devcel.2020.05.004

Massey, A. J., Williamson, D. S., Browne, H., Murray, J. B., Dokurno, P., Shaw, T., Macias, A. T., Daniels, Z., Geoffroy, S., Dopson, M., Lavan, P., Matassova, N., Francis, G. L., Graham, C. J., Parsons, R., Wang, Y., Padfield, A., Comer, M., Drysdale, M. J., & Wood, M. (2010). A novel, small molecule inhibitor of Hsc70/Hsp70 potentiates Hsp90 inhibitor induced apoptosis in HCT116 colon carcinoma cells. *Cancer Chemotherapy and Pharmacology*, *66*(3), 535–545. https://doi.org/10.1007/s00280-009-1194-3

Matsuo, Y., Ikeuchi, K., Saeki, Y., Iwasaki, S., Schmidt, C., Udagawa, T., Sato, F., Tsuchiya, H., Becker, T., Tanaka, K., Ingolia, N. T., Beckmann, R., & Inada, T. (2017). Ubiquitination of stalled ribosome triggers ribosome-associated quality control. *Nature Communications*, *8*(1), 1–13. https://doi.org/10.1038/s41467-017-00188-1

Maurel, M., Chevet, E., Tavernier, J., & Gerlo, S. (2014). Getting RIDD of RNA: IRE1 in cell fate regulation. *Trends in Biochemical Sciences*, *39*(5), 245–254. https://doi.org/10.1016/j.tibs.2014.02.008

McGranahan, N., Burrell, R. A., Endesfelder, D., Novelli, M. R., & Swanton, C. (2012). Cancer chromosomal instability: Therapeutic and diagnostic challenges. *EMBO Reports*, *13*(6), 528–538. https://doi.org/10.1038/embor.2012.61

Meyer, C., Garzia, A., Morozov, P., Molina, H., & Tuschl, T. (2020). The G3BP1-Family-USP10 Deubiquitinase Complex Rescues Ubiquitinated 40S Subunits of Ribosomes Stalled in Translation from Lysosomal Degradation. *Molecular Cell*, 1–13. https://doi.org/10.1016/j.molcel.2019.12.024

Meyer, H., & Weihl, C. C. (2014). The VCP/p97 system at a glance: Connecting cellular function to disease pathogenesis. *Journal of Cell Science*, *127*(18), 3877–3883. https://doi.org/10.1242/JCS.093831

Miao, Z. H., Player, A., Shankavaram, U., Wang, Y. H., Zimonjic, D. B., Lorenzi, P. L., Liao, Z. Y., Liu, H., Shimura, T., Zhang, H. L., Meng, L. H., Zhang, Y. W., Kawasaki, E. S., Popescu, N. C., Aladjem, M. I., Goldstein, D. J., Weinstein, J. N., & Pommier, Y. (2007). Nonclassic functions of human topoisomerase I: Genome-wide and pharmacologic analyses. *Cancer Research*, *67*(18), 8752–8761. https://doi.org/10.1158/0008-5472.CAN-06-4554

Miyata, Y. (2005). Hsp90 inhibitor geldanamycin and its derivatives as novel cancer chemotherapeutic agents. *Current Pharmaceutical Design*, *11*(9), 1131–1138. https://doi.org/10.2174/1381612053507585

Mizushima, N., Yoshimori, T., & Levine, B. (2010). Methods in Mammalian Autophagy Research. *Cell*, *140*(3), 313–326. https://doi.org/10.1016/j.cell.2010.01.028

Musacchio, A., & Salmon, E. D. (2007). The spindle-assembly checkpoint in space and time. *Nature Reviews Molecular Cell Biology*, *8*(5), 379–393. https://doi.org/10.1038/nrm2163

Muzzopappa, M., Murcia, L., & Milán, M. (2017). Feedback amplification loop drives malignant growth in epithelial tissues. *Proceedings of the National Academy of Sciences of the United States of America*, *114*(35), E7291–E7300. https://doi.org/10.1073/pnas.1701791114

Nasmyth, K., & Haering, C. H. (2009). Cohesin: Its roles and mechanisms. *Annual Review of Genetics*, *43*, 525–558. https://doi.org/10.1146/annurev-genet-102108-134233

Oromendia, A. B., & Amon, A. (2014). Aneuploidy: Implications for protein homeostasis and disease. *DMM Disease Models and Mechanisms*, *7*(1), 15–20. https://doi.org/10.1242/dmm.013391

Oromendia, A. B., Dodgson, S. E., & Amon, A. (2012). Aneuploidy causes proteotoxic stress in yeast. *Genes and Development*, *26*(24), 2696–2708. https://doi.org/10.1101/gad.207407.112

Ossareh-Nazari, B., Niño, C. A., Bengtson, M. H., Lee, J. W., Joazeiro, C. A. P., & Dargemont, C. (2014). Ubiquitylation by the Ltn1 E3 ligase protects 60S ribosomes from starvation-induced selective autophagy. *Journal of Cell Biology*, *204*(6), 909–917. https://doi.org/10.1083/jcb.201308139

Padovani, C., Jevtić, P., & Rapé, M. (2022). Quality control of protein complex composition. *Molecular Cell*, *82*(8), 1439–1450. https://doi.org/10.1016/j.molcel.2022.02.029

Panas, M. D., Ivanov, P., & Anderson, P. (2016). Mechanistic insights into mammalian stress granule dynamics. *Journal of Cell Biology*, *215*(3), 313–323. https://doi.org/10.1083/jcb.201609081

Pechmann, S., Willmund, F., & Frydman, J. (2013). The Ribosome as a Hub for Protein Quality Control. *Molecular Cell*, *49*(3), 411–421. https://doi.org/10.1016/j.molcel.2013.01.020

Peters, J. M. (2006). The anaphase promoting complex/cyclosome: A machine designed to destroy. *Nature Reviews Molecular Cell Biology*, *7*(9), 644–656. https://doi.org/10.1038/nrm1988

Pfau, S. J., & Amon, A. (2012). Chromosomal instability and aneuploidy in cancer: from yeast to man. *EMBO Reports*, *13*(6), 515–527. https://doi.org/10.1038/EMBOR.2012.65

Pines, J., & Hunter, T. (1991). Cyclin-dependent kinases: a new cell cycle motif? *Trends in Cell Biology*, *1*(5), 117–121. https://doi.org/https://doi.org/10.1016/0962-8924(91)90116-Q

Reich, M., Liefeld, T., Gould, J., Lerner, J., Tamayo, P., & Mesirov, J. P. (2006). GenePattern 2.0. *Nature Genetics*, *38*(5), 500–501. https://doi.org/10.1038/ng0506-500

Rutledge, S. D., Douglas, T. A., Nicholson, J. M., Vila-Casadesús, M., Kantzler, C. L., Wangsa, D., Barroso-Vilares, M., Kale, S. D., Logarinho, E., & Cimini, D. (2016). Selective advantage of trisomic human cells cultured in non-standard conditions. *Scientific Reports*, *6*(March), 1–12. https://doi.org/10.1038/srep22828

Santaguida, S., & Amon, A. (2015a). Aneuploidy triggers a TFEB-mediated lysosomal stress response. *Autophagy*, *11*(12), 2383–2384. https://doi.org/10.1080/15548627.2015.1110670

Santaguida, S., & Amon, A. (2015b). Short- and long-term effects of chromosome mis-segregation and aneuploidy. *Nature Reviews Molecular Cell Biology*, *16*(8), 473–485. https://doi.org/10.1038/nrm4025

Santaguida, S., & Musacchio, A. (2009). The life and miracles of kinetochores. *EMBO Journal*, *28*(17), 2511–2531. https://doi.org/10.1038/emboj.2009.173

Santaguida, S., Richardson, A., Iyer, D. R., M'Saad, O., Zasadil, L., Knouse, K. A., Wong, Y. L., Rhind, N., Desai, A., & Amon, A. (2017). Chromosome Mis-segregation Generates Cell-Cycle-Arrested Cells with Complex Karyotypes that Are Eliminated by the Immune System. *Developmental Cell*, *41*(6), 638-651.e5. https://doi.org/10.1016/j.devcel.2017.05.022

Santaguida, S., Tighe, A., D'Alise, A. M., Taylor, S. S., & Musacchio, A. (2010). Dissecting the role of MPS1 in chromosome biorientation and the spindle checkpoint through the small molecule inhibitor reversine. *Journal of Cell Biology*, *190*(1), 73–87. https://doi.org/10.1083/jcb.201001036

Santaguida, S., Vasile, E., White, E., & Amon, A. (2015). Aneuploidy-induced cellular stresses limit autophagic degradation. *Genes and Development*, *29*(19), 2010–2021. https://doi.org/10.1101/gad.269118.115

Santaguida, S., Vernieri, C., Villa, F., Ciliberto, A., & Musacchio, A. (2011). Evidence that Aurora B is implicated in spindle checkpoint signalling independently of error correction. *EMBO Journal*, *30*(8), 1508–1519. https://doi.org/10.1038/emboj.2011.70

Schmidt, E. K., Clavarino, G., Ceppi, M., & Pierre, P. (2009). SUnSET, a nonradioactive method to monitor protein synthesis. *Nature Methods*, *6*(4), 275–277. https://doi.org/10.1038/nmeth.1314

Schuller, A. P., & Green, R. (2018). Roadblocks and resolutions in eukaryotic translation. *Nature Reviews Molecular Cell Biology*, *19*(8), 526–541. https://doi.org/10.1038/s41580-018-0011-4

Schvartzman, J. M., Duijf, P. H. G., Sotillo, R., Coker, C., & Benezra, R. (2011). Mad2 is a critical mediator of the chromosome instability observed upon Rb and p53 pathway inhibition. *Cancer Cell*, *19*(6), 701–714. https://doi.org/10.1016/j.ccr.2011.04.017

Settembre, C., Di Malta, C., Polito, V. A., Arencibia, M. G., Vetrini, F., Erdin, S., Erdin, S. U., Huynh, T., Medina, D., Colella, P., Sardiello, M., Rubinsztein, D. C., & Ballabio, A. (2011). TFEB links autophagy to lysosomal biogenesis. *Science*, *332*(6036), 1429–1433. https://doi.org/10.1126/science.1204592

Settembre, C., Fraldi, A., Medina, D. L., & Ballabio, A. (2013). Signals from the lysosome: a control centre for cellular clearance and energy metabolism. *Nature Reviews Molecular Cell Biology*, *14*(5), 283–296. https://doi.org/10.1038/nrm3565

Settembre, C., Zoncu, R., Medina, D. L., Vetrini, F., Erdin, S., Erdin, S., Huynh, T., Ferron, M., Karsenty, G., Vellard, M. C., Facchinetti, V., Sabatini, D. M., & Ballabio, A. (2012). A lysosome-to-nucleus signalling mechanism senses and regulates the lysosome via mTOR and TFEB. *EMBO Journal*, *31*(5), 1095–1108. https://doi.org/10.1038/emboj.2012.32

Shao, S., & Hegde, R. S. (2016). Target Selection during Protein Quality Control. *Trends in Biochemical Sciences*, *41*(2), 124–137. https://doi.org/10.1016/j.tibs.2015.10.007

Shao, S., Von der Malsburg, K., & Hegde, R. S. (2013). Listerin-dependent nascent protein ubiquitination relies on ribosome subunit dissociation. *Molecular Cell*, *50*(5), 637–648. https://doi.org/10.1016/j.molcel.2013.04.015

Sheltzer, J. M., & Amon, A. (2011). The aneuploidy paradox: Costs and benefits of an incorrect karyotype. *Trends in Genetics*, *27*(11), 446–453. https://doi.org/10.1016/j.tig.2011.07.003

Sheltzer, J. M., Torres, E. M., Dunham, M. J., & Amon, A. (2012). Transcriptional consequences of aneuploidy. *Proceedings of the National Academy of Sciences of the United States of America*, *109*(31), 12644–12649. https://doi.org/10.1073/pnas.1209227109

Siegel, J. J., & Amon, A. (2012). New Insights into the Troubles of Aneuploidy. *Annual Review of Cell and Developmental Biology*, *28*(1), 189–214. https://doi.org/10.1146/annurev-cellbio-101011-155807

Sigoillot, F. D., Lyman, S., Huckins, J. F., Adamson, B., Chung, E., Quattrochi, B., & King, R. W. (2012). A bioinformatics method identifies prominent off-targeted transcripts in RNAi screens. *Nature Methods*, *9*(4), 363–366. https://doi.org/10.1038/nmeth.1898

Simms, C. L., Yan, L. L., Qiu, J. K., & Zaher, H. S. (2019). Ribosome Collisions Result in +1 Frameshifting in the Absence of No-Go Decay. *Cell Reports*, *28*(7), 1679-1689.e4. https://doi.org/10.1016/j.celrep.2019.07.046

Simms, C. L., Yan, L. L., & Zaher, H. S. (2017). Ribosome Collision Is Critical for Quality Control during No-Go Decay. *Molecular Cell*, *68*(2), 361-373.e5. https://doi.org/10.1016/j.molcel.2017.08.019

Sinha, N. K., Ordureau, A., Best, K. M., Saba, J. A., Zinshteyn, B., Sundaramoorthy, E., Fulzele, A., Garshott, D. M., Denk, T., Thoms, M., Paulo, J. A., Harper, J. W., Bennett, E. J., Beckmann, R., & Green, R. (2020). EDF1 coordinates cellular responses to ribosome collisions. *ELife*, *9*, 1–84. https://doi.org/10.7554/ELIFE.58828

Sitron, C. S., & Brandman, O. (2020). Detection and Degradation of Stalled Nascent Chains via Ribosome-Associated Quality Control. *Annual Review of Biochemistry*, *89*, 417–442. https://doi.org/10.1146/annurev-biochem-013118-110729

Soto, M., García-Santisteban, I., Krenning, L., Medema, R. H., & Raaijmakers, J. A. (2018). Chromosomes trapped in micronuclei are liable to segregation errors. *Journal of Cell Science*, *131*(13). https://doi.org/10.1242/jcs.214742

Soto, M., Raaijmakers, J. A., & Medema, R. H. (2019). Consequences of Genomic Diversification Induced by Segregation Errors. *Trends in Genetics*, *35*(4), 279–291. https://doi.org/10.1016/j.tig.2019.01.003

Stingele, S., Stoehr, G., Peplowska, K., Cox, J., Mann, M., & Storchova, Z. (2012). Global analysis of genome, transcriptome and proteome reveals the response to aneuploidy in human cells. *Molecular Systems Biology*, *8*(608). https://doi.org/10.1038/msb.2012.40

Stingele, S., Stoehr, G., & Storchova, Z. (2013). Activation of autophagy in cells with abnormal karyotype. *Autophagy*, *9*(2), 246–248. https://doi.org/10.4161/auto.22558

Subramanian, A., Tamayo, P., Mootha, V. K., Mukherjee, S., Ebert, B. L., Gillette, M. A., Paulovich, A., Pomeroy, S. L., Golub, T. R., Lander, E. S., & Mesirov, J. P. (2005). Gene set enrichment analysis: A knowledge-based approach for interpreting genome-wide expression profiles. *Proceedings of the National Academy of Sciences of the United States of America*, *102*(43), 15545–15550. https://doi.org/10.1073/pnas.0506580102

Sun, N., Malide, D., Liu, J., Rovira, I. I., Combs, C. A., & Finkel, T. (2017). A fluorescence-based imaging method to measure in vitro and in vivo mitophagy using mt-Keima. *Nature Protocols*, *12*(8), 1576–1587. https://doi.org/10.1038/nprot.2017.060

Sundaramoorthy, E., Leonard, M., Mak, R., Liao, J., Fulzele, A., & Bennett, E. J. (2017). ZNF598 and RACK1 Regulate Mammalian Ribosome-Associated Quality Control Function by Mediating Regulatory 40S Ribosomal Ubiquitylation. *Molecular Cell*, *65*(4), 751-760.e4. https://doi.org/10.1016/j.molcel.2016.12.026

Täckholm, G. (1922). *Zytologische Studien über die Gattung Rosa*. Almqvist & Wiksells boktr. https://www.biodiversitylibrary.org/item/52699

Taipale, M., Jarosz, D. F., & Lindquist, S. (2010). HSP90 at the hub of protein homeostasis: Emerging mechanistic insights. *Nature Reviews Molecular Cell Biology*, *11*(7), 515–528. https://doi.org/10.1038/nrm2918

Tanaka, T., Fuchs, J., Loidl, J., & Nasmyth, K. (2000). Cohesin ensures bipolar attachment of microtubules to sister centromeres and resists their precocious separation. *Nature Cell Biology*, *2*(8), 492–499. https://doi.org/10.1038/35019529

Tang, Y. C., & Amon, A. (2013). Gene copy-number alterations: A cost-benefit analysis. *Cell*, *152*(3), 394–405. https://doi.org/10.1016/j.cell.2012.11.043

Tang, Y. C., Williams, B. R., Siegel, J. J., & Amon, A. (2011). Identification of aneuploidy-selective antiproliferation compounds. *Cell*, *144*(4), 499–512. https://doi.org/10.1016/j.cell.2011.01.017

Taniuchi, S., Miyake, M., Tsugawa, K., Oyadomari, M., & Oyadomari, S. (2016). Integrated stress response of vertebrates is regulated by four eIF2α kinases. *Scientific Reports*, *6*, 1–11. https://doi.org/10.1038/srep32886

Taylor, S. S., Scott, M. I. F., & Holland, A. J. (2004). The spindle checkpoint: A quality control mechanism which ensures accurate chromosome segregation. *Chromosome Research*, *12*(6), 599–616. https://doi.org/10.1023/B:CHRO.0000036610.78380.51

Thompson, S. L., & Compton, D. A. (2010). Proliferation of aneuploid human cells is limited by a p53-dependent mechanism. *Journal of Cell Biology*, *188*(3), 369–381. https://doi.org/10.1083/jcb.200905057

Torres, E. M., Sokolsky, T., Tucker, C. M., Chan, L. Y., Boselli, M., Dunham, M. J., & Amon, A. (2007). Effects of aneuploidy on cellular physiology and cell division in haploid yeast. *Science*, *317*(5840), 916–924. https://doi.org/10.1126/SCIENCE.1142210

Torres, E. M., Williams, B. R., & Amon, A. (2008). Aneuploidy: Cells Losing Their Balance. *Genetics*, *179*(2), 737–746. https://doi.org/10.1534/GENETICS.108.090878

Tye, B. W., Commins, N., Ryazanova, L. V., Wühr, M., Springer, M., Pincus, D., & Churchman, L. S. (2019). Proteotoxicity from aberrant ribosome biogenesis compromises cell fitness. *ELife*, *8*, 1–29. https://doi.org/10.7554/eLife.43002

Uetake, Y., & Sluder, G. (2010). Prolonged prometaphase blocks daughter cell proliferation despite normal completion of mitosis. *Current Biology*, *20*(18), 1666–1671. https://doi.org/10.1016/j.cub.2010.08.018

Umbreit, N. T., Zhang, C. Z., Lynch, L. D., Blaine, L. J., Cheng, A. M., Tourdot, R., Sun, L., Almubarak, H. F., Judge, K., Mitchell, T. J., Spektor, A., & Pellman, D. (2020). Mechanisms generating cancer genome complexity from a single cell division error. *Science*, *368*(6488). https://doi.org/10.1126/science.aba0712

Uphoff, C. C., & Drexler, H. G. (2002). Comparative PCR analysis for detection of mycoplasma infections in continuous cell lines. *In Vitro Cellular and Developmental Biology - Animal*, *38*(2), 79–85. https://doi.org/10.1290/1071-2690(2002)038<0079:CPAFDO>2.0.CO;2

Vitale, M., Bakunts, A., Orsi, A., Lari, F., Tadé, L., Danieli, A., Rato, C., Valetti, C., Sitia, R., Raimondi, A., Christianson, J. C., & Van Anken, E. (2019). Inadequate BiP availability defines endoplasmic reticulum stress. *ELife*, *8*, 1–17. https://doi.org/10.7554/eLife.41168

Walter, P., & Ron, D. (2011). The unfolded protein response: from stress pathway to homeostatic regulation. *Science (New York, N.Y.)*, *334*(6059), 1081–1086. https://doi.org/10.1126/science.1209038

Wang, R. W., MacDuffie, E., & Santaguida, S. (2018). Generation and isolation of cell cycle-arrested cells with complex karyotypes. *Journal of Visualized Experiments*, *2018*(134), 1–6. https://doi.org/10.3791/57215

Wang, R. W., Viganò, S., Ben-David, U., Amon, A., & Santaguida, S. (2021). Aneuploid senescent cells activate NF-κB to promote their immune clearance by NK cells. *EMBO Reports*, *22*(8), 1–16. https://doi.org/10.15252/embr.202052032

Weaver, B. A., & Cleveland, D. W. (2008). The Aneuploidy Paradox in Cell Growth and Tumorigenesis. *Cancer Cell*, *14*(6), 431–433. https://doi.org/10.1016/j.ccr.2008.11.011

Williams, B. R., Prabhu, V. R., Hunter, K. E., Glazier, C. M., Whittaker, C. a, Housman, D. E., & Amon, A. (2008). Aneuploidy Affects Proliferation and Spontaneous Immortalization in Mammalian Cells. *Science*, *322*(October), 703–710.

Wu, C. C. C., Peterson, A., Zinshteyn, B., Regot, S., & Green, R. (2020). Ribosome Collisions Trigger General Stress Responses to Regulate Cell Fate. *Cell*, *182*(2), 404-416.e14. https://doi.org/10.1016/j.cell.2020.06.006

Yahya, G., Menges, P., Amponsah, P. S., Ngandiri, D. A., Schulz, D., Wallek, A., Kulak, N., Mann, M., Cramer, P., Savage, V., Räschle, M., & Storchova, Z. (2022). Sublinear scaling of the cellular proteome with ploidy. *Nature Communications*, *13*(1), 1–13. https://doi.org/10.1038/s41467-022-33904-7

Yanagitani, K., Juszkiewicz, S., & Hegde, R. S. (2017). UBE2O is a quality control factor for orphans of multiprotein complexes. *Science*, *357*(6350), 472–475. https://doi.org/10.1126/science.aan0178

Yang, Y., Liu, L., Naik, I., Braunstein, Z., Zhong, J., & Ren, B. (2017). Transcription Factor C/EBP Homologous Protein in Health and Diseases. *Frontiers in Immunology*, *8*, 1612. https://doi.org/10.3389/fimmu.2017.01612

Ye, J., Rawson, R. B., Komuro, R., Chen, X., Davé, U. P., Prywes, R., Brown, M. S., & Goldstein, J. L. (2000). ER stress induces cleavage of membrane-bound ATF6 by the same proteases that process SREBPs. *Molecular Cell*, *6*(6), 1355–1364. https://doi.org/10.1016/s1097-2765(00)00133-7

Young, J. C., Moarefi, I., & Ulrich Hartl, F. (2001). Hsp90: A specialized but essential protein-folding tool. *Journal of Cell Biology*, *154*(2), 267–273. https://doi.org/10.1083/jcb.200104079

Zhang, C. Z., Spektor, A., Cornils, H., Francis, J. M., Jackson, E. K., Liu, S., Meyerson, M., & Pellman, D. (2015). Chromothripsis from DNA damage in micronuclei. *Nature*, *522*(7555), 179–184. https://doi.org/10.1038/nature14493

Zhang, F., Gu, W., Hurles, M. E., & Lupski, J. R. (2009). Copy number variation in human health, disease, and evolution. *Annual Review of Genomics and Human Genetics*, *10*, 451–481. https://doi.org/10.1146/annurev.genom.9.081307.164217

Zhao, T., Chen, Y. M., Li, Y., Wang, J., Chen, S., Gao, N., & Qian, W. (2019). Disome-seq reveals widespread ribosome collisions that recruit co-translational chaperones. *Genome Biology*, 1–35.

Zhu, P. J., Khatiwada, S., Cui, Y., Reineke, L. C., Dooling, S. W., Kim, J. J., Li, W., Walter, P., & Costa-Mattioli, M. (2019). Activation of the ISR mediates the behavioral and neurophysiological abnormalities in down syndrome. *Science*, *366*(6467), 843–849. https://doi.org/10.1126/science.aaw5185

Zuo, J., Rungger, D., & Voellmy, R. (1995). Multiple layers of regulation of human heat shock transcription factor 1. *Molecular and Cellular Biology*, *15*(8), 4319–4330. https://doi.org/10.1128/mcb.15.8.4319